VOLUME 34 MARCH 1956 NUMBER 3

Canadian Journal of Physics

Editor: G. M. VOLKOFF

Associate Editors:

L. G. ELLIOTT, *Atomic Energy of Canada, Ltd., Chalk River*
J. S. FOSTER, *McGill University*
G. HERZBERG, *National Research Council of Canada*
L. LEPRINCE-RINGUET, *Ecole Polytechnique, Paris*
R. W. PRINGLE, *University of Manitoba*
B. W. SARGENT, *Queen's University*
Sir FRANCIS SIMON, *Clarendon Laboratory, University of Oxford*
W. H. WATSON, *University of Toronto*

Published by THE NATIONAL RESEARCH COUNCIL

OTTAWA CANADA

CANADIAN JOURNAL OF PHYSICS

(Formerly Section A, Canadian Journal of Research)

Under the authority of the Chairman of the Committee of the Privy Council on Scientific and Industrial Research, the National Research Council issues THE CANADIAN JOURNAL OF PHYSICS and six other journals devoted to the publication, in English or French, of the results of original scientific research. Matters of general policy concerning these journals are the responsibility of a joint Editorial Board consisting of: members representing the National Research Council of Canada; the Editors of the Journals; and members representing the Royal Society of Canada and four other scientific societies.

EDITORIAL BOARD

Representatives of the National Research Council

A. N. Campbell, *University of Manitoba*
G. E. Hall, *University of Western Ontario*
E. G. D. Murray, *McGill University*
D. L. Thomson, *McGill University*
W. H. Watson (Chairman), *University of Toronto*

Editors of the Journals

D. L. Bailey, *University of Toronto*
T. W. M. Cameron, *Macdonald College*
J. B. Collip, *University of Western Ontario*
G. A. Ledingham, *National Research Council*
Léo Marion, *National Research Council*
R. G. E. Murray, *University of Western Ontario*
G. M. Volkoff, *University of British Columbia*

Representatives of Societies

D. L. Bailey, *University of Toronto*
Royal Society of Canada
T. W. M. Cameron, *Macdonald College*
Royal Society of Canada
J. B. Collip, *University of Western Ontario*
Canadian Physiological Society
R. G. E. Murray, *University of Western Ontario*
Canadian Society of Microbiologists
H. G. Thode, *McMaster University*
Chemical Institute of Canada
T. Thorvaldson, *University of Saskatchewan*
Royal Society of Canada
G. M. Volkoff, *University of British Columbia*
Royal Society of Canada; Canadian Association of Physicists

Ex officio

Léo Marion (Editor-in-Chief), *National Research Council*
F. T. Rosser, Director, Division of Administration, *National Research Council*

Manuscripts for publication should be submitted to Dr. Léo Marion, Editor-in-Chief, Canadian Journal of Physics, National Research Council, Ottawa 2, Canada.
(For instructions on preparation of copy, see **Notes to Contributors** (inside back cover).)

Proof, correspondence concerning proof, and orders for reprints should be sent to the Manager, Editorial Office (Research Journals), Division of Administration, National Research Council, Ottawa 2, Canada.

Subscriptions, renewals, requests for single or back numbers, and all remittances should be sent to Division of Administration, National Research Council, Ottawa 2, Canada. Remittances should be made payable to the Receiver General of Canada, credit National Research Council.

The journals published, frequency of publication, and prices are:

Canadian Journal of Biochemistry and Physiology	Bimonthly	$3.00 a year
Canadian Journal of Botany	Bimonthly	$4.00 a year
Canadian Journal of Chemistry	Monthly	$5.00 a year
Canadian Journal of Microbiology	Bimonthly	$3.00 a year
Canadian Journal of Physics	Monthly	$4.00 a year
Canadian Journal of Technology	Bimonthly	$3.00 a year
Canadian Journal of Zoology	Bimonthly	$3.00 a year

The price of single numbers of all journals is 75 cents.

"Reprinted in entirety by photo-offset from the original issue"

Canadian Journal of Physics

Issued by THE NATIONAL RESEARCH COUNCIL OF CANADA

VOLUME 34 MARCH 1956 NUMBER 3

THE POSSIBILITY OF A PHASE CHANGE IN NUCLEAR MATTER[1]

BY L. E. H. TRAINOR AND W. R. DIXON

ABSTRACT

The possibility is discussed that Livesey's hypothesis of a constant nuclear temperature at low excitations is indicative of a phase change in nuclear matter.

INTRODUCTION

In the study of nuclear physics where the basic theory is so little understood, it has sometimes been very fruitful to investigate analogies with situations in other fields of physics—situations which are presumably more familiar and better understood. For sufficiently large nuclei, thermodynamic concepts such as heat energy, temperature, and evaporation have been introduced, and much attention has been given to statistical models, such as the Fermi-gas model and the liquid drop model. These analogies have proved very helpful in the description of certain nuclear phenomena. In the present note we wish to draw attention to the possibility of another thermodynamic analogy for nuclei, namely, that of a phase change in the nuclear matter. This suggestion (Trainor and Dixon 1955) arose specifically out of a hypothesis by Livesey (1955) that the nuclear temperature is essentially constant for excitations below about 10 Mev. The idea of a phase change has been put forward independently by Weisskopf (1953, 1955) on other grounds.

EVIDENCE FOR A CONSTANT NUCLEAR TEMPERATURE

In the application of statistical thermodynamics to nuclei, the entropy S can be defined as the logarithm of the level density (thermodynamic probability) w, and a nuclear temperature T is introduced in the usual way to relate the entropy to the excitation energy E,

$$dE = T\,dS. \tag{1}$$

An equation of state relating E and T then determines the entropy $S(E)$ and the level density $w(E)$. Simple models give

$$S \sim E^n \tag{2}$$

where n lies between $\frac{1}{2}$ (degenerate Fermi gas) and 1 (constant nuclear temperature), depending upon the nuclear model.

[1]Manuscript received September 28, 1955.
Contribution from the Physics Department, Queen's University, Kingston, Ontario, and the Radiology Section, Division of Applied Physics, National Research Council, Ottawa. Issued as N.R.C. No. 3856.

Lang and LeCouteur (1954) find that for nuclear excitations in excess of about 10 Mev. the experimental data are generally consistent with the model of a degenerate Fermi gas. Other experiments suggest, however, that at low excitation energies the entropy variation is stronger than the $E^{\frac{1}{2}}$ variation of the Fermi-gas model. For example, the energy distributions of particles emitted in (p, n) reactions (Gugelot 1951), in the inelastic scattering of neutrons (Graves and Rosen 1953), and in photonuclear reactions (Dawson 1955, Dixon 1955) can be fitted using a constant nuclear temperature, which would imply a linear variation of entropy with excitation energy. (Cohen (1953) has suggested an even stronger dependence of S upon E.) Livesey (1955) has reviewed a wide range of experimental data, and suggests that they may be brought together if one assumes that the nuclear temperature is effectively constant below 10 Mev. excitation at a value of the order of that given by the Fermi-gas model at 10 Mev., viz. $T \approx 10\,A^{-\frac{1}{2}}$ Mev.

The evidence for a constant nuclear temperature is by no means conclusive, since reliable experiments are difficult to perform and the interpretation of the results is far from straightforward. For example, in deriving nuclear temperatures from the energy distributions of emitted particles, direct effects must be excluded. If they are erroneously included, there are too many high-energy particles, and the derived temperatures are too high for low energies of excitation in the residual nucleus. The subtraction of direct effects is particularly important in considering the energy distributions of charged particles, since the Coulomb barrier discriminates severely against the evaporation process.

Aside from questions concerned with the applicability of the compound-nucleus description (for example, the changing mean free path of nucleons in nuclear matter (Feshbach, Porter, and Weisskopf 1954), and the influence of direct effects insofar as these cannot be separated out), there are difficulties in the determination of nuclear temperatures within the framework of that description. Blatt and Weisskopf (1952) write the energy distribution $I(e)$ of neutrons evaporated from a compound nucleus as

$$I(e)\,de = \text{const.}\; e\,\sigma_c(e, E)\,w(e_{\max}-e), \tag{3}$$

where $e_{\max}$ is the maximum energy with which a neutron may be emitted, $w(e_{\max}-e)$ is the level density in the residual nucleus at an excitation energy $E = e_{\max}-e$, and $\sigma_c(e, E)$ is the cross section for formation of a compound nucleus when a neutron of energy e is incident upon the residual nucleus in the state of excitation E. Unfortunately this cross section cannot be measured directly, since experimentally a bombarded nucleus is initially in its ground state. It is usually assumed that for neutrons σ_c is independent of both e and E. A marked energy dependence of this quantity however could significantly affect all conclusions concerning level densities and nuclear temperatures. The possibility should also be noted that the experimentally derived temperature might depend on the particular reaction being studied, through a selection of only certain of the levels of a given energy in the residual nucleus.

THE POSSIBILITY OF A NUCLEAR CHANGE OF PHASE

Although there is no conclusive evidence to support the hypothesis of a constant nuclear temperature at excitations below about 10 Mev., it is nevertheless interesting to speculate upon its possible thermodynamical significance. We have suggested (Trainor and Dixon 1955) that Livesey's hypothesis may indicate a first order phase change in nuclear matter, in which energy, entropy, and volume increase without change in temperature and pressure.

If the notion of a phase change in nuclei is a sensible one, two quantities are of immediate interest, viz. the latent heat and the temperature at which the phase change occurs. To a first approximation one can consider that the composition and density of nuclear matter are independent of atomic mass number A, from which it follows that both the latent heat per unit volume and the transition temperature should be independent of A. The excitation energy at which the phase change sets in (which must be low according to the experimental results), and the excitation energy at which the phase change ceases,

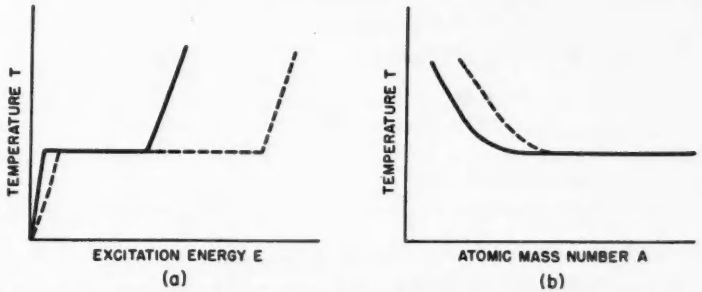

FIG. 1. Illustrating possible behavior associated with a nuclear change of phase. (*a*) Nuclear temperature T versus excitation energy E for given mass number A. The dashed curve is for the larger value of A. (*b*) Nuclear temperature T versus mass number A for given excitation energy E. The dashed curve is for the larger value of E.

should both increase linearly with A. This general scheme of things is illustrated in Fig. 1(*a*), where the temperature T is plotted against excitation energy for two hypothetical values of A.

Since the transition temperature has been supposed essentially independent of A, and since it can be measured at any energy in the transition region, it can be determined experimentally in a variety of ways. It is not so easy to measure the latent heat. In principle, the latent heat could be measured for a particular nucleus by determining the graph of temperature versus excitation energy, but this is difficult to do in practice. However if the latent heat per unit volume is independent of A, its value can also be inferred from a graph of temperature versus A for a given excitation energy, as illustrated in Fig. 1(*b*). For a particular nucleus there is an excitation energy which is just sufficient to "melt" that nucleus. With the same excitation energy, nuclei heavier than this critical one will be only partially "melted", and the measured

temperature will be the transition temperature. The same excitation energy in nuclei lighter than the critical one, however, will be sufficient to complete the phase change and to heat the nucleus to some point beyond the transition temperature. The latent heat per unit volume is then just the ratio of the excitation energy used in the experiment to the volume of the critical nucleus.

Present experimental results however do not permit an accurate determination of the latent heat per unit volume. In Fig. 2 the experimental temperatures found in the photoproton work of Dawson (1955) and in the photoneutron

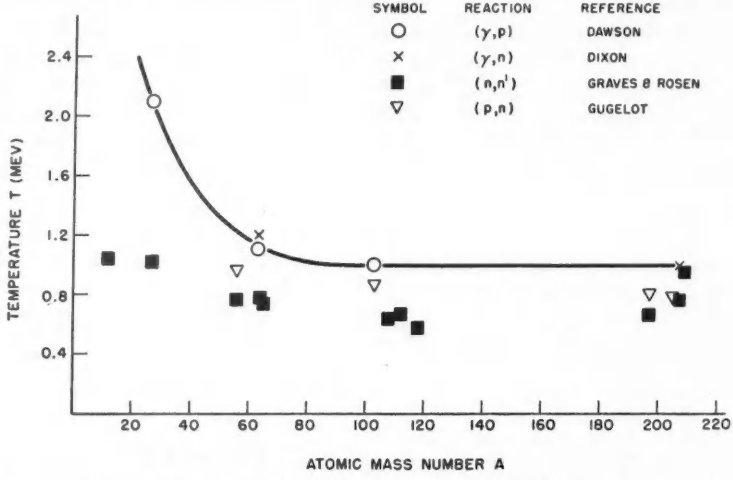

FIG. 2. Experimental values of the nuclear temperature. The solid curve has been drawn through the photonuclear results.

work of Dixon (1955) are plotted as a function of A. The analysis of the photoproton results has involved taking into account the direct emission of protons, according to the theory of Courant (1951), and the analysis of the photoneutron results has involved a small correction for $(\gamma, 2n)$ reactions. The temperatures determined from the (n, n') work of Graves and Rosen (1953) and from the (p, n) work of Gugelot (1951) are also plotted in Fig. 2. The data of Graves and Rosen are uncorrected for multiple neutron reactions which tend to give too many low-energy neutrons and too low a value for the nuclear temperature. In the case of the (p, n) and (n, n') experiments the temperatures shown have been determined for excitation energies of the residual nucleus of about 10–12 Mev., while for the photonuclear experiments the average excitation energies are about 5–7 Mev. The results of Gugelot (1954) on the inelastic scattering of protons have not been included in Fig. 2 because they are not considered to give reliable values for the temperatures owing to the presence of direct effects (Eisberg 1954).

It is not clear from the experimental results shown in Fig. 2 that the break in the curve for the photonuclear results occurs at a smaller value of A than

for the particle reactions, as is to be expected from the relative excitation energies. It is also not clear whether the transition temperature is actually independent of A, as in the simplest picture, or whether it perhaps varies as $A^{-\frac{1}{3}}$, as in Livesey's hypothesis. Assuming that the transition temperature is independent of A, however, a rough determination of the latent heat per nucleon can be made, and one obtains a figure of about 0.1 Mev. per nucleon from the photonuclear results.

In conclusion, it should be emphasized that the above discussion has been quite speculative. There is not yet sufficient experimental evidence to determine if the idea of a phase change in nuclear matter is useful for the description of certain nuclear phenomena.

ACKNOWLEDGMENTS

The authors wish to thank Drs. D. L. Livesey and G. E. Tauber for valuable discussions. One of us (L.E.H.T.) is indebted to the Summer Research Institute of the Canadian Mathematical Congress for a Summer Research Fellowship.

REFERENCES

BLATT, J. M. and WEISSKÖPF, V. F. 1952. Theoretical nuclear physics. John Wiley & Sons, Inc., New York. Chap. VIII.
COHEN, B. L. 1953. Phys. Rev. **92**: 1245.
COURANT, E. D. 1951. Phys. Rev. **82**: 703.
DAWSON, W. K. 1955. Photonuclear Conference, Cleveland, May.
DIXON, W. R. 1955. Can. J. Phys. **33**: 785.
EISBERG, R. M. 1954. Phys. Rev. **94**: 739.
FESHBACH, H., PORTER, C. E., and WEISSKOPF, V. F. 1954. Phys. Rev. **96**: 448.
GRAVES, E. R. and ROSEN, L. 1953. Phys. Rev. **89**: 343.
GUGELOT, P. C. 1951. Phys. Rev. **81**: 51.
——— 1954. Phys. Rev. **93**: 425.
LANG, J. M. B. and LECOUTEUR, K. J. 1954. Proc. Phys. Soc. (London), A, **67**: 586.
LIVESEY, D. L. 1955. Can. J. Phys. **33**: 391.
TRAINOR, L. E. H. and DIXON, W. R. 1955. Bull. Am. Phys. Soc. **30**(No. 4): 29.
WEISSKOPF, V. F. 1953. Proc. Am. Acad. Arts Sci. **82**(No. 7): 360.
——— 1955. Photonuclear Conference, Cleveland, May.

GROWTH TWINS IN GERMANIUM[1]

By G. F. Bolling, W. A. Tiller,[2] and J. W. Rutter

ABSTRACT

The occurrence of growth twins in germanium was investigated as a function of the thermal, constitutional, and crystallographic conditions of solidification; it was found to be very markedly dependent upon these growth conditions. In every case the nucleation of a twin could be traced to a condition of supercooling, either absolute or constitutional, during solidification. A new type of substructure was also observed to form under certain growth conditions.

INTRODUCTION

During recent years, a great deal of interest has been focused upon the production of single crystals of the semiconductors germanium and silicon. The demands of industry necessitated the immediate production of crystals, and consequently very little time was devoted to the understanding of why these semiconductors solidified as they did in a manner different from the solidification of metal crystals from the melt.

The most apparent difference between the solidification of semiconductors and metals is the frequency of occurrence of growth twins in semiconductors. Ellis and Fageant (1954) investigated the orientation relationships in cast germanium, and have shown that all major regions in a progressively solidified ingot of germanium were related through successive orders of octahedral twinning. It was suggested that the entire ingot grew from one nucleus formed in initial freezing, and that all subsequent orientations originated through nucleation on the surface of the existing solid. Ellis and Treuting (1951) showed theoretically that twinned regions can occur with relative ease in the diamond cubic structure. This fact is consistent with the existence of twins in a cast structure, but it does not explain how or why they occur.

The investigation of Billig (1954), who studied growth twins in germanium and silicon, gives further insight into the phenomenon. He concludes, in accordance with earlier investigators, that the observed twinning initiates at the solid–liquid interface and is not a solid state transformation. His study shows that a crystal attempts to grow with one of its {111} planes aligned as closely as possible with its maximum temperature gradient. If necessary, it will twin to do this. His observations indicate that twinning is not a haphazard event, and that it can be promoted by an unevenness in growth rate.

Experience at the University of Toronto derived from growing germanium crystals from the melt supports the following. If a specimen is grown under linear heat flow conditions such that the solid–liquid interface is approximately a plane, then a single crystal will usually be obtained. However, when the heat flow is not linear, the isotherms in the liquid adjacent to the interface become curved. The interface will attempt to adopt the curvature of the freezing-point isotherm. Twinning is observed each time before this can be accomplished.

[1]Manuscript received October 31, 1955.
Contribution from the Department of Metallurgical Engineering, University of Toronto, Toronto, Ontario.
[2]Now at Westinghouse Research Laboratories, East Pittsburgh, Pennsylvania.

The present work is an attempt to explain the occurrence of twinning in terms of thermal, crystallographic, and constitutional conditions. The observations are qualitative in nature but lead to an explanation for twinning in germanium.

EXPERIMENTAL PROCEDURES

Crystals of zone-refined germanium of approximately 10 ohm-cm. resistivity were grown from the melt in a horizontal carbon boat using the Chalmer's technique (1953). Approximately linear heat flow was produced by soldering a water-cooled copper block to seed crystals of desired crystallographic orientation. The crystals were grown under various growth rates and different temperature gradients. The solid–liquid interface of each crystal was exposed and preserved by separating the solid from the liquid using the accelerated decanting technique of Elbaum and Chalmers (1955). The curvature of the interface could then be observed, and the orientation of the twin crystals determined by X-raying the interface.

Measurements of the temperature configuration at the solid–liquid interface were made by placing a protected thermocouple into the melt. For a desired growth rate and imposed temperature conditions, this thermocouple was frozen into the crystal and a time–temperature plot of this trial run was recorded. The crystal was remelted, and then resolidified under identical conditions. Decanting was effected just before the solid–liquid interface reached the thermocouple. In this way, both the growth rate and the temperature gradient in the liquid at the interface were known from the trial run, and the interface was preserved.

EXPERIMENTAL OBSERVATIONS

Thermal Effects

Crystals were grown using the same seed at rates of growth $R = 0.16$, 0.5, 1.5 cm./min. It was observed that as the rate of growth increased, the interface was further outside the furnace and, therefore, the amount of lateral

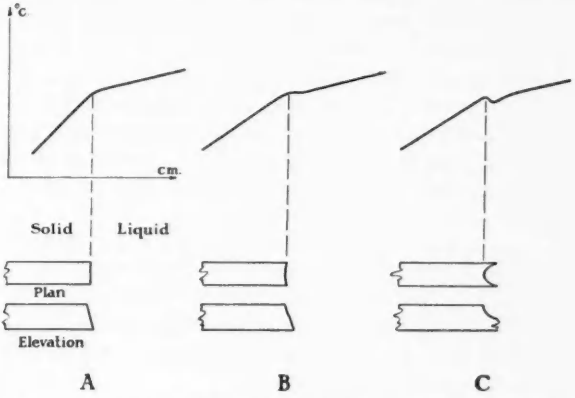

FIG. 1. Temperature distributions in the germanium near the interface for various growth rates. Corresponding interface shapes for these cases are shown.

heat loss from the liquid increased. The distance–temperature plots for these crystals were as shown in Fig. 1A. It can be seen that, as the rate of growth increases, the temperature gradient in the liquid, G, decreases from a positive value, through zero, to a negative value; that is, at high growth rates a small zone of absolute supercooling exists ahead of the interface.

In the system that was used, it was impossible to vary R and G independently. For example, when R was increased by increasing the rate of furnace movement, G decreased. However, both factors could be measured separately, and similar experimental results were obtained on different samples provided that the ratio G/R was the same, even though R and G individually were different for each. As a consequence, it is sufficient to use the parameter G/R to describe the general growth conditions.

A plane interface shape could be maintained at high values of R if G were also high, keeping G/R high. With a plane interface, no twins occurred. As the lateral heat loss increased, the interface altered shape from a plane to a concave parabolic form, as shown schematically in Fig. 1B. Beyond any slight curvature, as the ratio G/R decreased, the following events were observed:

(i) Growth twins appeared, a few lamellar twins appearing for small curvatures and twin crystals for large curvatures. The density of twinning increased inversely as the ratio G/R.

(ii) All the growth twins extended to at least one outer surface.

(iii) Under the condition of G approximately zero at the interface, a substructure appeared on the bottom of the crystal projecting into the liquid. This structure is centered by a lamellar twin and is shown in Fig. 9. The length of projection ahead of the general interface increased as the ratio G/R decreased. This structure is not a simple dendrite because its axis is not the dendrite direction.

(iv) Before shape changes of the interface became too pronounced, the twin crystals were examined by X-rays. It was observed that the interface of each twin was (within a few degrees) of the $\{h, h-l, l\}$ family. These are families of planes perpendicular to one of the {111} planes.

Crystal Orientation Effects

A single crystal seed was used to grow specimens turned in orientation $\pm 10°$ respectively from the seed axis, as shown in Fig. 2. A value of G/R was used such that the solid–liquid interface was close to a plane and an absence of twins would be expected in the resulting crystal. One specimen became aligned within 2° of a [111] direction. It exhibited a regularly spaced structure on both sides of the crystal. The structure habit was like twinning and appeared lamellar. Some "fragmentation" appeared in the center of the crystal where the lamellae from each side met.

The other crystal was rotated away from the particular [111] direction mentioned above. The structure appeared again but was more favored on one side, as is shown diagrammatically.

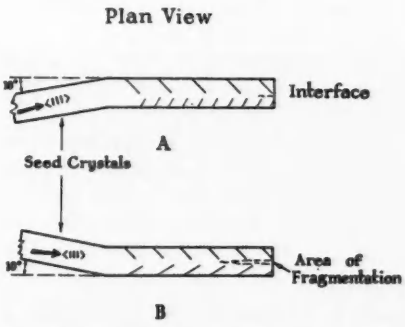

FIG. 2. Two samples with their growth axes related to <111> directions. A regular structure appears as shown.

Constitutional Effects

Seed crystals of 35 ohm-cm. resistivity germanium, having a [321] axis, were used to grow crystals containing from 0.014 atomic per cent to 0.75 atomic per cent additions of gallium. These crystals were grown under values of G/R such that no twins would appear in the pure germanium.

Internally bounded growth twins like those in Fig. 3 began to appear at 0.043 atomic per cent gallium, and when the gallium content was increased to 0.13 atomic per cent twin lamellae appeared on two different {111} planes as shown in Fig. 4. As the gallium content was increased, the twin density increased greatly.

By scratching the surface and also by casting the shadow of a graticule on the surface, it was observed that the twin lamellae projected a very short distance ahead of the rest of the interface.

It was observed that the germanium liquid does not completely wet high-resistivity solid germanium. This is evident from the observation that a drop of liquid clings to the solid during decanting, as shown in Fig. 5. The gallium content increases in a clockwise motion from the upper right in the figure. It can be seen that, as the gallium content increases, the contact angle decreases toward zero so that the wetting of the solid by the liquid must increase.

On the basis of considerations by Walton *et al.* (1955), it would be expected that a transition from a smooth interface to a cellular interface should occur as the gallium content is increased. However, the interface exhibits a pox-like structure which tends to cluster at twin boundaries, as shown in Fig. 6, long after one would expect a cellular interface. Near 0.2 atomic per cent gallium, the crystal interface has broken down to exhibit an array of well-developed pyramidal cells, as shown in Figs. 7 and 8.

Crystals were also grown with antimony additions. At 0.1 atomic per cent antimony, a huge dendrite which projected 1½ cm. into the liquid was preserved; it is shown in Fig. 10. X-ray investigation showed the dendrite direction to be the [11$\bar{2}$] direction, and the upper surface to be a (111) plane. Multiple

beam interferometry showed that the upper surface was flat to within 200 Å. The lower surface of the dendrite was also a (111) plane, but it was very irregular.

DISCUSSION

The solidification of a semiconducting element like germanium differs essentially from the solidification of a metal in that for germanium a metallic liquid is in contact with a covalent solid rather than a metallic solid. For germanium, there is thus less bonding between solid and liquid than for a metal, so that the solid–liquid interface has a higher interfacial energy. Because of the directional nature of the bonds, interfaces of different orientations will differ greatly in energy and the crystal will find it easier to attach atoms to the solid in certain directions rather than in others.

Thermal and Crystal Orientation Effects

From the observations it appears that germanium finds it easiest to grow in the $\langle h, h-l, l\rangle$ directions and that it tries at all times to have an interface of the $\{h, h-l, l\}$ type. This is consistent with the observations of Billig (1954, 1955). He finds that germanium prefers to grow by the extension of that set of {111} planes most closely perpendicular to the interface. In his study of dendritic growth in germanium, Billig shows that dendritic growth in crystals with the diamond structure proceeds mainly by the extension of one or more sets of the {111} family of planes, and is especially favored along one of the $\langle 112\rangle$ directions in these planes.

The present observations could therefore be accounted for by consideration of Fig. 11(*a*). Consider a germanium crystal growing with AA' as the interface with one {111} plane perpendicular to both AA' and the page. AA' will be of the family $\{h, h-l, l\}$ which is preferred. Then if $BB''B'$ represents the freezing point isotherm distorted by lateral heat losses, the region of liquid between AA' and $BB''B'$ is supercooled. The greatest supercooling is at the outer edges $A'B'$. If this supercooling becomes large enough, a twin will nucleate at the outer surface along one {111} plane not perpendicular to the page. The interface of the twin can be of the $\{h, h-l, l\}$ family of AA' but at an angle to it. The twin crystal can then proceed inwards to absorb the supercooling and allow the interface to adjust to the freezing point isotherm.

To explain the observations for other crystal orientations, Fig. 11(*b*) must be considered. The preferred $\{h, h-l, l\}$ plane is represented by CC'. It is oblique to the direction of general heat flow. $DD''D'$ represents the freezing point isotherm. If CC' can exist, there will be supercooling and it will be greatest at the edge CD. A twin lamella can nucleate here to favorably alter the interface shape, but, as it grows into the crystal, its usefulness disappears and another twin must nucleate and so forth. At $C'D'$, to a smaller extent, this cyclic arrangement will also appear. If the thermally determined solid–liquid interface is a {111} plane, it will be as far away as possible from the preferred type. The appearance of a twin structure would be symmetrically favorable at the outer edges and a balanced cycling would appear.

PLATE I

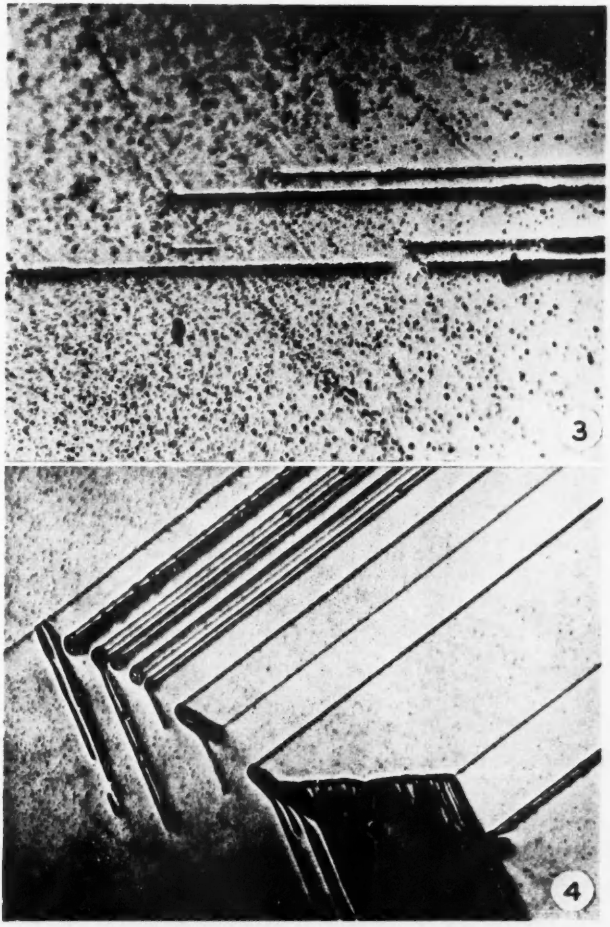

FIG. 3. An internally bounded structure parallel to the trace of a {111} plane appears on the decanted interface when some gallium is added (300×).

FIG. 4. The structure of Fig. 3 appears on two different {111} traces at higher gallium concentration. There is a preference for the pock-marked background in some regions (100×).

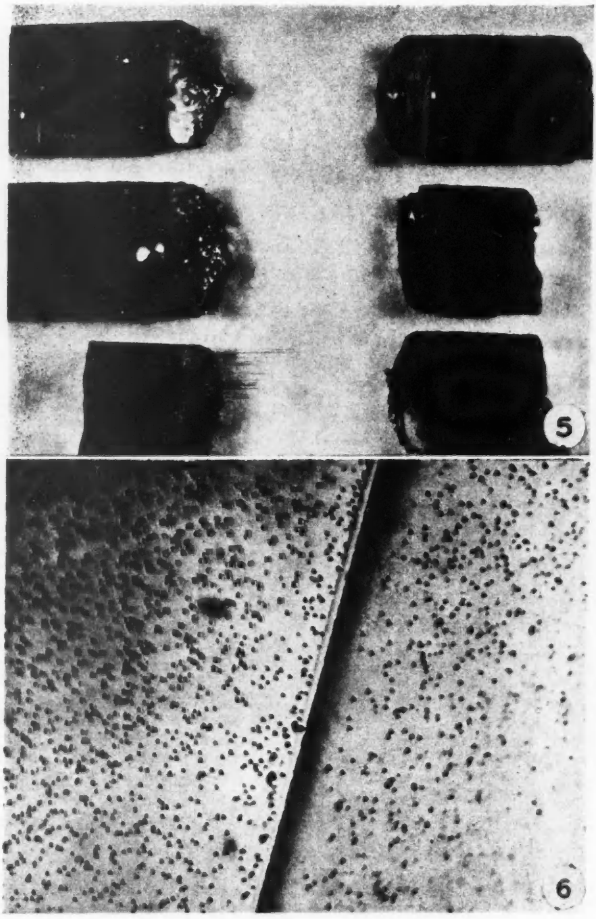

FIG. 5. Germanium interfaces (1½×). The gallium content increases for the samples, viewed in a clockwise sense from the upper right corner. The "contact angle" decreases indicating increased wetting with gallium addition.

FIG. 6. A twin boundary at the interface shows a preference for the pock marks (1000×).

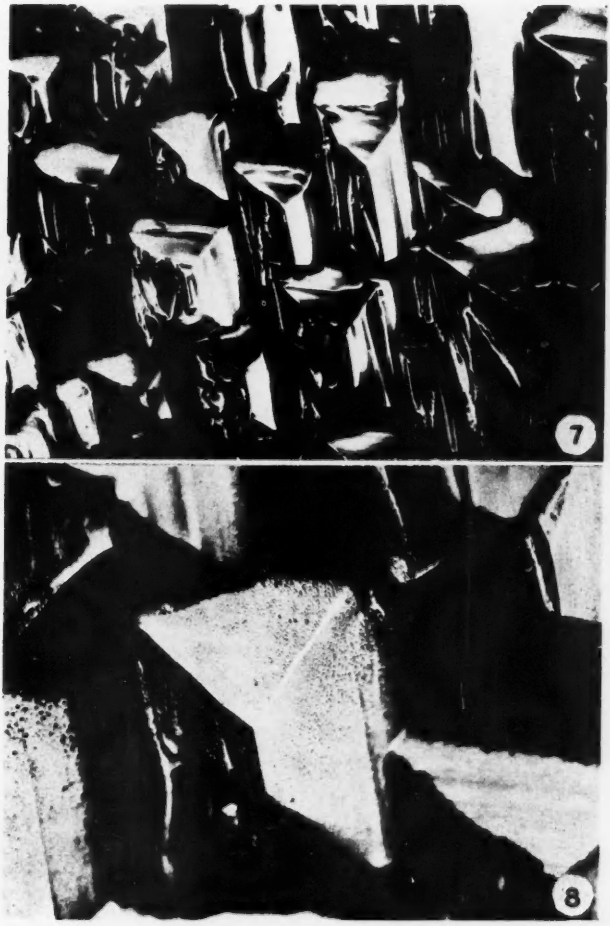

FIG. 7. With large amounts of gallium added, the interface exhibits pyramidal cells (150×).
FIG. 8. A single pyramid obliquely illuminated (500×).

FIG. 9. A germanium sample viewed on its lower surface which solidified in contact with the boat. Projecting structures centered by a twin lamella were revealed at the interface by decanting (7×).

FIG. 10. A very flat dendrite grown with antimony added to the germanium (7×).

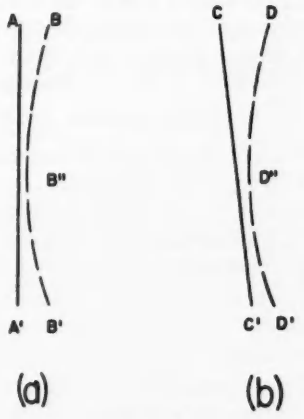

FIG. 11.

Crystals of unfavorable orientations may then be grown only if a critical supercooling for the nucleation of a twin is not reached. This could be achieved by controlled temperature gradients in the liquid.

Solute Effect

On the basis of considerations concerning the distribution of solute at the growing interface by Tiller *et al.* (1953), it would be expected that even under the addition of 0.01 atomic per cent of gallium, a zone of constitutional supercooling must exist adjacent to the solid–liquid interface. In metallic systems, the interface would alter shape from a smooth interface to a cellular interface, as studied by Rutter and Chalmers (1953). However, the interface does not develop an array of hexagonal projections, and this may indicate either that the growth mechanism is unable to form these projections, or that the increase of interfacial energy which must accompany the formation of this substructure is too great to allow its formation.

Thus, constitutional supercooling does exist, resulting in the occurrence of twins. As the degree of constitutional supercooling increases, the instability is great enough to allow even the nucleation of a second less favorably oriented twin system. Constitutional supercooling would most probably be equal over the whole interface. The critical supercooling necessary for twin formation could then occur first away from the outer edges, giving rise to internally bounded twins. This occurrence of internally bounded twins lends support to the necessity of supercooling as a prerequisite to twin formation.

As can be seen from the addition of gallium, the liquid wets the solid much better at higher alloy concentrations than at low. This increased bonding between liquid and solid indicates that the interfacial energy of the germanium has decreased; that is, it is becoming more like a metal. When the alloy concentration is high enough, the interface does break down to an array of projections which are similar to the cellular projections previously mentioned. The occurrence of well-developed projections which exhibit a pyramidal

form indicates either that the surface energy has become low enough to allow the transition, or that the growth mechanism has changed. It is difficult on the basis of few experiments to separate these two effects. Similar structures were observed indirectly by Ellis (1955) in the growth of germanium–silicon alloys.

CONCLUSIONS

(i) The growth mechanism is such that the germanium exhibits a strong tendency to grow in the $\langle h, h-l, l \rangle$ directions.

(ii) The occurrence of twins requires the existence of supercooling, either constitutional or absolute. The nucleation of twins requires a certain minimum of supercooling for their occurrence. The frequency of twinning increases as the supercooling increases.

(iii) The interfacial energy of solid germanium against liquid germanium was lowered by gallium additions.

(iv) At a certain degree of constitutional supercooling, a smooth interface becomes unstable with respect to an interface which exhibits a regular array of pyramidal projections.

ACKNOWLEDGMENTS

This work was carried out in the Department of Metallurgical Engineering, University of Toronto. The authors are grateful to Canadian Patents and Development, Limited, and the National Research Council of Canada for financial assistance.

REFERENCES

BILLIG, E. 1954. J. Inst. Metals, **53**: Oct.
——— 1955. Proc. Roy. Soc. A, **229**: 346.
CHALMERS, B. 1953. Can. J. Phys. **31**: 132.
ELBAUM, C. and CHALMERS, B. 1955. Can. J. Phys. **33**: 196.
ELLIS, S. G. 1955. J. Appl. Phys. **26**: 1140.
ELLIS, W. C. and FAGEANT, J. 1954. J. Metals, **6**: 291.
ELLIS, W. C. and TREUTING, R. G. 1951. J. Metals, **3**: 53.
RUTTER, J. and CHALMERS, B. 1953. Can. J. Phys. **31**: 15.
TILLER, W. A., JACKSON, K. A., RUTTER, J. W., and CHALMERS, B. 1953. Acta metallurgica, **1**: 428.
WALTON, D., TILLER, W. A., RUTTER, J. W., and WINEGARD, W. C. 1955. J. Metals, **7**: 1023.

THE PHOTODISINTEGRATION OF OXYGEN NUCLEI INTO FOUR ALPHA-PARTICLES[1]

By W. K. Dawson[2] and D. L. Livesey[3]

ABSTRACT

A total of 323 four-prong stars found in photographic plates exposed to bremsstrahlung of maximum energy 70 Mev. have been identified as due to the disintegration of O^{16} nuclei into four alpha-particles. The excitation function of the reaction exhibits pronounced peaks at 22.5 Mev. and 32.5 Mev. as well as maxima at intermediate energies, and the integrated cross sections for various energy ranges have been estimated. The mechanism of the process has been investigated and most of the disintegrations proceed via known excited levels in C^{12} and various states of Be^8.

1. INTRODUCTION

When a photographic plate is exposed to high energy X-rays many types of multiple nuclear disintegration occur, leading to the production of identifiable stars when the light nuclei of the gelatin are involved. Several authors have published accounts of the photodisintegration of C^{12} nuclei into three alpha-particles and of O^{16} into four alpha-particles. The following properties of these reactions have been established with some degree of certainty:

(*a*) the excitation functions exhibit a series of narrow resonances grouped into larger peaks which alone are detected when the energy resolution is not of a high order (see Goward and Wilkins 1952*b*, 1953), Livesey and Smith (1952); the same kind of behavior is shown by the (γ, n) reactions in these nuclei according to Katz *et al.* (1954) and Spicer *et al.* (1954);

(*b*) the mode of disintegration of these even–even light nuclei is predominately via excited levels in the intermediate nuclei C^{12} and Be^8 according to Goward and Wilkins (1955), Livesey and Smith (1953), and Hsiao and Telegdi (1953);

(*c*) the preferred states of C^{12} and Be^8 are determined to some extent by isotopic-spin selection rules, in that above about 25 Mev. electric-dipole absorption leads to $T = 1$ states which then break up via $T = 1$ states of the intermediate nuclei in agreement with the predictions of Gell-Mann and Telegdi (1953).

The oxygen reaction

$$O^{16} + h\nu = 4He^4 - 14.5 \text{ Mev.}$$

has been studied by the authors quoted above, also by Dawson and Bigham (1953) and by Millar and Cameron (1953). The method of identifying the four-pronged stars produced by this reaction is well-known, and the variation of yield with photon energy for 700 stars has been published by Goward and Wilkins (1952*b*). Analysis of the modes of disintegration of the nuclei involved

[1]Manuscript received October 19, 1955.
Contribution from the Department of Physics, Queen's University, Kingston, Ontario.
[2]Present address: Suffield Experimental Station, Ralston, Alberta.
[3]National Research Council Postdoctorate Fellow. Present address: Oundle School, Northants., England.

has been carried out by Livesey and Smith (1953), by Goward and Wilkins (1952*a*), and by Millar and Cameron (1953). However, the behavior of the reaction above 30 Mev. has not been studied in detail, and no detailed analysis of a large number of stars has yet appeared. This paper describes the results of analyses carried out on 323 oxygen stars produced in Ilford C-2 plates exposed to bremsstrahlung of maximum energy 70 Mev. from the electron synchrotron at Queen's University. In a later section the deductions are compared with those of other authors.

2. EXPERIMENTAL PROCEDURE

Ilford C-2 nuclear emulsions, 200 μ thick, coated on 1 in. by 3 in. glass backings were irradiated in the unfiltered 70 Mev. X-ray beam from the electron synchrotron at Queen's University. All irradiations were monitored by Baldwin–Farmer BD-2 ionization chambers placed near the beam edge. These chambers were calibrated against a Victoreen thimble placed behind 7.3 cm. of lucite at the position the plates later occupied. The plates were placed at a distance of 2 meters from the synchrotron target with the emulsion face perpendicular to the beam direction. Plate dosages varied from about 10 to 50 roentgens.

A standard temperature-change method was used for processing the plates. They were first immersed in a 2% sodium carbonate solution at room temperature, then placed in a refrigerator kept at 3° C. and left there for several hours. Next they were transferred to a cold developing bath also at 3° C. consisting of 1 gm. hydroquinone, 20 gm. sodium sulphite, and 1 gm. potassium bromide in 2 liters of distilled water. (This developer has been found to give good discrimination between different types of particles.) The cold soak continued for at least 12 hr. and was followed by a development period of about 30 min. in the same type developer at 20° C. Development was arrested by immersing the plates in a $\frac{3}{4}$% acetic acid solution for 30 min. Fixation started with a 30 min. soak in fixer at 3° C. followed by a transfer of the plates to fixer at 20° C. where they were left for about five hours. Kodak formula F-5 which contains a hardening solution was used for the fixer. A mechanical rocker was used for all processing carried out at 20° C. Following a five-hour wash in running water the plates were immersed in a 30% glycerin solution for about 45 min. before being placed out to dry.

Measurement of the shrinkage factor was carried out as follows. Immediately after an irradiation the thickness of the glass backing plus emulsion was measured at 10 different places on the plate using a bench gauge which read consistently to 0.0001 in. After processing but before the plates were put out to dry, the emulsion was removed from each corner of the plate. Thus it was possible to measure the glass thickness at these points with the bench gauge and to determine the original emulsion thickness at the intermediate points. The processed emulsion thickness was measured at the same intermediate points using the microscope fine-focus adjustment and the same set of objective and eyepieces that would later be used for star measurement. Under reasonably favorable conditions this method allows the shrinkage factor to be

determined to within about 5%. The values of the shrinkage factor for the various plates used lay between 0.9 and 1.4. This method has the advantage that it calibrates the fine-focus adjustment of the microscope against the bench gauge. Day-to-day checks of the processed emulsion thickness were made in order to allow for variations occasioned by changing humidity and temperature.

Measurement of the stars was carried out using a combination of objective and eyepieces which gave a field of view about 110 μ in diameter. The stars were identified using the momentum balance principle described by Goward and Wilkins (1950).

The correction for stars not measured because any prong is not entirely contained in the emulsion was determined experimentally as follows. A plot of the number of stars versus star thickness (the distance between two planes parallel to the emulsion surface which just enclose the star) was made for each of the energy groups indicated in the yield curve. In group A, for example, 70% of the stars have thicknesses less than 10 μ while all the stars in this energy group have thicknesses less than 20 μ. Hence, if all the stars in group A were situated 2.5 μ (one-half the average thickness) from the emulsion surface about 70% would be entirely contained in the emulsion. At a distance of 7.5 μ from the surface approximately all group A stars would be contained in the emulsion. A curve of fraction of stars contained in the emulsion versus distance of the vertex from the emulsion surface was made for each energy group. The area under each curve out to one-half the emulsion thickness is divided by the area that would have been obtained had there been no loss, giving the fraction of stars entirely contained in the emulsion. The inverse of this quantity is then the required correction. Values of the correction factor varied from 1.02 for group A to 1.12 for group E, in the yield curve (Fig. 1*b*).

3. RESULTS AND DISCUSSION

The first step in the analysis of the oxygen stars consisted of the calculation of the balance of momentum in each of the three dimensions as already mentioned, and a star was accepted only if the net error in momentum balance (Δ) was less than 50 photon units. In these units the energy of a photon in Mev. is numerically equal to its momentum. The energy of the photon responsible for each star was found under the assumption that none of the energy was lost in excitation of the product nuclei. The number of stars per 0.5 Mev. interval was then plotted against photon energy, as is shown in Fig. 1*a*, and this yield curve exhibits several peaks similar to those reported by Livesey and Smith (1953) and by Goward and Wilkins (1952*b*). The estimated error on each energy determination is of the order of ± 0.5 Mev., and this severely limits the resolution of the different energy groups. In order to improve the resolution slightly and to select a group of stars suitable for detailed analysis, a second yield curve is plotted in Fig. 1*b* with data from stars in which the value of Δ did not exceed 35 photon units. This histogram is based on figures from 263 stars and it shows well-defined peaks close to 22.5 Mev. and 32.5 Mev. with possible groups at 29 Mev., 35 Mev., and between 26 and 28 Mev. For the purpose of further analysis the stars were divided into six groups, marked on the diagram, but,

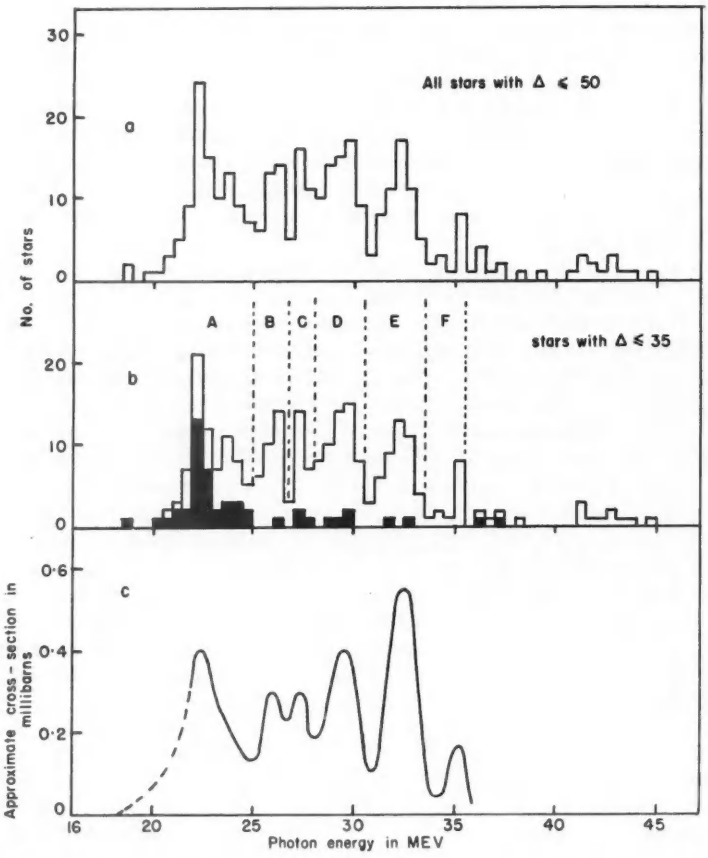

FIG. 1. (*a*) Yield curve for 323 stars with $\Delta \leqslant 50$ photon units. (*b*) Yield curve for 263 stars with $\Delta \leqslant 35$ photon units, used in detailed analysis, with stars involving Be^8 in the ground state shown shaded. (*c*) Estimated cross section curve for the reaction after corrections for escape of particles and the bremsstrahlung spectrum.

owing to the limited resolution of the method, these groups are not sharply defined.

The actual excitation function for the reaction is derived from the yield curve by applying corrections for the escape of tracks from the emulsion boundaries and for the shape of the spectrum of bremsstrahlung emitted from the synchrotron target. The Schiff spectrum was used in this work (see Trainor and Brown 1955), and the dosage in roentgens as measured by the Victoreen chamber was used to find the integrated cross sections for the various groups. In Table I the energy limits of the groups and the corresponding cross sections are shown. The total integrated cross section up to 35.5 Mev. is approxi-

TABLE I

ENERGY GROUPS AND INTEGRATED CROSS SECTIONS

Group	Energy range in Mev.	Integrated cross section in Mev-millibarns
A	Up to 25.0	1.0
B	25.0–26.5	0.3
C	26.5–28.0	0.2
D	28.0–30.5	0.5
E	30.5–33.5	0.6
F	33.5–35.5	0.2

mately 2.8 Mev-mb. Our result of 1.5 Mev-mb. is in agreement with the estimate of 1.4 Mev-mb. for the energy range up to 28 Mev. given by the data of Goward and Wilkins (1952*b*).

The variation of the cross section with photon energy is shown in Fig. 1*c* and, although there are considerable errors both in the energy resolution and in the absolute value of the cross section, the function shows marked resonance effects with the maximum cross section occurring near 32.5 Mev. At low energies the dotted line allows for losses of low-energy stars with tracks too short for measurement. The position of group A agrees fairly closely with the peak in the "giant resonance" curve shown by the (γ, n) and (γ, p) reactions in oxygen, but, as will be shown later, this group is probably complex in structure. Group B agrees in position with a peak in the excitation function published by Goward and Wilkins (1952*b*), but the peaks corresponding to groups D and E have not previously been detected. It is interesting to note that the cross section tends to increase over the energy range between 25 and 30 Mev., where the cross sections of the (γ, n) and (γ, p) reactions are believed to decrease rapidly. This effect may be due to some competition between the various reactions, as has been discussed by Goward and Wilkins (1953) in connection with the photodisintegration of C^{12} nuclei.

A notable feature of many stars, especially those belonging to group A, is the occurrence of two alpha-particle tracks of similar length very close together. This happens much more often than a random orientation of the tracks would allow, and it is clear that each pair of tracks arises from the intermediate nucleus Be^8 in its ground state. After allowing for a small number of stars of this kind as arising from chance juxtaposition of tracks, 49 stars were allotted to the "ground-state" category, and these are shown heavily shaded in Fig. 1*b* and also in Fig. 4. This yield curve exhibits a single well-marked peak at 22.3 ± 0.2 Mev., but a small proportion of the stars at all the energies investigated belong to this category.

In any star showing a pair of tracks derived from Be^8 in the ground state it is possible to calculate two values of the excitation energy of C^{12} as an intermediate nucleus. Of these only one in each case can be significant, so the histogram of all calculated C^{12} excitation energies, shown in Fig. 2, should consist of a continuum of non-significant results with superimposed peaks where any level of C^{12} makes an appreciable contribution to the process. The only clear evidence of a peak is at 10.8 ± 0.2 Mev., but examination of the individual

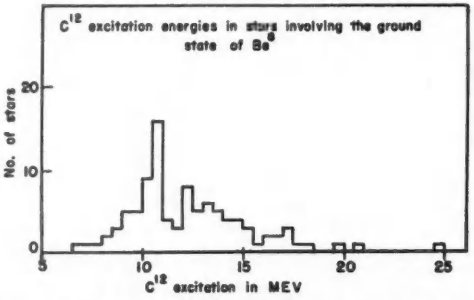

FIG. 2. Histogram of calculated excitation energies of C^{12} as intermediate nuclei in 49 stars involving Be^8 in the ground state. One-half of the values only may be significant.

stars shows that a single level cannot explain all the stars observed, and the known level at 9.6 Mev. in C^{12} (see Ajzenberg and Lauritsen 1955) must be invoked to account for about 30% of them. The present evidence for levels at 9.6 Mev. and 10.8 Mev. agrees with the results of Goward and Wilkins (1952*a*) and those of Livesey and Smith (1953).

The stars not involving the ground state of Be^8 were analyzed to determine if any levels of C^{12} were operative, but here each star yielded four values of the excitation energy, of which only one can be significant. In general it was found

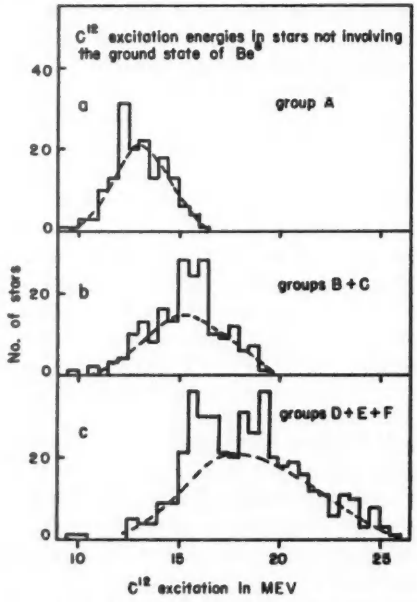

FIG. 3. Histograms of calculated excitation energies of C^{12} in stars not involving Be^8 in the ground state: (*a*) for group A stars; (*b*) for groups B+C; (*c*) for groups D+E+F. One-fourth of the values may be significant.

that the groups B and C behaved similarly, likewise the groups D, E, and F, so in Fig. 3 we show three histograms of C^{12} excitation values, for groups A, B+C, and D+E+F respectively. In the case of group A there is a possible peak at 12.3±0.3 Mev., but this does not rise significantly above the dotted curve estimated for a random orientation of tracks. In groups B+C, however, there is clear evidence of a peak between 15 and 16 Mev., and it is probable that here the well-known $T = 1$ levels of C^{12} at 15.1 and 16.1 Mev. are involved. This is in agreement with the theory of Gell-Mann and Telegdi (1953) and with previous experimental results by Hsiao and Telegdi (1953). The D+E+F histogram also shows evidence of the level at 16 Mev., and a second peak between 18 and 19 Mev. This latter peak is probably due to the levels at 18.3 and 18.9 Mev., which are known to lead to the emission of three alpha-particles (Goward and Wilkins 1953).

The Be^8 excitation energies for different pairs of tracks in all the stars included in Fig. 1*b* have been worked out, and the appropriate histograms are shown in Fig. 4. Here the significant values number only one-sixth of the total

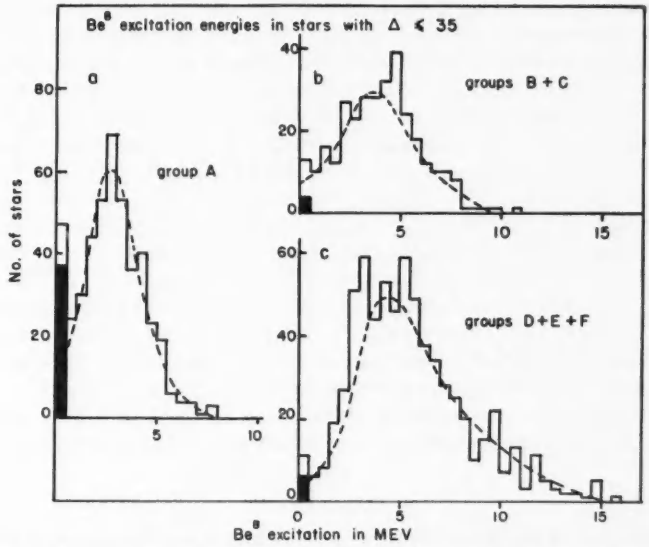

FIG. 4. Histograms of calculated Be^8 excitation values in stars belonging to different energy groups: (*a*) for group A stars; (*b*) for groups B+C; (*c*) for groups D+E+F. One-sixth or one-third of the values may be significant according to the mechanism postulated.

if the reaction proceeds by successive emission of single alpha-particles, and one-third of the total if two Be^8 nuclei are formed from the oxygen nucleus, but no clear evidence of the latter reaction has been obtained and the foregoing evidence on C^{12} levels seems to rule out the possibility except in a small proportion of cases. The diagram for group A stars shows a well-marked peak for the ground state stars, and it is of interest to note that the average ground

state energy relative to two free alpha-particles calculated from these data is 0.09 ± 0.02 Mev., in agreement with more precise determinations quoted by Van Patter and Whaling (1954). There is no evidence of the 3 Mev. level of Be^8 occurring in this group, but it is almost impossible to detect this level in the presence of a large number of non-significant values distributed about a mean close to 2.9 Mev. The behavior of groups B+C is markedly different from that of group A, and it seems to be quite clear that the 3 Mev. level does not occur in these stars. The histogram shows a peak near 5 Mev. which is of particular interest in the light of recent evidence for Be^8 levels in this region. Goward and Wilkins have reported the presence of a 4.1 ± 0.1 Mev. Be^8 level in $C^{12}(\gamma, He^4)Be^{8*}$ stars, and Gibson and Prowse (1955) have published evidence of Be^8 levels at 4.1 and 5.3 Mev. in the $Li^7(d, n)Be^{8*}$ reaction. However, the present data do not give definite information on the point and they do not confirm the suggestion of Livesey and Smith that the supposed level at 4.1 Mev. is responsible for group B stars. Again, in groups D+E+F there is no clear evidence of Be^8 levels except a peak near 3 Mev. which seems to be significant when compared with the trend of the expected random curve in its vicinity.

These results are in good agreement with previous deductions concerning this reaction. Above 28 Mev. the dominant mode of disintegration is via levels in C^{12} at 16.1, 18.3, and 18.9 Mev. leading to the broad 3 Mev. level in Be^8. It is believed that the level at 16.1 Mev. in C^{12} is of the type (2^+, $T = 1$) (Inglis 1953), and this would readily yield that Be^8 level with the emission of an *s*-wave alpha-particle, but one cannot rule out the possibility that some of the levels quoted are of the type 1^-. The stars in group A show evidence of at least three different modes of disintegration and no clear indication of the spin relations has been obtained. The remaining groups B and C show some trace of the $T = 1$ level in C^{12} at 15.1 Mev., and this is believed to be of the type 1^+, in which case transitions to the 2^+ level in Be^8 at 3 Mev. require the emission of a *d*-wave alpha-particle. It is not surprising, therefore, that this mode does not occur very often, but, on the other hand, no other even-parity levels in Be^8 (which alone can give two alpha-particles) are favored. Until the difficult question of the existence of Be^8 levels in the 4 to 5 Mev. region is settled, one cannot draw definite conclusions concerning the stars in groups B and C.

4. CONCLUSIONS

A great deal of this work has been in the nature of a confirmation of previous results with rather more accurate data. We summarize here the salient points emerging from the analysis:

(i) the excitation function of the reaction shows definite peaks at 22.5 and 32.5 Mev. and possible peaks at 26.0, 27.5, 29.5, and 35.2 Mev.;

(ii) a small proportion of stars at all energies proceed via the ground state of Be^8, and the yield of this type of star shows a sharp peak at 22.3 Mev.;

(iii) the stars in group A (below 25 Mev.) may disintegrate via levels in C^{12} at 9.6 and 10.8 Mev., leading to the ground state of Be^8, or by other mechanisms not ascertained;

(iv) the stars in groups B and C (25 to 28 Mev.) disintegrate to some extent via the $T = 1$ levels in C^{12} at 15.1 and 16.1 Mev.;

(v) the high energy stars (28 to 35 Mev.) proceed chiefly via C^{12} levels at 16.1, 18.3, and 18.9 Mev. and the broad 3 Mev. level in Be^8.

ACKNOWLEDGMENTS

We are greatly indebted to Dr. B. W. Sargent for his help and encouragement and to Dr. J. A. Gray who initiated this work at Queen's University. Sincere thanks are due to Dr. C. B. Bigham and Mr. T. J. Rock for making available to us their unpublished results, to Mr. H. Janzen for operating the synchrotron, and to Mrs. E. MacPhail and Mrs. A. Cameron for microscope measurements. Both of us wish to thank the National Research Council for financial assistance. This work was part of the synchrotron program at Queen's University receiving financial support from the Atomic Energy Control Board.

REFERENCES

AJZENBERG, F. and LAURITSEN, T. 1955. Rev. Mod. Phys. **27**: 77.
DAWSON, W. K. and BIGHAM, C. B. 1953. Can. J. Phys. **31**: 167.
GELL-MANN, M. and TELEGDI, V. L. 1953. Phys. Rev. **91**: 169.
GIBSON, W. M. and PROWSE, D. J. 1955. Phil. Mag. **46**: 807.
GOWARD, F. K. and WILKINS, J. J. 1950. Proc. Phys. Soc. (London), A, **63**: 662.
——— 1952*a*. A.E.R.E. Rept. G/M 100, Harwell.
——— 1952*b*. Proc. Phys. Soc. (London), A, **65**: 671.
——— 1953. Proc. Roy. Soc. (London), A, **217**: 375.
——— 1955. Proc. Roy. Soc. (London), A, **228**: 376.
HSIAO, C. A. and TELEGDI, V. L. 1953. Phys. Rev. **90**: 494.
INGLIS, D. R. 1953. Revs. Mod. Phys. **25**: 390.
KATZ, L., HASLAM, R. N. H., HORSLEY, R. J., CAMERON, A. G. W., and MONTALBETTI, R. 1954. Phys. Rev. **95**: 464.
LIVESEY, D. L. and SMITH, C. L. 1952. Proc. Phys. Soc. (London), A, **65**: 758.
——— 1953. Proc. Phys. Soc. (London), A, **66**: 689.
MILLAR, C. H. and CAMERON, A. G. W. 1953. Can. J. Phys. **31**: 723.
SPICER, B. M., PENFOLD, A. S., and GOLDEMBERG, J. 1954. Phys. Rev. **95**: 629.
TRAINOR, L. E. H. and BROWN, S. B. 1955. Can. J. Phys. **33**: 110.
VAN PATTER, D. M. and WHALING, W. 1954. Revs. Mod. Phys. **26**: 402.

THE FAR ULTRAVIOLET ($C-X$) BANDS OF N_2^+ [1]

By P. G. Wilkinson

ABSTRACT

Emission bands of the N_2^+ $C-X$ system in the vacuum ultraviolet have been obtained under high resolution. The rotational analysis confirms the assignment as a $^2\Sigma_u^+ \rightarrow {}^2\Sigma_g^+$ transition and the rotational constants obtained are in substantial agreement with previous investigations. The unusual intensity distribution in the $v' = 3$ progression and perturbations in the $v' = 0$, 1, and 2 levels of the C state are in agreement with the theory of inverse predissociation in the $v' = 3$ level.

A. INTRODUCTION

Three band systems of N_2^+ have been reported, the $C^2\Sigma_u^+ \rightarrow X^2\Sigma_g^+$ system in the vacuum ultraviolet, the $B^2\Sigma_u^+ \rightarrow X^2\Sigma_g^+$ system in the near ultraviolet, and the $A^2\Pi_u \rightarrow X^2\Sigma_g^+$ system, first discovered in auroral emissions in the near infrared. The rotational structure of the ultraviolet bands has been studied by Childs (1932), Coster and Brons (1932), Crawford and Tsai (1935), Parker (1933), and Douglas (1952). Douglas showed that the $B^2\Sigma_u^+$ state has a dissociation energy at 70358 cm^{-1}, which value gives strong support to the 9.756 ev. dissociation energy of nitrogen. The auroral bands were obtained under low resolution by Meinel (1951), and soon after duplicated in the laboratory (Dalby and Douglas 1951; Douglas 1953). Watson and Koontz (1934) made a vibrational analysis of the $C-X$ system which was corrected by Setlow (1948) and Miescher and Baer (1952). Takamine *et al.* (1939) and Tanaka (1953) have made intensity studies of these bands excited under different conditions. The present paper reports a high resolution study of a number of the $C-X$ bands, and several intensity anomalies are discussed.

B. EXPERIMENTAL

The $C-X$ bands were excited in an iron hollow cathode discharge tube operating at 0.2 to 0.6 amp. in a mixture of flowing tank helium and nitrogen (1%) at a pressure of 10 mm. The photographs were taken on a 21-ft. normal incidence vacuum spectrograph (Wilkinson and Mulliken 1955) employing a Bausch and Lomb concave diffraction grating (30,000 lines per inch, 150 mm. by 45 mm.). The plate dispersion was 1.33 Å per mm. in the first order, and under favorable conditions a resolving power of 90,000 was obtained in the 1500Å–2000Å region using Ilford Q2 photographic plates. The exposure times were about one hour. The plates were reduced in the usual way employing FeI and FeII lines as wavelength standards (Green 1939).

C. RESULTS

An enlargement of the 4–10 and 3–9 bands is shown in Fig. 1. The bands possess only P and R branches, which are resolved almost to the head, and the expected intensity alternation (even N strong, odd N weak) is exhibited. The

[1]Manuscript received October 26, 1955.

Contribution from the Laboratory of Molecular Structure and Spectra, Department of Physics, The University of Chicago, Chicago, 37, Illinois, U.S.A.

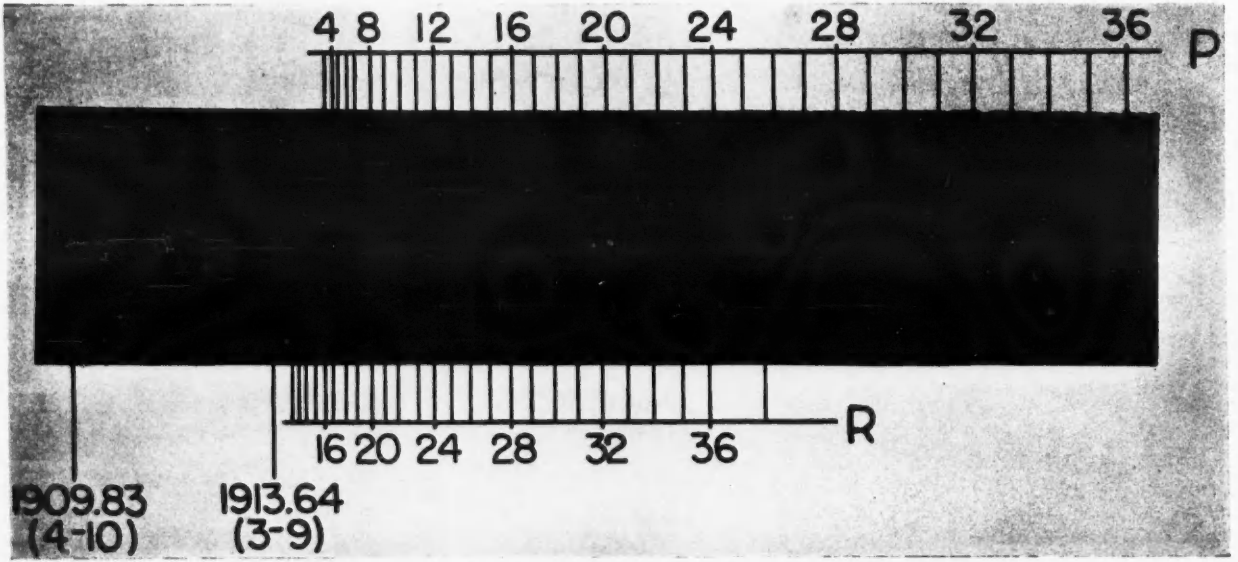

FIG. 1. Enlargement of the 4–10 and 3–9 bands of the N_2^+ $C^2\Sigma_u^+ \rightarrow X^2\Sigma_g^+$ system.

classification of the transition as $^2\Sigma_u^+ \rightarrow {}^2\Sigma_g^+$ (Setlow 1948) is confirmed but no spin fine structure doubling is observed under the resolving power employed. The bands possess exactly the same structure as a $^1\Sigma - {}^1\Sigma$ transition except that the lines are numbered N instead of J (Hund's Case b). The wave numbers of the 3–6, 3–8, 3–9, 3–10, 4–10, and 4–11 bands are given in Table I. The data

TABLE I

WAVE NUMBERS OF THE $C-X$ BANDS

	3–6		3–8		3–9		3–10	
N	$R(N)$	$P(N)$	$R(N)$	$P(N)$	$R(N)$	$P(N)$	$R(N)$	$P(N)$
4					52256.32*	52224.53*	50384.19*	50357.64*
5	58079.02*	58047.00	54162.88*	54125.06*	56.32*	18.64*	84.19*	52.05
6	79.02*	40.60	62.88*	23.83	56.32*	16.62	84.19*	46.03
7	79.02*	33.52	62.88*	18.59*	56.32*	12.10*	84.19*	39.59
8	79.02*	24.36	62.88*	09.86	56.32*	05.12*	84.19*	33.21
9	76.06	17.83	58.92	03.65*	53.92	52197.76*	84.19*	27.94*
10	69.41	06.86	56.60	54095.40*	52.06	89.97*	81.46	18.72
11	65.33	57999.26	53.81	84.98	49.61	82.09*	79.28	10.62
12	61.29	86.41	50.38	75.45	46.71	71.89	76.89	02.19
13	53.20	75.75	46.40	65.39	43.19	62.47	74.16	50293.39
14	50.67	63.92	41.82	55.14	39.10	52.57	70.73	83.95
15	44.64	48.27	36.66	43.95	34.79	42.13	66.95	74.40
16	37.77	38.94	31.21	32.49	29.82	31.28	63.07	63.94
17	30.26	24.34	25.06*	20.36	24.53*	19.95	57.64*	53.30
18	22.21	11.59	18.59*	07.78	18.64*	08.38	52.97	42.09
19	13.66	57896.77	11.38	53994.69	12.10*	52095.73	47.40	30.58
20	04.10	81.56	03.65*	81.34	05.12*	83.09	41.31	18.75
21	57994.21	65.45	54095.40*	66.83	52197.76*	69.64	35.10	06.25
22	83.72	49.21	86.74	52.30	89.97*	55.92	27.94*	50193.39
23	72.19	32.28	77.61	37.14	82.02*	41.64	20.69	80.10
24	60.83	14.63	67.64	21.41	73.25	26.94	13.28	66.35
25	57796.52	57948.27	57.74	05.13	64.11	11.79	04.64	52.19
26	77.42	35.55	46.54	53888.28	54.26	51996.10	50295.99	37.48
27	57.93	22.16	34.13	69.70	43.98	79.91	86.28	22.75
28	38.05	07.97	23.39	53.28	33.38	63.28	77.33	07.13
29	17.16	57892.88	11.11	35.30	22.21	46.35		
30	57696.15	78.07	53998.22	16.30	10.56	28.76		50075.16
31	74.98		84.72	53796.90	52098.34	10.81		
32	51.91		70.97	77.29	85.91	51892.36		
33			58.65	57.05	72.97	73.52		
34			41.36	36.11	59.44	54.20		
35				15.07	44.92	33.94		
36			10.39	53693.03	30.92	13.95		

	4–10		4–11	
N	$R(N)$	$P(N)$	$R(N)$	$P(N)$
1			50518.27*	50509.34*
2		52341.52*	20.41*	05.43*
3		36.95*	22.15*	01.12*
4	52359.09*	31.96	24.49*	50496.48*
5	60.57*	26.57*	24.49*	91.33
6	60.57*	20.63	24.49*	85.75
7	60.57*	16.14	24.49*	79.76
8	60.57*	09.52*	24.49*	73.44
9	59.09*	00.16	24.49*	66.66
10	57.28	52292.45*	22.15*	59.36
11	52.29	86.35*	20.41*	51.78
12	49.17	77.90*	18.27*	43.56
13	45.55	66.32	15.66	35.26
14	41.52*	56.32	12.58	26.36
15	36.95*	46.71	09.34*	16.65
16	33.52	34.79	05.43*	07.14
17	26.57*	24.53	01.12*	50396.88
18	22.54	12.10	50496.48*	86.18
19	14.28	52197.76		
20	09.52*	89.97		
21	02.35	73.25		
22	52292.45*	62.47		
23	86.35*			
24	77.90*	31.28		

*Lines uncertain because of overlapping.

represent an improvement over previous work in that P and R branches are resolved, making possible independent determinations of the rotational

constants in the upper and lower states. A summary of the rotational constants found, along with the band heads and origins, is given in Table II. The con-

TABLE II

ROTATIONAL CONSTANTS AND BAND POSITIONS OBTAINED FROM ANALYSIS OF THE $C-X$ BANDS (BH—band head; ν_0—band origin)

v'	v''	B' (cm^{-1})	$D'.10^6$ (cm^{-1})	B'' (cm^{-1})	$D''.10^6$ (cm^{-1})	ν_0 (cm^{-1})	BH (cm^{-1})
3	6	1.499	4.5	1.805_3	6.16	58070.3_0	58079.0_2
3	8	1.499_0	4.6	1.765_4	6.25	54152.8_2	54162.8_8
3	9	1.499_0	4.6	1.745_6	6.20	52246.2_6	52256.3_2
3	10	1.499_4	4.6	1.724_5	6.2	50373.0_6	50384.1_3
4	10	1.478	4.5	1.724_5	6.2	52350.1_8	52360.5_7
4	11					50512.9	50524.8
4	9					54222.4*	54232.0
5	10					54294.8*	54305.1
5	11					52459.5*	52470.6

*Band origin computed from band head position and rotational constants.

stants B and D were computed from the combination relations, $\Delta_2F'(N) = R(N)-P(N)$ and $\Delta_2F''(N) = R(N-1)-P(N+1)$ (Herzberg 1950). The rotational constants obtained for the $X^2\Sigma_g^+$ ground state are consistent with the data of Crawford and Tsai (1935) and Douglas (1952). Since the usual B_v versus v plot is nonlinear in this case, it is necessary to introduce a $(v+\frac{1}{2})^2$ term in order to fit the data properly. The resulting equation, $B_v = 1.925_8-0.0174_3(v+\frac{1}{2})-0.00016_4(v+\frac{1}{2})^2$, fits the present data within ±0.0005 cm^{-1} and previous work within ±0.002 cm^{-1}. The value of B_e (1.926 cm^{-1}) is smaller than previously given (Douglas 1952), and the corresponding value of r_e (1.118 Å) is somewhat higher. The combined data of Crawford and Tsai (1935), Douglas (1952), and the present work are given in Fig. 2. The only rotational constants for the upper state previously available are those of Setlow (1948): $B_3' = 1.493$ and $B_4' = 1.480$ cm^{-1}, which compare with 1.499 and 1.478 obtained in the present work.

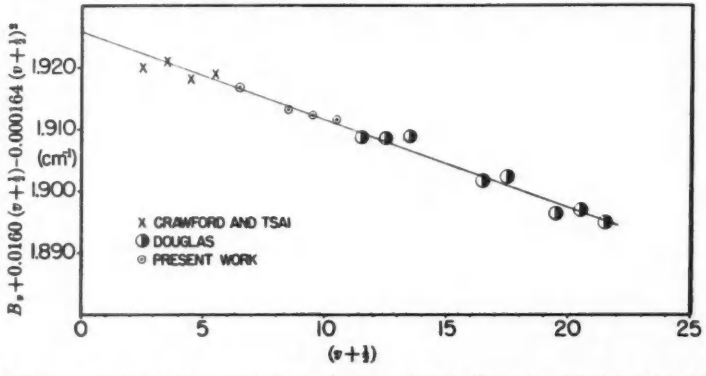

FIG. 2. B_v graph for the ground electronic state of N_2^+. The value $0.0160(v+\frac{1}{2})-0.000164\times(v+\frac{1}{2})^2$ has been added to B_v in order to allow a large-scale linear plot.

D. DISCUSSION OF RESULTS

Vibrational perturbations are observed in the $v' = 0$, 1, and 2 levels of the $C^2\Sigma_u^+$ state as may be seen in Fig. 3. Tanaka's (1953) band head data were used

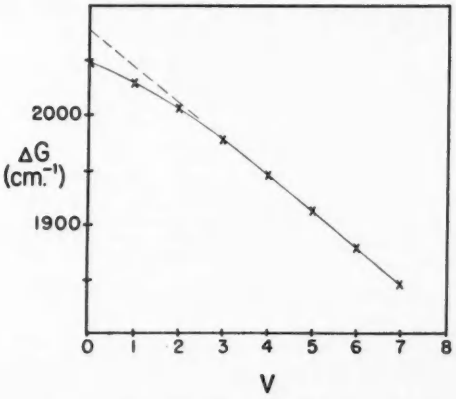

FIG. 3. ΔG curve for the $C^2\Sigma_u^+$ state of N_2^+. The curve was constructed from the data of Tanaka (1953). None of the points should be in error by more than a few cm^{-1}.

to construct the $\Delta G_{v+\frac{1}{2}}$ versus v plot in the figure. Although the use of band heads undoubtedly introduces an error, this is only about 2.5 cm^{-1},[2] whereas the $\Delta G_{v+\frac{1}{2}}$ curve in Fig. 3 deviates 33 cm^{-1} at $v' = 0$, 16 cm^{-1} at $v' = 1$, and 7 cm^{-1} at $v' = 2$ from a linear relationship. Douglas (1952) has considered that the unusual shape of the $\Delta G_{v+\frac{1}{2}}$ versus v curve in the $B^2\Sigma_u^+$ state is caused by interaction with the first three vibrational levels of $C^2\Sigma_u^+$ and predicts that B_0, B_1, and B_2 will be anomalously large in $C^2\Sigma_u^+$. Setlow (1948) reported $B_0 = 1.62$ cm^{-1}, which is unusually large, but this value must be considered uncertain since it was obtained by analysis of several only partially resolved bands (0–5, 0–6).

There are a number of peculiarities in the observed intensity distribution of the $C-X$ bands which depend on the excitation conditions. Transitions from $v' = 3$ and 4 are by far the strongest especially in helium–nitrogen mixtures. This was explained by Watson and Koontz (1934) as resonance excitation by He^+ ^2S since the ionization potential of helium (24.580 ev.) nearly coincides with the energy of the $v' = 3$ level of the $C^2\ \Sigma_u^+$ state (24.330 ev. above $v = 0$ of N_2 $X^1\Sigma_g^+$). The intensity distribution in the various bands as given by Tanaka (1953) is shown in Table III (top) and as found under the present conditions (bottom). In this work the excitation of the $v' = 3$ and 4 progressions was by far the strongest and the 3–9 band was the strongest in the system; in addition, these progressions appeared only in the pressure range 10–20 mm. Above 20 mm. the bands were very weak or absent. If the mechanism involves resonance excitation by He^+ (24.580 ev.) then the

[2]This error was estimated using reasonable rotational constants obtained from Setlow (1948), Douglas (1952), and this research.

TABLE III

INTENSITIES IN THE $C-X$ BANDS. DATA GIVEN BY TANAKA[a] ARE AT THE TOP AND DATA FOUND IN THE PRESENT WORK ARE AT THE BOTTOM[b]

v' \ v''	0	1	2	3	4	5	6	7	8	9	10	11	12	13	14	15
0						0	0									
1							0	0	0							
2								0	0	0						
3	3	3	2	5	4	3	6		6	6	7	3				
4	2		3	2	5	5			0	3	5	6	2			
5										0	0	4	5	1		
6											0		3	3	0	
7														0	1	0
8															0	0
3							4		6	10	6					
4										1	6	5				
5											0	0				

[a]Y. Tanaka (1953). The 0–5, 0–6, 1–6, 1–7, 1–8, 2–7, 2–8, and 2–9 bands were obtained in disruptive discharge of nitrogen and nitric oxide. All other bands were obtained in nitrogen and helium mixtures.

[b]Intensities obtained in hollow cathode discharge through He – 1% N_2.

$v' = 4$ level (24.575 ev.) should be preferentially excited rather than the $v' = 3$ level (24.330 ev.) (Tanaka 1953). Douglas has suggested (1952) that the excitation mechanism may be a case of inverse predissociation. This is supported by the observations that the dissociation energy of the $B^2\Sigma_u^+$ state is 70358 cm^{-1} (above $v = 0$ of N_2^+ $X^2\Sigma_g^+$),[3] which is 269 cm^{-1} below the energy of the $v = 3$ level of $C^2\Sigma_u^+$, and that under certain discharge conditions (see above) band progressions with $v' = 3$ and 4 do not appear. The existence of vibrational perturbations in the $v' = 0$, 1, and 2 levels as well as the appearance of strong NI and NII lines in the spectra also lends support to this theory (Tanaka 1953). It is reasonable to suppose that both processes (resonance excitation by He^+ and inverse predissociation) may be operating in tubes containing helium. Predissociation in the $v' = 3$ level is consistent with either the 7.373 or the 9.756 ev. dissociation energy of nitrogen although a potential hill of 0.029 ev. must be involved in either process.

Although the perturbations in the $C^2\Sigma_u^+$ state are undoubtedly real, and it seems possible there could be interaction with $B^2\Sigma_u^+$ (Douglas 1952), it appears that the perturbations and predissociation in $C^2\Sigma_u^+$ could also be understood from an interaction with a slightly attractive state with its asymptote at approximately 70600 cm^{-1} (8.75 ev.). If the 9.756 ev. dissociation energy of nitrogen is assumed (corresponding to 8.721 ev. for the dissociation energy of N_2^+), then the products of the predissociation of N_2^+ at 8.75 ev. must be $N^+(^3P) + N(^4S)$. Consideration of selection rules gives the result that possible predissociating states are $^2\Sigma_u^+$, $^4\Sigma_u^+$, $^6\Sigma_u^+$, $^2\Pi_u$, $^4\Pi_u$, and $^6\Pi_u$.

If the Franck–Condon principle is employed to predict relative band intensities (Setlow 1948) one can see immediately that $3 \rightarrow 9$ is the most probable transition and that $3 \rightarrow 8$ and $3 \rightarrow 10$ should be weaker and about equal in intensity in agreement with experiment (Table III). One would also

[3]A small discrepancy exists between the experimental dissociation energy of N_2^+ as derived from the $B-X$ bands (Douglas 1952) and that derived from the dissociation energy of nitrogen (Douglas and Herzberg 1951) and the ionization potentials of the nitrogen atom and the nitrogen molecule. The latter gives 70396 cm^{-1} and must be considered the more reliable.

predict the $3 \rightarrow 7$ and $3 \rightarrow 6$ transitions with decreasing intensities. In actual fact the $3 \rightarrow 7$ band was not observed in the present work and the $3 \rightarrow 6$ band appears nearly as strong as the $3 \rightarrow 8$.[4]

I wish to thank Professor R. S. Mulliken of the University of Chicago and Dr. Y. Tanaka of the Air Force Cambridge Research Center, for many helpful discussions. This research was assisted in part by the Geophysics Research Directorate of the Air Force Cambridge Research Center, Air Research and Development Command, under Contract No. AF19(604)-1019 with the University of Chicago.

REFERENCES

CHILDS, W. H. J. 1932. Proc. Roy. Soc. (London), A, **137**: 641.
COSTER, D. and BRONS, H. H. 1932. Z. Physik, **73**: 747.
CRAWFORD, F. H. and TSAI, P. M. 1935. Proc. Am. Acad. Arts Sci. **69**: 407.
DALBY, F. W. and DOUGLAS, A. E. 1951. Phys. Rev. **84**: 843.
DOUGLAS, A. E. 1952. Can. J. Phys. **30**: 302.
——— 1953. Astrophys. J. **117**: 380.
DOUGLAS, A. E. and HERZBERG, G. 1951. Can. J. Phys. **29**: 294.
GREEN, L. C. 1939. Phys. Rev. **55**: 1209.
Herzberg, G. 1950. Spectra of diatomic molecules. D. Van Nostrand Company, Inc., New York.
MEINEL, A. B. 1951. Astrophys. J. **114**: 431.
MIESCHER, R. and BAER, P. 1952. Nature, **169**: 581.
PARKER, A. E. 1933. Phys. Rev. **44**: 90, 914.
SETLOW, R. B. 1948. Phys. Rev. **74**: 153.
TAKAMINE, T., SUGA, T., and TANAKA, Y. 1939. Sci. Papers Inst. Phys. Chem. Research (Tokyo), **36**: 437.
TANAKA, Y. 1953. J. Chem. Phys. **21**: 1402.
WATSON, W. W. and KOONTZ, P. G. 1934. Phys. Rev. **46**: 32.
WILKINSON, P. G. and MULLIKEN, R. S. 1955. J. Chem. Phys. **23**: 1895.

[4]Setlow (1948) considered that the 3–6 band had an anomalously high intensity and offered the explanation that it really was the 2–5 band. This must be rejected since in the present experiments the upper and lower state rotational constants (Table II) are exactly correct if the 3–6 identification is assumed.

HIGH-ENERGY FORBIDDEN β-RAY TRANSITIONS FROM Cs^{134} (2.3 yr.), Co^{60} (5.3 yr.), Sc^{46} (84 d.), and Hg^{203} (47.9 d.)[1]

By J. L. Wolfson[2]

ABSTRACT

Beta-ray transitions of energies 1478±6 kev. from Co^{60} (5.3 yr.) and 1475±6 kev. from Sc^{46} (84 d.) were observed with intensities of $(1.0\pm0.2)\times10^{-4}$ and $(3.6\pm0.7)\times10^{-6}$ β-rays per disintegration respectively. Forbidden spectrum shapes were obtained for both transitions. No evidence was obtained for the β-ray transition of energy 1451 kev. from Cs^{134} (2.3 yr.), nor for the transition of energy 473 kev. from Hg^{203} (47.9 d.), and upper limits of 5×10^{-6} and 3×10^{-4} β-rays per disintegration respectively are placed upon the intensities of these transitions. The log f_0t values are >14.5, 14.0±0.1, 13.0±0.1, and >11.3 for the transitions referred to from Cs^{134}, Co^{60}, Sc^{46}, and Hg^{203} respectively.

1. INTRODUCTION

The magnitude of the matrix elements operative in beta decay is expressed in terms of the *ft* value (or log *ft*), the quantity *ft* being proportional to the inverse square of the nuclear matrix element. The *ft* values are known for a large number of β-ray transitions (Goeppert-Mayer 1955), but the vast majority are for allowed and first-forbidden transitions. In particular, only a relatively small number are known for forbidden transitions of the second order, partly because of the scarcity of simple spectra of high orders of forbiddenness, and partly because, among the more complex modes of disintegration, the transitions of higher orders of forbiddenness must compete with the much more probable allowed or first-forbidden transitions, and their experimental observation becomes difficult. Nevertheless, since these forbidden transitions have higher energies than those transitions of lower orders of forbiddenness with which they compete, it is possible to observe at least the higher energy portion of their spectra, and thence deduce their intensities. In the present work this has been attempted with the β-ray transitions proceeding from the decay of Cs^{134} (2.3 yr.), Co^{60} (5.3 yr.), Sc^{46} (84 d.), and Hg^{203} (47.9 d.). The transitions sought from the decay of the first three nuclides are expected to be second forbidden, whereas that from the decay of Hg^{203} is expected to be first forbidden.

In all of the transitions studied it was of importance to correct for or to avoid the detection of conversion or secondary electrons from the relatively high energy and high intensity gamma-ray transitions in the daughter nuclei. The second of these alternatives was chosen by restricting the region studied to that portion of the β-ray spectrum of energy greater than that of the most energetic γ-ray emitted from the source. While this procedure rendered the detection of the weak β-ray transitions rather difficult, it did possess the virtue of yielding unambiguous results.

[1]Manuscript received November 4, 1955.
Contribution from Physics Division, Atomic Energy of Canada Limited, Chalk River Laboratory, Chalk River, Ontario. Issued as A.E.C.L. No. 281.
[2]Present address: Jewish General Hospital, Montreal, Quebec.

A report of the results obtained in these studies was presented at a meeting of the Canadian Association of Physicists at London, Ontario, in May, 1953.

2. APPARATUS AND METHOD

The method employed in each of these studies, as indicated in Section 1, involved a detailed examination of the spectrum sought at energies in excess of the most energetic γ-ray emitted by the daughter nucleus. A double-lens magnetic spectrometer was used, adjusted for a line width of about 0.9% in momentum at half-maximum intensity. The transmission of the spectrometer was about 0.4% of 4π steradians. The low level of the background counting rate achieved by the spectrometer, as discussed elsewhere (Elliott *et al.* 1954), constitutes a most valuable feature of the instrument. The background was further reduced in these investigations by employing pulse height selection, using a single-channel pulse height analyzer. In the studies with Cs^{134}, Co^{60}, and Sc^{46}, a NaI(Tl) crystal, sufficiently thick to stop all electrons whose energies lay in the range of interest, was used as detector. For examination of the spectrum from decay of Hg^{203}, the NaI crystal was replaced by an anthracene crystal 1 mm. thick.

The sources were all prepared by neutron irradiation in the NRX reactor. Since only those regions of the spectra near their end-points were examined, the thickness of the sources was not as important a consideration as it usually is in studies of spectrum shapes. Nevertheless, considerable effort was made to obtain the highest possible specific activities, as well as uniform deposition of the source material. In general the sources were prepared by evaporation of salts from nitric acid solution on backings of 2.3 mgm./cm.^{2} aluminum foil. The sources were all approximately 2 mm. in diameter.

The intensity of a transition whose spectrum was detected was found by extrapolation of the spectrum to zero energy, followed by comparison of the area underneath the spectrum with that of the K internal conversion line of the most energetic γ-ray transition. The intensity of the β-ray transition was then deduced from the known K conversion coefficient and the quantum intensity. This method has the advantage of minimizing the effects of source thickness, since all electrons observed are of high energy.

3. RESULTS

Cs^{134} (2.3 yr.)

The source was about 9 mgm./cm.^{2} thick and about 0.75 mc. in activity. The results of an examination of the spectrum above 1300 kev. are shown in Fig. 1. The arrow in the right-hand figure at about 6320 gauss-cm. indicates the end-point expected for the 1451 kev. beta spectrum. There is no evidence for this spectrum. If the disintegration scheme of Keister, Lee, and Schmidt (1955) is correct, an upper limit of 5×10^{-5} β-rays per disintegration can be placed on the intensity of this transition. The corresponding log f_0t value is >14.5. These figures are based on Keister, Lee, and Schmidt's (1955) values for the intensity of the 1367 kev. γ-ray transition and its K conversion coefficient.

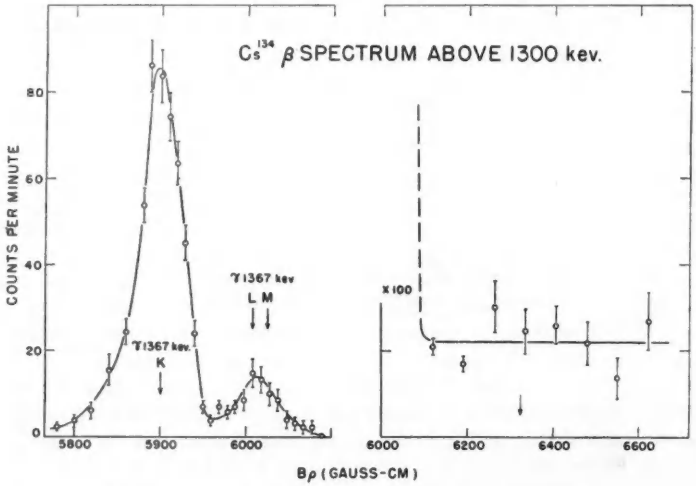

FIG. 1. The β-ray spectrum of Cs^{134} (2.3 yr.) above 1300 kev. The K, L, and M internal conversion lines of the 1367 kev. γ-ray transition in Ba^{134} are shown on the left. The counting rates at energies greater than 1367 kev. are shown on the right. The arrow indicates the end-point of the expected 1451 kev. β-ray spectrum. There is no evidence for the existence of this spectrum. The vertical bars through the experimental points indicate the standard deviations.

Co^{60} (5.3 yr.)

The source was about 9 mgm./cm.^{2} thick and approximately 1 mc. in activity. The results of an examination of the beta spectrum above 1270 kev. are shown in Fig. 2. A forbidden Fermi plot, using the shape factor C_{2T} (Greuling 1942) corresponding to a spin change of three without parity change (Section 4), is shown in the inset. The extrapolated end-point of the plot is 1478 ± 6 kev. in satisfactory agreement with the expected end-point of 1481 ± 3 kev. Further, the straight-line shape of the plot is consistent with a spin change of three without parity change for the transition.* The intensity of the transition is $(1.0\pm0.2)\times10^{-4}$ β-rays per disintegration. This value is based on a total conversion coefficient of 1.32×10^{-4} for the 1332 kev. γ-ray transition, as required for $E2$ radiation. Using the curves of Moszkowski (1951) and Davidson (1951), the corresponding log f_0t and log f_2t values are 14.0 ± 0.1 and 13.6 ± 0.1 respectively.

Sc^{46} (84 d.)

The source was about 6 mgm./cm.^{2} thick and about 2.7 mc. in activity. The results of the examination of the beta spectrum above 1050 kev. are shown in Fig. 3. An allowed Fermi plot of the data is shown in the inset. The plot is somewhat concave toward the energy axis, and has an extrapolated

*While the data found here are not sufficiently extensive to rule out the possibility of a $\Delta I = 2$ transition, the evidence is overwhelmingly in favor of the $\Delta I = 3$ transition (Section 4), and the corresponding shape factor has been used in finding the intensity of the transition.

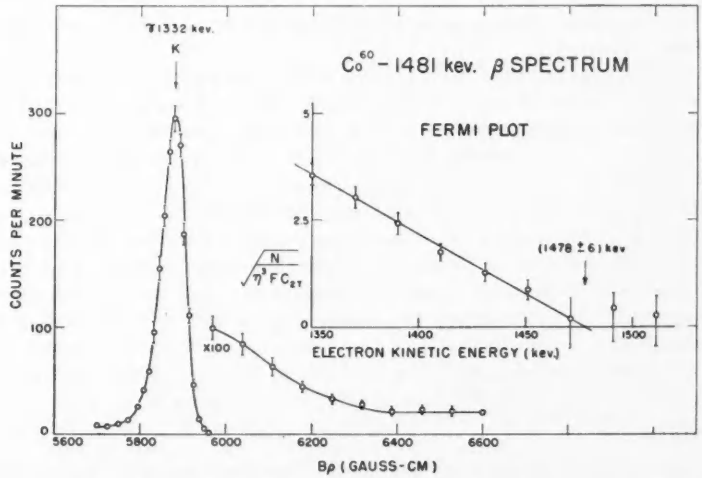

FIG. 2. The 1481 kev. β-ray spectrum of Co^{60} (5.3 yr.). The K internal conversion line of the 1332 kev. γ-ray transition in Ni^{60} is shown on the left. The L and M internal conversion lines are not resolved from the K line. The inset shows a forbidden Fermi plot of the data obtained at energies greater than 1350 kev., using the shape factor C_{2T} applicable to a $\Delta I = 3$ (no) transition. The vertical bars indicate the standard deviations. For the point at 6600 gauss-cm. the standard deviation is less than the radius of the circle describing the point.

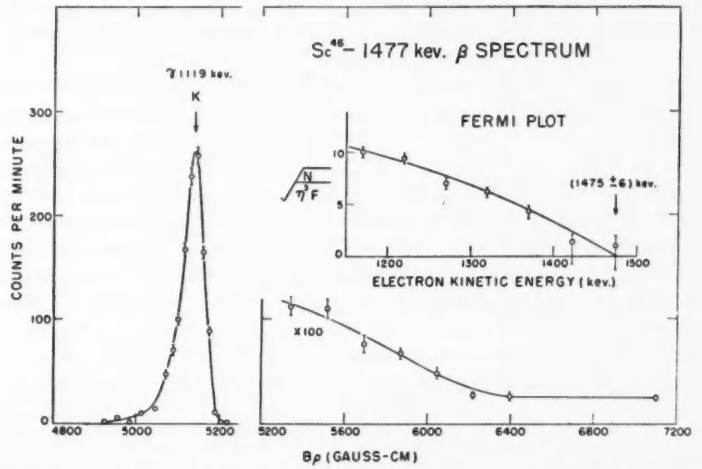

FIG. 3. The 1477 kev. β-ray spectrum of Sc^{46} (84 d.). The K internal conversion line of the 1119 kev. γ-ray transition in Ti^{46} is shown on the left. The L and M internal conversion lines are not resolved from the K line. The inset shows an allowed Fermi plot of the data obtained at energies greater than 1150 kev. The vertical bars indicate the standard deviations.

end-point of 1475±6 kev. in agreement with the expected end-point of 1477±8 kev. (provided that the 2+ state in Ti^{46} is at 890 kev.). This finding will be discussed in Section 4.

Since it is expected that the spectrum is characterized by a spin change of two without parity change (Section 4), the shape of the spectrum is not expected to be unique. Inasmuch as only a very small portion of the spectrum has been observed, no attempt has been made to derive the shape factor C_{2T} which will fit the experimental points. The shape factor S_2^2 ($[p^2+0.6q^2]$, as for Cl^{36} (Wu 1955)) has been found to give a satisfactory fit,* but this is not of great significance since any factor involving the square of the momentum will have much the same effect for the restricted high-energy portion of the spectrum observed. When the S_2^2 factor is applied for the purpose of extrapolating the spectrum to zero energy, an intensity of $(3.6\pm0.7)\times10^{-5}$ β-rays per disintegration is found for the 1477 kev. transition. This value is based on a total conversion coefficient of 9.86×10^{-5} for the 1119 kev. γ-ray transition as required for $E2$ radiation. The corresponding $\log f_0 t$ value is 13.0±0.1.

Hg^{203} (47.9 d.)

In the attempt to detect a 473 kev. β-ray transition from Hg^{203}, Hg enriched to 95% in the isotope Hg^{202} was used in the irradiation in order to obtain the highest possible specific activity. The low energy of the β-rays, as compared with those from Co^{60} and Sc^{46}, makes the source thickness of greater importance in this case. The source was about 6 mgm./cm.^{2} thick and approximately 0.5 mc. in activity.

The results of the study are given in Fig. 4. Two runs taken 113 days apart are shown. It is immediately evident that the spectrum above 310 kev. decays at a rate much slower than that corresponding to the K internal conversion line of the 278.3 kev. γ-ray transition. Eight very weak K internal conversion lines (not shown in the figure) have been observed in the spectrum. These have been identified with those resulting from the decay of 270 d. Ag^{110}. Corresponding to two of these K lines, two L conversion lines have been observed, the $K-L$ difference in each case being in excellent agreement with the $K-L$ difference in Cd. Two β-ray transitions of energies 520 kev. and 2.9 Mev. occur in the decay of 270 d. Ag^{110}, of which the former is intense and the latter weak. The β-ray spectrum shown in Fig. 4 is consistent with the assumption that it results from the decay of 270 d. Ag^{110}. The major part of the spectrum ends at about 520 kev. (shown by the arrow in Fig. 4), while the portion above 520 kev. can be accounted for by the weak 2.9 Mev. component. The curious hump in the region of 520 kev. is probably caused by the conversion lines in that vicinity.

The decay of the spectrum is also consistent with a half-life of 270 days.

*$S_2^2 \backsim p^2+\lambda q^2$ for the five known twice-forbidden non-unique spectra, where $\lambda = 0.6$ for the Cl^{36} spectrum, $\backsim 2$ for the Tc^{99} spectrum, and >10 for the Cs^{135}, Cs^{137}, and I^{129} spectra (Wu 1955). A good experimental value for λ can clearly only be found if the low-energy portion of the spectrum is available for study. The arbitrary choice of $\lambda = 0.6$ for the 1475 kev. spectrum is justified only by the necessity of making some choice, and Sc^{46} is similar to Cl^{36} in that both are low Z odd–odd nuclei. If $\lambda > 0.6$ the intensity of the 1475 kev. transition will have been underestimated, by about 20% if $\lambda = 1$, and almost a factor of 2 if $\lambda = 2$.

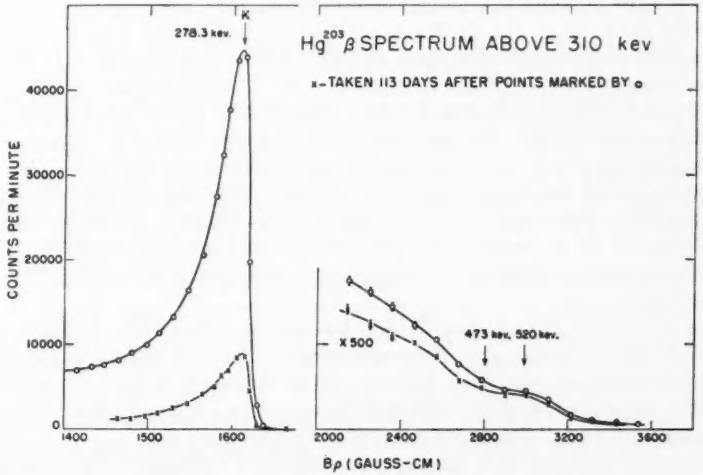

FIG. 4. The β-ray spectrum of Hg^{203} (47.9 d.) above 310 kev. Two runs taken 113 days apart are shown. The K internal conversion line of the 278.3 kev. γ-ray transition in Tl^{203} is shown on the left. The β-ray spectrum is shown on the right. The expected end-point of the 473 kev. β-ray spectrum of Hg^{203} is marked by an arrow. The spectrum observed is due to 270 d. Ag^{110} which occurs as a contaminant in the source. The arrow at 520 kev. indicates the end-point of the 520 kev. β-ray component of Ag^{110} (270 d.). The vertical bars shown indicate the standard deviations. Where no bars are shown the standard deviations are about the same as, or less than, the magnitudes of the symbols marking the experimental points.

About 10% of the spectrum can however be assigned to a component of half-life longer than 270 days without being inconsistent with the experimental data, but there is no evidence for a component with a half-life as short as 47.9 days.

From the above it appears certain that the spectrum observed is due largely if not entirely to 270 d. Ag^{110} contained as an impurity in the sample material.

From the results shown in Fig. 4 an upper limit of 3×10^{-4} β-rays per disintegration can be placed on the occurrence of the 473 kev. β-ray transition. This figure is based upon a K conversion coefficient of 0.13 ± 0.01, and $K/(L+M) = 2.75$, as measured by the author. The $\log f_0 t$ value corresponding to this limit is 11.3. If the transition is of the $\Delta I = 2$ (yes) type (Section 4), then, using the curves of Davidson (1951), a value of >10.2 is obtained for $\log f_1 t$.

A summary of the results of these investigations is given in Table I.

TABLE I

Nucleus	Energy of β-ray transition (kev.)	Intensity of β-ray transition	$\log f_0 t$
Cs^{134} (2.3 yr.)	1451	$<5\times10^{-6}$	>14.5
Co^{60} (5.3 yr.)	1478	$(1.0\pm0.2)\times10^{-4}$	14.0 ± 0.1*
Sc^{46} (84 d.)	1475	$(3.6\pm0.7)\times10^{-6}$	13.0 ± 0.1
Hg^{203} (47.9 d.)	473	$<3\times10^{-4}$	>11.3†

*$\log f_1 t = 13.6\pm0.1$.
†$\log f_1 t > 10.2$, if spectrum is of $\Delta I = 2$ (yes) type.

4. DISCUSSION

Cs^{134} (2.3 yr.)

The transition sought in the decay of 2.3 yr. Cs^{134} is that proceeding from the ground state of Cs^{134} to the 605 kev. state in Ba^{134} with an energy of 1451 kev. A 2+ state in Ba^{134} at 605 kev. has been proposed by both Cork *et al.* (1953) and Keister *et al.* (1955). Further, Klema (1955) has just reported that experiments conducted at Oak Ridge are in agreement with the disintegration scheme proposed by Keister *et al.* However the possibility remains that the 2+ state in Ba^{134} is of energy 797 kev. rather than 605 kev., in which case the transition sought, of energy 1259 kev., would not have been detected, since examination of the spectrum was restricted to energies greater than that of the 1367 kev. γ-ray.

The spin of the ground state of Cs^{134} has been determined by Bellamy and Smith (1953) to be four, and from shell structure considerations its parity is expected to be even. The β-ray transition to the 2+ state in Ba^{134} is therefore expected to be characterized by a spin change of two without parity change; i.e. it is a transition of the second order of forbiddenness.

From what has been said, the upper limit of 5×10^{-5} β-rays per disintegration for the 1451 kev. transition is significant only if a 2+ state in Ba^{134} exists at 605 kev. However, data shown in Fig. 1 are otherwise useful in demonstrating the extremely low level of scattering within the spectrometer. The counting rate at energies just greater than that of the γ-rays shows no contribution whatsoever from conversion electrons scattered into the detector. This observation supplements previous findings (Elliott *et al.* 1954) of the excellent performance of the spectrometer with respect to background levels in general.

Co^{60} (5.3 yr.)

The transition sought in the decay of Co^{60} (5.3 yr.) proceeds from the ground state of Co^{60} to the 1332 kev. level in Ni^{60}. The energy of the intense transition to the 2504 kev. level in Ni^{60} has recently been measured by Bolla *et al.* (1954), who obtain a value of 309 ± 3 kev., whence the transition to the state in Ni^{60} at 1332 kev. has an energy of 1481 ± 3 kev. From shell structure, the parity of the ground state of Co^{60} is expected to be even. An assignment of spin five to this state is consistent with most experimental evidence (Goldhaber and Hill 1952). An assignment of 2+ to the 1332 kev. level in Ni^{60} is in accord with all experimental evidence (Goldhaber and Hill 1952). The 1481 kev. β-ray transition is therefore expected to be characterized by a spin change of three without change of parity. The spectrum shape will accordingly be unique (Wu 1955).

Keister and Schmidt (1954) have recently reported observing this spectrum with an intensity of 0.15% of the total number of disintegrations. The shape of the spectrum obtained by them does not however correspond to a spin change of three, but rather to a spin change of two. To account for this they propose a disintegration scheme for Co^{60} in which the ground state of Co^{60} is assigned a spin of four and the 10.7 min. state of Co^{60} a spin of one, both with even parity. This latter proposal is not in accord with the failure of

Deutsch and Scharff-Goldhaber (1951) to observe a β-ray transition from the 10.7 min. level in Co^{60} to the ground state of Ni^{60}.

The results obtained in this investigation differ from those reported by Keister and Schmidt (1954). The intensity of the transition found by these workers, 0.15% of the disintegrations, is more than an order of magnitude greater than that found in this study. Further, over the restricted range of the spectrum here studied, the shape of the spectrum has been found to be consistent with a $\Delta I = 3$ (no) transition, in agreement with the requirements of all other experimental results (Deutsch and Scharff-Goldhaber 1951; Goldhaber and Hill 1952).

The spectrum of the secondary electrons does not affect the results obtained in the present work since measurements were taken only at energies greater than those of all γ-rays emitted by the source. This however does not hold for the investigations of Keister and Schmidt (1954), who extended their observations to much lower energies, and it is possible that their spectrum shape and deduced intensity may be accounted for by insufficient correction for the intensity of the secondary electron component in their measured spectrum.

Sc^{46} (84 d.)

An assignment of 4+ is probable for the ground state of Sc^{46} and an assignment of 2+ for the first excited state in Ti^{46} (Goldhaber and Hill 1952). The high-energy β-ray spectrum is therefore expected to be characterized by a spin change of two without parity change, and accordingly will be second forbidden (Wu 1955).

Keister and Schmidt (1954) and Whalen *et al.* (1953) have reported the detection of a β-ray component of energy about 1.25 Mev. with an intensity of 0.1% according to the former, and $<0.1\%$ according to the latter.

The results obtained here differ from those obtained by Keister and Schmidt (1954) as to both intensity and energy. The intensity of the high-energy β-ray component as found by Keister and Schmidt is about 30 times greater than that reported here. The energy of the transition given by them, viz. 1.25 Mev., requires that the 2+ state in Ti^{46} be at 1.12 Mev., whereas the energy of the transition found here, 1475 kev., requires the 2+ state to be at 890 kev. In this connection, Heydenburg and Temmer (1955) have recently reported a value of 890 kev. for this state in Ti^{46}, as found in Coulomb excitation experiments. The remarks made above regarding Keister and Schmidt's results for the high-energy spectrum detected by them in the decay of Co^{60} (5.3 yr.) apply also to their results in the present case.

Hg^{203} (47.9 d.)

The transition sought in the decay of 47.9 d. Hg^{203} proceeds from the ground state of Hg^{203} to the ground state of Tl^{203}. The main transition is from the ground state of Hg^{203}, via a 195 ± 2 kev. β-ray transition, to a 278.3 ± 0.5 kev. state in Tl^{203}. Both of these measurements have been made by the author. The energy of the high-energy β-ray transition is therefore 473.3 kev. From shell structure considerations the odd neutron in Hg^{203} is in either a $p_{3/2}$

or an $f_{5/2}$ state. The parity of the state is therefore expected to be odd. The parity of the ground state of Tl^{203}, from shell structure, is even, and the spin of the state has been measured to be 1/2 (Jackson 1932). The β-ray transition to the ground state of Tl^{203} is therefore expected to involve a change of parity, and possibly a spin change of two. In this case the spectrum has a unique shape (Wu 1955). Wapstra *et al.* (1954) have recently reported an upper limit of 1.5% for the occurrence of this transition.

The lower limit of 10.2 obtained here for log f_1t of the transition, while somewhat high, is nevertheless not inconsistent with a $\Delta I = 2$ (yes) transition. The presence of the 270 d. Ag^{110} contaminant unfortunately rendered the experiment less sensitive than it would otherwise have been.

ACKNOWLEDGMENT

The author wishes to acknowledge the provision, by the U.S. Atomic Energy Commission, of the Hg enriched in the isotope Hg^{202} used in the experiments. It is a pleasure also to acknowledge the advice and criticism rendered to the author by Dr. L. G. Elliott.

REFERENCES

BELLAMY, E. H. and SMITH, K. F. 1953. Phil. Mag. **44**: 33.
BOLLA, G., TERRANI, S., and ZAPPA, L. 1954. Nuovo cimento, **12**: 875.
CORK, J. M., LE BLANC, J. M., NESTER, W. H., MARTIN, D. W., and BRICE, M. K. 1953. Phys. Rev. **90**: 444.
DAVIDSON, J. P., JR. 1951. Phys. Rev. **83**: 48.
DEUTSCH, M. and SCHARFF-GOLDHABER, G. 1951. Phys. Rev. **83**: 1059.
ELLIOTT, L. G., PRESTON, M. A., and WOLFSON, J. L. 1954. Can. J. Phys. **32**: 153.
GOEPPERT-MAYER, M. 1955. Beta- and gamma-ray spectroscopy. *Edited by* K. Siegbahn. North-Holland Pub. Co., Amsterdam. p. 433.
GOLDHABER, M. and HILL, R. D. 1952. Revs. Mod. Phys. **24**: 179.
GREULING, E. 1942. Phys. Rev. **61**: 568.
HEYDENBERG, N. P. and TEMMER, G. M. 1955. Phys. Rev. **99**: 617.
JACKSON, D. A. 1932. Z. Physik, **75**: 223.
KEISTER, G. L., LEE, E. B., and SCHMIDT, F. H. 1955. Phys. Rev. **97**: 451.
KEISTER, G. L. and SCHMIDT, F. H. 1954. Phys. Rev. **93**: 140.
KLEMA, E. D. 1955. Phys. Rev. **100**: 66.
MOSZKOWSKI, S. A. 1951. Phys. Rev. **82**: 35.
WAPSTRA, A. H., MAEDER, D., NIJGH, G. J., and ORNSTEIN, L. TH. M. 1954. Physica, **20**: 169.
WHALEN, J. A., PORTER, F. T, and COOK, C. S. 1953. Phys. Rev. **89**: 902.
WU, C. S. 1955. Beta- and gamma-ray spectroscopy. *Edited by* K. Siegbahn. North-Holland Pub. Co., Amsterdam. p. 314.

AN EXAMINATION OF VERWEY'S MODEL FOR THE LATTICE STRUCTURE OF THE FREE SURFACE OF ALKALI HALIDE CRYSTALS[1]

By G. C. Benson, H. P. Schreiber,[2] and D. Patterson[3]

ABSTRACT

The Verwey model for the free surface structure of alkali halide crystals at 0° K. has been used to estimate the effect of surface distortion on the surface energy of these crystals. It appears that the contributions from distortion are considerably larger than previously reported. In the case of some lithium salts the corrected surface energy becomes negative; the mechanical stability of the solid is considered in the light of this. Several aspects of the Verwey model have been examined. These include the effect of various repulsive potentials and forms of distortion.

1. INTRODUCTION

The Born–Mayer lattice model has been widely adapted for the computation of surface energies, particularly for the alkali halides. The problem is complicated by the presence of an unsymmetrical electric field at the crystal surface, which gives rise to some form of surface deformation. The effect of these deformations on the surface energy has been discussed by various authors (Lennard-Jones and Dent 1928; Dent 1929; Molière, Rathje, and Stranski 1949; Glauberman 1949). Perhaps the most realistic model to date has been proposed by Verwey (1946) who, following Madelung's (1919) suggestion, has examined the displacements of the positive and negative surface ions of alkali halides perpendicular to the surface plane. Polarization of the surface ions has also been taken into account, and a lowering of the surface energy due to surface relaxation predicted. As more accurate experimental values of the surface energies of certain alkali halides may be obtained in the foreseeable future, it seems timely to re-examine the theoretical work.

This paper is divided into the following sections. First, an expression is developed for the change in energy of an infinite crystal as it is separated along a plane into two semi-infinite hemi-crystals, the surfaces of the hemi-crystals being allowed to deform in the Verwey manner. The development of this expression seemed justified by a first examination of the Verwey model, which yielded a surprisingly large lowering of the surface energy of NaCl and NaBr. In fact it is shown later that in the case of LiF and LiI, the final surface energy is negative. This unexpected result may be due to the inapplicability of the model, but there did not seem to be an a priori reason to reject a negative surface energy as impossible, apart from the obvious consideration of mechanical stability of the crystal. The expression, though not necessary to our main

[1]Manuscript received November 17, 1955.
Contribution from the Division of Pure Chemistry, National Research Council, Ottawa, Canada. Issued as N.R.C. No. 3869.
[2]National Research Laboratories Postdoctorate Fellow 1953–1955. Present address: Central Research Laboratories, C.I.L., McMasterville, Que.
[3]National Research Laboratories Postdoctorate Fellow 1953–1955. Present address: Département de Chimie, Université de Montréal, Montréal, Que.

argument, is useful in discussing the plausibility of the negative surface energy; thus, it seems worth while to present the mathematical analysis attending its derivation. The normal surface energy as discussed by Verwey can be obtained by considering the change in energy when the two hemi-crystals are at an infinite distance. In the second section, the ionic displacements calculated by Verwey are checked for NaCl and NaBr, and the corresponding distortion energies and surface energies calculated and discussed. In the light of the results of this section, a third section is devoted to an examination of the effects on the surface energy of assuming various possible forms of the repulsive potential between ions, and of assuming various displacement and polarization characteristics. Finally, the distortion and surface energies of LiF and LiI are calculated, and the results discussed with the aid of the above-mentioned model.

2. THE CHANGE IN ENERGY WHEN AN INFINITE CRYSTAL IS SEPARATED INTO TWO HEMI-CRYSTALS

The model (shown in Fig. 1) assumes that the Verwey distortion is restricted to the first layer S of each hemi-crystal. The structure of the inner layers I is regular. The lattice nearest neighbor distance a is taken as a convenient unit

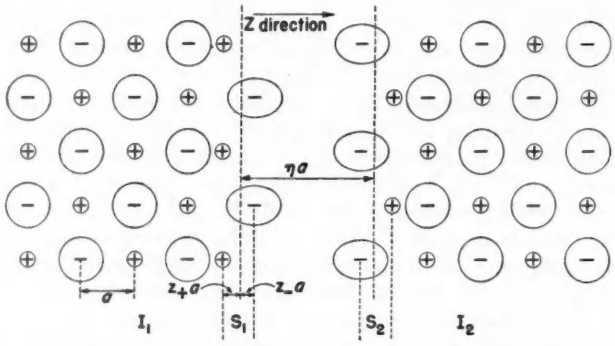

FIG. 1. Model for the calculation of the change in energy when an infinite crystal is separated into two hemi-crystals.

of length. At any separation ηa, measured between the positions of the undistorted first layers of the hemi-crystals, the displacements of the positive and negative ions of the left-hand surface layer are* z_+a and z_-a; these have positive value if the ions have moved to the right of their undistorted positions. The corresponding displacements of the ions of the right-hand surface are then $-z_+a$ and $-z_-a$. For simplicity, only the polarization of the negative ions of the surface layers is considered. These ions have moment μ in the direction Z for ions in surface 1, and $-\mu$ for ions in surface 2.

*Our notation z_+a corresponds to Verwey's displacement z_1.

For $\eta = 1$, the two hemi-crystals coalesce to form a perfect infinite crystal. Here all displacements and dipole moments must vanish. At any separation η, $U(\eta)$ is the total energy of the system relative to the free ions and stated per ion pair in the combined surface planes of parts 1 and 2. This quantity is of course infinite, but for any two values of the separation a finite change in it can be computed. Adopting the regular infinite crystal as a reference state, the change in energy is denoted by $\Delta U(\eta)$, where

$$\Delta U(\eta) = U(\eta) - U(1) . \tag{1}$$

The energy $U(\eta)$ is computed by summing interactions between pairs of ions and pertinent internal energy contributions from the ions. In general, the interaction energy for two ions i and j with charge e_i and e_j and dipole moments $\boldsymbol{\mu}_i$ and $\boldsymbol{\mu}_j$ is taken to be

$$u_{ij} = e_i e_j r_{ij}^{-1} - e_i(\mathbf{r}_{ij}\cdot\boldsymbol{\mu}_j)r_{ij}^{-3} + e_j(\mathbf{r}_{ij}\cdot\boldsymbol{\mu}_i)r_{ij}^{-3} - \boldsymbol{\mu}_j\cdot\left(\frac{3(\mathbf{r}_{ij}\cdot\boldsymbol{\mu}_i)\mathbf{r}_{ij}}{r_{ij}^{5}} - \frac{\boldsymbol{\mu}_i}{r_{ij}^{3}}\right) + R(r_{ij}), \tag{2}$$

where $\mathbf{r}_{ij}$ is the position vector of the jth ion relative to the ith, and $R(r_{ij})$ is the repulsive energy. The dipoles are considered to be permanent and subsequently a correction for the quasi-elastic energy is introduced as an internal energy contribution.

It is convenient to further divide $U(\eta)$ into two parts: $U_{12}(\eta)$ and $U_{11}(\eta)$. The former is composed of terms representing the interactions of ions in part 1 with those in part 2; the latter represents interaction terms between pairs of ions in either of the two parts together with all pertinent internal energy contributions. Hence we can write

$$\Delta U(\eta) = \Delta U_{11}(\eta) + \Delta U_{12}(\eta) . \tag{3}$$

Because of the symmetry when the surface is a {100} plane, $U_{11}(\eta)$ can be computed by considering terms arising from part 1 alone. Stating this per ion pair in the surface of the hemi-crystal

$$\Delta U_{11}(\eta) = U_{11}(\eta) - U_{11}(1) = \sum_{j}^{I_1} u_{+j} + \sum_{j}^{I_1} u_{-j} + \tfrac{1}{2}\sum_{j}^{S_1} u_{+j} + \tfrac{1}{2}\sum_{j}^{S_1} u_{-j} + \frac{\mu^2}{2\alpha} , \tag{4}$$

where the first two sums represent respectively the interactions of a positive and negative surface ion in S_1 with all ions in I_1, the next two sums are analogously defined for interactions between surface ions, and the last term is the quasi-elastic energy of a negative surface ion with polarizability α.

The electrostatic lattice sums in equation (4) can be treated by the method of van der Hoff and Benson (1953), leading to the equation*

*It may be noted that η does not appear explicitly in equation (5), but implicitly through the displacements and dipole moment.

$$(5)\quad \Delta U_{11}(\eta) = \frac{e^2}{a}\left[\left(1-\frac{1}{2\sqrt{2}}\right)\frac{T}{2}(z_- - z_+)^2 \right.$$

$$-8\sum_{l_1\text{odd}}^{\infty}\sum_{l_2\text{odd}}^{\infty}\frac{1}{\sqrt{(l_1^2+l_2^2)}.[1+\exp\{-\pi\sqrt{(l_1^2+l_2^2)}\}]}\{\exp[-\pi(1+z_+)\sqrt{(l_1^2+l_2^2)}]$$

$$\left.+\exp[-\pi(1+z_-)\sqrt{(l_1^2+l_2^2)}]-2\exp[-\pi\sqrt{(l_1^2+l_2^2)}]\}\right]$$

$$-\frac{e}{a^2}\mu\left[\left(1-\frac{1}{2\sqrt{2}}\right)T(z_- - z_+)+8\pi\sum_{l_1\text{odd}}^{\infty}\sum_{l_2\text{odd}}^{\infty}\frac{\exp[-\pi(1+z_-)\sqrt{(l_1^2+l_2^2)}]}{1+\exp[-\pi\sqrt{(l_1^2+l_2^2)}]}\right]$$

$$+\frac{\mu^2}{2}\left[\frac{T}{2\sqrt{2}.a^3}+\frac{1}{\alpha}\right]+\Delta R_{11}(\eta),$$

where $T = 9.0336217$ is a constant representing a lattice sum originally computed by Topping (see van der Hoff and Benson 1953). Terms in $(z_- - z_+)$ of higher than square order have been neglected.

In evaluating the repulsive contributions $\Delta R_{11}(\eta)$, it is assumed for the moment that the Born–Mayer form is applicable, so that $R(r_{ij})$ may be equated to $b_{ij}\exp(-r_{ij}/\rho) = bc_{ij}\exp[(r_i+r_j)/\rho]\exp(-r_{ij}/\rho)$. Here r_i and r_j are the two ionic radii and the c_{ij} are the Pauling factors for $++$, $+-$, and $--$ interactions. These have the respective values 2.00, 1.375, and 0.75 for lithium halides, and 1.25, 1, and 0.75 for other alkali halides. The value of ρ is 0.345×10^{-8} cm. The value of b is determined for each alkali halide by making the spacing at the minimum of the total potential energy curve for the uniform dilatation of the crystal agree with the experimental value of the nearest neighbor distance. Following Verwey, only repulsions between nearest neighbor ions and next-nearest neighbor negative ions are considered.

Thus,

$$(6)\quad \Delta R_{11}(\eta) = b_{+-}[\exp[-(a/\rho)(1+z_+)]+\exp[-(a/\rho)(1+z_-)]$$

$$+4\exp\{-(a/\rho)\sqrt{[1+(z_- - z_+)^2]}\}-6\exp(-a/\rho)]$$

$$+4b_{--}[\exp\{-(a/\rho)\sqrt{[1+(1+z_-)^2]}\}-\exp[-(a/\rho)\sqrt{2}]].$$

Some modifications of the repulsive contribution will be discussed later.

In a similar way, it may be shown that

$$(7)\quad \Delta U_{12}(\eta) = \frac{e^2}{a}\left[8\sum_{l_1\text{odd}}^{\infty}\sum_{l_2\text{odd}}^{\infty}\frac{1}{\sqrt{(l_1^2+l_2^2)}.\{1+\exp[-\pi\sqrt{(l_1^2+l_2^2)}]\}}\right.$$

$$\times\left\{\exp[-\pi(1+\eta-z_+)\sqrt{(l_1^2+l_2^2)}]\right.$$

$$+\exp[-\pi(1+\eta-z_-)\sqrt{(l_1^2+l_2^2)}]-2\exp[-2\pi\sqrt{(l_1^2+l_2^2)}]$$

$$\left.\left.-\frac{\exp[-\pi(2+\eta)\sqrt{(l_1^2+l_2^2)}]-\exp[-3\pi\sqrt{(l_1^2+l_2^2)}]}{1+\exp[-\pi\sqrt{(l_1^2+l_2^2)}]}\right\}\right.$$

$$+2\sum_{\substack{l_1\\ l_1+l_2\text{even}}}^{\infty}\sum_{l_2}^{\infty}\frac{1}{\sqrt{(l_1^2+l_2^2)}}\left\{(-1)^{l_2}[\exp[-\pi(\eta-2z_+)\sqrt{(l_1^2+l_2^2)}]\right.$$

$$\left.+\exp[-\pi(\eta-2z_-)\sqrt{(l_1^2+l_2^2)}]-2\exp[-\pi\sqrt{(l_1^2+l_2^2)}]\right]$$

$$-2[\exp[-\pi(\eta-z_+-z_-)\sqrt{(l_1^2+l_2^2)}]-\exp[-\pi\sqrt{(l_1^2+l_2^2)}]]\Big\}\Big]$$

$$+4\pi\frac{e}{a^2}\mu\Big[\sum_{\substack{l_1\\ l_1+l_2\text{even}}}^{\infty}\sum_{l_2}^{\infty}[\exp[-\pi(\eta-z_+-z_-)\sqrt{(l_1^2+l_2^2)}]$$

$$-(-1)^{l_2}\exp[-\pi(\eta-2z_-)\sqrt{(l_1^2+l_2^2)}]]$$

$$-2\sum_{l_1\text{odd}}^{\infty}\sum_{l_2\text{odd}}^{\infty}\frac{\exp[-\pi(1+\eta-z_-)\sqrt{(l_1^2+l_2^2)}]}{1+\exp[-\pi\sqrt{(l_1^2+l_2^2)}]}\Big]$$

$$+2\pi^2\frac{\mu^2}{a^3}\sum_{\substack{l_1\\ l_1+l_2\text{even}}}^{\infty}\sum_{l_2}^{\infty}(-1)^{l_2}\sqrt{(l_1^2+l_2^2)}\exp[-\pi(\eta-2z_-)\sqrt{(l_1^2+l_2^2)}]+\Delta R_{12}(\eta),$$

where

$$\Delta R_{12}(\eta) = b_{+-}[\exp[-(a/\rho)(\eta-z_+-z_-)]-\exp(-a/\rho)]$$
$$+2b_{--}[\exp\{-(a/\rho)\sqrt{[1+(\eta-2z_-)^2]}\}-\exp[-(a/\rho)\sqrt{2}]]\,.$$

Following Born and Heisenberg (1924), the variables z_+, z_-, and μ in the foregoing equations may be treated as independent. Then for any fixed η, the conditions for equilibrium are

$$\frac{\partial\Delta U(\eta)}{\partial z_+}=\frac{\partial\Delta U(\eta)}{\partial z_-}=\frac{\partial\Delta U(\eta)}{\partial\mu}=0.$$

A solution of these conditions yields the displacements and dipole moment. As a check on internal consistency it can be shown that at $\eta = 1$, the equations are simultaneously satisfied by $z_+ = z_- = \mu = 0$, and also that at this point $d\Delta U(\eta)/d\eta = 0$.

At infinite separation $U_{12}(\eta)$ vanishes and

$$\Delta U_{12}(\infty) = -U_{12}(1)\,. \tag{8}$$

Equation (8) is the surface energy per ion pair of the undistorted hemicrystal. The term $\Delta U_{11}(\infty)$ then is the "distortion energy", representing the correction to the surface energy arising from the displacement and polarization of the ions in the surface layer.

For the purpose of numerical calculations the electrostatic sums were simplified in a manner essentially equivalent to that adopted by Verwey. Thus, only the first term of each sum was considered and $\exp[-\pi\sqrt{(l_1^2+l_2^2)}]$ was neglected when compared with unity. These two simplifications have a compensating effect. The simplified expression for $\Delta U_{11}(\eta)$ is

$$\Delta U_{11}(\eta)=\frac{e^2}{a}\Big[\Big(1-\frac{1}{2\sqrt{2}}\Big)\frac{T}{2}(z_--z_+)^2$$

$$-\frac{8}{\sqrt{2}}\{\exp[-\pi(1+z_+)\sqrt{2}]+\exp[-\pi(1+z_-)\sqrt{2}]-2\exp(-\pi\sqrt{2})\}\Big]$$

$$-\frac{e}{a^2}\mu\Big[\Big(1-\frac{1}{2\sqrt{2}}\Big)T(z_--z_+)+8\pi\exp[-\pi(1+z_-)\sqrt{2}]\Big] \tag{9}$$

$$+\frac{\mu^2}{2}\Big[\frac{T}{2\sqrt{2}.a^3}+\frac{1}{\alpha}\Big]+\Delta R_{11}(\eta).$$

A similar simplified form of $\Delta U_{12}(\eta)$ can be derived. At infinite separation, equilibrium conditions demand that

$$\frac{\partial \Delta U_{11}(\infty)}{\partial z_+} = \frac{\partial \Delta U_{11}(\infty)}{\partial z_-} = \frac{\partial \Delta U_{11}(\infty)}{\partial \mu} = 0,$$

giving rise to the equations

$$(a)\quad 0 = \frac{\partial \Delta U_{11}(\infty)}{\partial z_+} = \frac{e^2}{a}\left[-\left(1-\frac{1}{2\sqrt{2}}\right)T(z_- - z_+) + 8\pi \exp[-\pi(1+z_+)\sqrt{2}]\right] + \frac{e}{a^2}\mu\left(1-\frac{1}{2\sqrt{2}}\right)T + \frac{\partial \Delta R_{11}(\infty)}{\partial z_+},$$

$$(10)\quad (b)\quad 0 = \frac{\partial \Delta U_{11}(\infty)}{\partial z_-} = \frac{e^2}{a}\left[\left(1-\frac{1}{2\sqrt{2}}\right)T(z_- - z_+) + 8\pi \exp[-\pi(1+z_-)\sqrt{2}]\right] + \frac{e}{a^2}\mu\left[-\left(1-\frac{1}{2\sqrt{2}}\right)T + 8\pi^2\sqrt{2}.\exp[-\pi(1+z_-)\sqrt{2}]\right] + \frac{\partial \Delta R_{11}(\infty)}{\partial z_-},$$

$$(c)\quad 0 = \frac{\partial \Delta U_{11}(\infty)}{\partial \mu} = -\frac{e}{a^2}\left[\left(1-\frac{1}{2\sqrt{2}}\right)T(z_- - z_+) + 8\pi \exp[-\pi(1+z_-)\sqrt{2}]\right] + \mu\left[\frac{T}{2\sqrt{2}.a^3} + \frac{1}{\alpha}\right].$$

The first two conditions have been obtained by Verwey by separately equating to zero the net force on a positive and negative surface ion, while the last equation corresponds to $\mu = \alpha E$, where E is the total electric field at a negative surface ion. Equation (10) (*c*) may be solved for μ as a function of z_+ and z_-, and the result employed in (10) (*a*) and (*b*). The numerical solution of these equations is tedious as Verwey has noted; in this work values of z_+ and z_- were estimated and refined by the Newton-Raphson (Whittaker and Robinson 1926) technique employing the derivatives of equations (10) (*a*) and (*b*).

3. A CHECK OF VERWEY'S DISPLACEMENTS FOR NaCl AND NaBr. THE SURFACE ENERGIES OF THESE SALTS

In order to carry out this computation in a manner analogous to Verwey, a further adjustment of the repulsive interaction terms had to be made. For surface displacements in which the interpenetration of ions was such that $r < r_+ + r_-$, the exponential power law was replaced by a "harder" inverse 12th power law (i.e. $R(r) = A + B/r^{12}$). The transition was effected by matching the force and potential statements of the two expressions at $r = r_+ + r_-$. The adjustment constant A was added in order to make the two terms identical at the chosen separation. The additional repulsive law constants were obtained from the equations

$$A+\frac{B}{(r_+ + r_-)^{12}} = b_{+-}\exp[-(r_+ + r_-)/\rho],$$

$$\frac{12B}{(r_+ + r_-)^{13}} = \frac{b_{+-}}{\rho}\exp[-(r_+ + r_-)/\rho]. \tag{11}$$

With the aid of equations described in the preceding section, the displacements of the surface ions of NaCl and NaBr were evaluated for $\eta = \infty$. The distortion energies ($\Delta U_{11}(\infty)$) and the surface energies were also obtained. The surface energy of a {100} surface at any separation η of the two hemicrystals is defined by

$$\sigma_{100}(\eta) = \Delta U(\eta)/2a^2 \tag{12}$$

where the factor $1/2a^2$ converts the result to a unit area basis. $\sigma_{100}(\infty)$ is then the normal surface energy of a {100} face. These results together with the values obtained by Verwey are shown in Table I. Values of the pertinent constants are also shown.

TABLE I

DISPLACEMENTS OF THE SURFACE IONS, DISTORTION AND SURFACE ENERGIES OF NaCl AND NaBr

	r_+	r_-	a	α,	z_+	z_-	μ,	$\frac{1}{2a^2}\Delta U_{11}(\infty)$	$\sigma_{100}(\infty)$
	cm.$\times 10^{-8}$			cm.$^3\times 10^{-24}$			debye	erg-cm.$^{-2}$	
NaCl This work	0.95	1.81	2.81	3.1	−.0586	.0173	0.9348	−77.1	52
Verwey	0.98	1.81	2.81	3.1	−.0534	.018	0.90	—	—
NaBr This work	0.95	1.95	2.97	4.2	−.0701	.0205	1.2082	−83.9	32
Verwey	0.98	1.95	2.97	4.2	−.0700	.0212	1.20	−32	90
								(−84)	(38)

The agreement between the two sets of displacements is good,* but the energy evaluation differs in the case of NaBr by about 50 erg/cm.^{2} We are most indebted to Dr. Verwey, who has kindly re-evaluated his result for NaBr and has reported in private communication a distortion energy value of −84 erg/cm.^{2} (bracketed terms in Table I) in agreement with our result. The surface energies are not in complete agreement because of differences in the formulation of the electrostatic term. Verwey simplified this to be proportional to $\exp(-\pi\sqrt{2})$ while in this work two additional terms were retained (i.e. $\exp(-\pi\sqrt{2}) - 2\exp(-2\pi\sqrt{2}) + \exp(-3\pi\sqrt{2})$). The surprisingly large distortion energies lower the values of the surface energies beyond the scope of the discussion at the end of Verwey's paper. In the case of NaCl the value is much smaller than that indicated by experimental data (Benson and Benson 1955) on the heat of solution of small particles.†

It must also be pointed out that the approximate corrections used by Shuttleworth (1949) for the distortion energy of the alkali halides and based on Verwey's NaBr result must be regarded as erroneous.

*Exact agreement could not be expected because of the different values of the ionic radius of Na^+ used. For consistency, the two Pauling radii were used in this work rather than the Goldschmidt radius for Na^+ used by Verwey.

†A direct comparison with these results is not valid since the experimental work was done at 298° K. while the theoretical model pertains to a crystal at absolute zero. However a rough estimate of the temperature correction which can be obtained from the data of Patterson, Morrison, and Thompson (1955) indicates that this effect is relatively small.

4. DEPENDENCE OF SURFACE ENERGY ON MODEL CHARACTERISTICS

Verwey has pointed out that the magnitude of the distortion energy is sensitive to the choice made for the function representing repulsive interactions between the ions. Furthermore, all other models used to describe the surface configuration lead to absolute values of the distortion energy substantially smaller than we obtained. The dependence of the distortion and surface energies on repulsive interaction and displacement characteristics has therefore been investigated.

(*a*) Displacements, distortion and surface energies for NaCl and NaBr were computed for three forms of the repulsive interaction. The data utilizing the inverse 12th power relationship have already been presented. Verwey's use of the inverse 12th power law was justified by the work of Verwey and de Boer (1940) where, in formulating the molecular energy of the diatomic alkali halides, the inverse power law was found best suited to represent repulsive interactions when the ions were separated by a distance smaller than the sum of the ionic radii. In a more recent paper, Rittner (1951) has shown preference for an altered exponential power law utilizing a value of $\rho = 0.31 \times 10^{-8}$ cm. A second set of data has therefore been computed using a combination of two exponential repulsive power laws which were matched in the same way as described in Section 3. Finally the single exponential form (with $\rho = 0.345 \times 10^{-8}$ cm.) was used to represent all repulsive interactions. The results are given in Table II.

TABLE II

DISPLACEMENTS, DISTORTION AND SURFACE ENERGIES FOR NaCl AND NaBr USING THREE FORMS OF REPULSIVE INTERACTION

	Repulsive terms	z_+	z_-	$\frac{1}{2a^2}\Delta U_{11}(\infty)$ erg-cm.$^{-2}$	$\sigma_{100}(\infty)$ erg-cm.$^{-2}$
NaCl	Exponential + inverse 12th	−.0586	+.0173	− 77.1	52
	Two exponential	−.0938	−.0059	− 89.7	39
	Single exponential	−.1105	−.0164	− 96.1	33
NaBr	Exponential + inverse 12th	−.0701	+.0205	− 83.9	32
	Two exponential	−.1034	−.0002	− 96.1	20
	Single exponential	−.1201	−.0103	−103.2	13

Although the energy values are rather sensitive to the choice of repulsive law function, none of the three methods of evaluation leads to an appreciably lower distortion energy. The present results then are more likely characteristic of the surface configuration than of any particular combination of repulsive interaction expressions.

(*b*) The dependence of the surface energy on surface configuration was investigated for the case of NaCl only. For simplicity, repulsive interactions were uniformly represented by the single exponential form. This seems justified because there is as yet no clear statement of preference for any one method of

formulation; moreover, the effect discussed in the preceding subsection appears to be of secondary magnitude. The following surface configurations were considered:*

(i) Positive and negative surface ions in a plane, which is free to move in Z-direction. No polarization. ($z_+ = z_-$, $\mu = 0$.)

(ii) Surface ions move separately. No polarization. ($z_+ \neq z_-$, $\mu = 0$.)

(iii) No displacements. Negative ions polarized. ($z_+ = z_- = 0$, μ_- finite.)

(iv) No displacement. Both types of surface ions polarized. ($z_+ = z_- = 0$, μ_+ and μ_- finite.) A value of $\alpha_{Na} = 0.18 \times 10^{-24}$ was used.

(v) Same as (i) but negative surface ions polarized. ($z_+ = z_-$, μ_- finite.)

(vi) Same as (i) but both types of surface ions polarized. (Lennard-Jones and Dent model, $z_+ = z_-$, μ_+ and μ_- finite.)

(vii) Verwey model ($z_+ \neq z_-$, μ_- finite).

The results are shown in Table III. The displacement in model (vi) is about

TABLE III

DEPENDENCE OF THE SURFACE ENERGY OF NaCl ON SURFACE CONFIGURATION

Model	z_+	z_-	μ_- (debye)	μ_+ (debye)	$\frac{1}{2a^2}\Delta U_{11}(\infty)$ (erg-cm.$^{-2}$)	$\sigma_{100}(\infty)$ (erg-cm.$^{-2}$)
(i)	−.0052	−.0052	0	0	0	129
(ii)	−.0193	−.0022	0	0	− 4	125
(iii)	0	0	0.385	0	−22	107
(iv)	0	0	0.414	−0.051	−24	105
(v)	−.030	−.030	0.440	0	−26	103
(vi)	−.0355	−.0355	0.484	−0.059	−27	102
(vii)	−.1105	−.0164	1.131	0	−96	33

half that given by Lennard-Jones and Dent (1928). This confirms criticism of their calculations by Molière, Rathje, and Stranski (1949). It is evident from the table that it is the combination of ion polarization and separate displacement which is instrumental in creating the large distortion energy. Thus the Verwey model appears to lead to the most stable surface structure of NaCl. This must, however, be regarded only in the light of the restricting assumptions inherent in the model. Inclusion of the van der Waals attractive forces for example may greatly alter these results. Further, no final conclusions can be reached until the problems of a more realistic formulation of the polarizability of ions in crystal lattices, and the connection between the repulsive term and the state of polarization of the ions, have been resolved. Mayer (Gomer and Smith 1953) has recently drawn attention to the importance of these questions.

*Equations (9) and (10) of Section 2 must be modified according to the needs of each model. In cases where μ_+ is finite, additional appropriate terms must of course be added to equation (9), and equations (10) augmented by a fourth equilibrium condition.

5. DISTORTION AND SURFACE ENERGIES OF LiF AND LiI

The importance of the distortion energy contribution to the surface energy appears to increase as the size difference between constituent ions increases. It was therefore interesting to calculate the distortion and surface energies of LiF and LiI. Verwey's values of the displacements and dipole moments were employed, and the inverse 12th power repulsive relationship applied under the appropriate conditions. The distortion energies of the halides were: -203 erg/cm.^{2} for the fluoride, -237 erg/cm.^{2} for the iodide, leading to respective surface energies of -93 and -142 erg/cm.^{2}

The negative surface energies could be taken to indicate the inapplicability of the classical Born–Mayer model to surface energy computations in these alkali halides. This may be a result of the inherent oversimplifications mentioned at the end of Section 4. The present results must in any case be considered with much caution. Not only have the important van der Waals interaction terms been omitted, but, in order to conform with Verwey's calculations, positive–positive ion repulsive interactions and third nearest neighbor repulsive terms have been neglected, although a crude calculation shows these terms to be still appreciable in the cases in point. It seems fairly certain, however, that inclusion of the additional repulsive terms would not alter the sign of the surface energy.

It has been pointed out in the introduction that no a priori reason exists for rejecting negative surface energies, if mechanical stability of the crystal can be maintained. The surface energy of LiF has therefore been computed for two small separations. In the course of this computation it was found that Verwey's displacements at $\eta = \infty$ did not satisfy the equilibrium conditions as well as might be expected. A new set of values was therefore computed and tabulated in Table IV together with values of the surface energy as a function of η. It will be noted that at $\eta = \infty$ the change in distortion energy from that based on Verwey's displacements is trivial.

TABLE IV

SURFACE CHARACTERISTICS AND SURFACE ENERGY OF LiF AS A FUNCTION OF CRYSTAL SEPARATION

η	1.0	1.1	1.5	∞
z_+	0	.0323	−.0686	−.0697
z_-	0	.0326	−.0039	+.0014
μ_-, debye	0	.0037	.5198	.5616
$\frac{1}{2a^2}\Delta U_{11}(\eta)$, erg-cm.$^{-2}$	0	7.0	−206	−207
$\frac{1}{2a^2}\Delta U_{12}(\eta)$, erg-cm.$^{-2}$	0	0.2	109	110
$\sigma_{100}(\eta)$, erg-cm.$^{-2}$	0	7.2	− 97	− 97

Initially there is an increase in the energy which goes through a maximum for a separation of η in the vicinity of 1.1 and then decreases rapidly to its final negative value in the region $\eta = 1.5$. It is possible, therefore, that the initial increase of energy serves to preserve the mechanical stability of the infinite crystal at 0° K.

In summary it appears that the Verwey model leads to surface energies of the alkali halides which are smaller than can be justified by the few experimental data available or by extrapolation from the liquid state. Undoubtedly the picture of separate displacement of positive and negative surface ions is a more realistic approach than used by previous workers. However, quantitative results for the distortion and associated energy change calculated by the classical Born–Mayer method with simple polarization corrections must be considered with some caution. It is suggested that the difficulty is a fundamental one and requires a more detailed treatment of the polarization and repulsive terms.

ACKNOWLEDGMENT

We should like to express our sincere thanks to Dr. E. J. W. Verwey for his courtesy in supplying details of his calculations.

REFERENCES

BENSON, G. C. and BENSON, G. W. 1955. Can. J. Chem. **33**: 232.
BORN, M. and HEISENBERG, W. 1924. Z. Physik, **23**: 388.
DENT, B. M. 1929. Phil. Mag. **8**: 530.
GLAUBERMAN, A. E. 1949. Zhur. Fiz. Khim. **23**: 124.
GOMER, R. and SMITH, C. S. 1953. Structure and properties of solid surfaces. The University of Chicago Press, Chicago. p. 181 *et seq.*
VAN DER HOFF, B. M. E. and BENSON, G. C. 1953. Can. J. Phys. **31**: 1087.
LENNARD-JONES, J. E. and DENT, B. M. 1928. Proc. Roy. Soc. A, **121**: 247.
MADELUNG, E. 1919. Physik. Z. **20**: 494.
MOLIÈRE, K., RATHJE, W., and STRANSKI, I. N. 1949. Discussions Faraday Soc. No. **5**: 21.
PATTERSON, D., MORRISON, J. A., and THOMPSON, F. W. 1955. Can. J. Chem. **33**: 240.
RITTNER, E. S. 1951. J. Chem. Phys. **19**: 1030.
SHUTTLEWORTH, R. 1949. Proc. Phys. Soc. A, **62**: 167.
VERWEY, E. J. W. 1946. Rec. trav. chim. **65**: 521.
VERWEY, E. J. W. and DE BOER, J. H. 1940. Rec. trav. chim. **59**: 633.
WHITTAKER, E. J. and ROBINSON, G. 1926. The calculus of observations. Blackie & Son, Ltd., London.

THE RADIATION FORCE ON A SPHERICAL OBSTACLE IN A CYLINDRICAL SOUND FIELD[1]

By T. F. W. Embleton

ABSTRACT

The corresponding problems of the radiation forces acting on a spherical obstacle in a plane or spherical progressive sound field have been examined previously by King (Proc. Roy. Soc. (London), A, 147: 212. 1934) and Embleton (J. Acoust. Soc. Amer. 26: 40. 1954) respectively. In these cases the sound field and scattering obstacle both have symmetry of revolution about the line joining the center of the obstacle to the origin of the sound field, but for a cylindrical sound field there exists only a much lower degree of symmetry. A general expression has been obtained for the radiation force in terms of the complex amplitudes of spherical harmonics required to synthesize the incident sound field—for the cases of greatest symmetry this reduces to the simpler expression previously obtained. The first 20 non-zero amplitudes have been evaluated for a cylindrical sound field and it is shown that the force is one of attraction near to the source, becomes zero at a certain distance, and is a force of repulsion at a greater distance. Qualitatively, this force is the same as for spherical waves but for any size of obstacle and frequency of the sound field the point of zero force is always nearer to the source in a cylindrical wave.

I. INTRODUCTION

The importance of dealing theoretically with the radiation force in a sound field where there is no simple relation between the mean kinetic and mean potential energy densities has been dealt with in a previous paper (Embleton 1954) where the field considered was spherical. This present paper deals with a cylindrical sound field where, in addition, there is a lower degree of symmetry of the field and consequently terms remain here which have vanished from previous analyses. The method used is similar to that employed by King (1934) who considered a spherical obstacle in a plane field—other work using essentially King's method but of no direct connection with the present paper is that of Awatani (1955) who derived the radiation force of plane waves on a circular disk.

II. SYMBOLS

δp pressure variation from undisturbed state.

ρ_0 density of propagation medium in undisturbed state.

t time coordinate.

ϕ velocity potential.

a_1, ρ_1, M radius, mean density, and mass of spherical obstacle.

c phase velocity of sound.

ρ, θ, Ω spherical coordinates; equilibrium position of center of sphere as origin, O; the line OL from O perpendicular to the line source as the zero direction of θ; the plane containing the line source and O as the zero plane of Ω, see Fig. 1.

r, l distance of any element δl of line source from the center of the sphere O and the point L respectively.

r_0 mean distance of the center of the sphere from the line source (the length of the line OL).

[1]Manuscript received November 14, 1955.
Contribution from the Division of Applied Physics, National Research Council, Ottawa, Canada. Issued as N.R.C. No. 3873.

III. THEORY

(*a*) *Boundary Conditions*

The pressure variation in the propagation medium (most commonly, air) may be written entirely in terms of the velocity potential using the form of Bernoulli's equation applicable to non-steady flow

$$\delta p = \rho_0 \dot{\phi} + \frac{1}{2}\frac{\rho_0}{c^2}\dot{\phi}^2 - \frac{1}{2}\rho_0(\nabla\phi)^2. \tag{1}$$

This equation is correct to the order of $(\nabla\phi)^2/c^2$ and so ϕ may be expressed as any solution of the simple wave equation, $(\nabla^2+k^2)\phi = 0$, where the wave number k defines the frequency of the sound field. Equation (1) may be integrated over the surface of the sphere to obtain the net force acting on the sphere. The last two terms represent a unidirectional force when integrated over the surface; the first term will give rise to dynamical equations of motion of the sphere if it is free to move. If u is the linear velocity of the sphere determined in this way with respect to the origin O of the velocity potential field, then in place of $\dot{\phi}$ we must have $\dot{\phi} - u.\nabla\phi$. The last term of this expression gives rise to a contribution to δp of the same order of magnitude as the last two terms of Equation (1), which now becomes

$$\delta p = \rho_0 \dot{\phi} - \rho_0 u.\nabla\phi + \frac{1}{2}\frac{\rho_0}{c^2}\dot{\phi}^2 - \frac{1}{2}\rho_0(\nabla\phi)^2. \tag{2}$$

From the degree of symmetry of the cylindrical sound field and the spherical obstacle the only resultant forces acting on the sphere will be along the line OL, Fig. 1. It is assumed that the sphere is rigid, that its surface is impervious

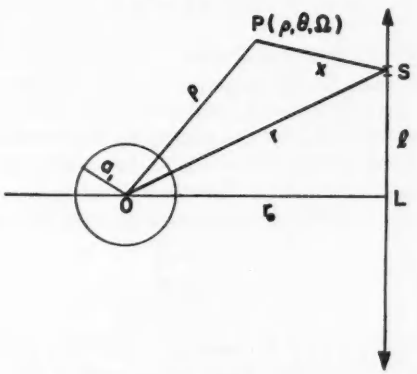

FIG. 1.

to the sound field, but that it is free to move. The sphere will execute small oscillations along the line OL under a law of force given by

$$M\dot{u} = -2a_1^2 \int_0^{\pi}\int_0^{\pi} \rho_0 \dot{\phi} \sin\theta.\cos\theta.\, d\theta.\, d\Omega. \tag{3}$$

Integrating Equation (3) with respect to time, the oscillatory motion of the sphere is obtained as

$$Mu = -2a_1^2\rho_0 \int_0^{\pi}\int_{-1}^{1} \phi\mu \,.\, d\mu \,.\, d\Omega \tag{4}$$

where $\mu = \cos\theta$.

Since the fluid medium must remain in contact with the sphere at all points on its surface, the velocity potential must satisfy the boundary condition that

$$-\left(\frac{\partial\phi}{\partial\rho}\right)_{\rho=a_1} = u\cos\theta. \tag{5}$$

(*b*) *Solution of the Wave Equation*

From the nature of the boundary conditions it is most convenient to adopt a solution of the wave equation in terms of spherical coordinates, in which the wave equation is separable, based on the center of the sphere as origin. The velocity potential may then be written as

$$\phi = \sum_{n=0}^{\infty} \{A_n\psi_n(k\rho)+A_n'f_n(k\rho)\} \,.\, (k\rho)^n \,.\, S_n(\mu, \Omega) \tag{6}$$

where S_n is a surface harmonic of order n, a function of both θ (or μ) and Ω. $\psi_n(z)$, $\Phi_n(z)$, and $f_n(z)$ are spherical wave functions equal to $(-d/z\,dz)^n$ operating on $(\sin z)/z$, $(\cos z)/z$, and e^{-iz}/z respectively. From the nature of these functions the term

$$\phi_i = \sum_{n=0}^{\infty} A_n\psi_n(k\rho) \,.\, (k\rho)^n . S_n \tag{7}$$

represents the incident velocity potential and the coefficients A_n may be made to satisfy the conditions of a line source whose nearest point to the origin is at a distance r_0. Equation (6) can be made to satisfy Equation (5), the boundary condition over the surface of the sphere, by suitable choice of the coefficients A_n' of the scattered waves in terms of the coefficients A_n of the incident waves. This has been described in sufficient detail in previous papers (King 1934; Embleton 1954); here it is only necessary to state that A_n' was written as

$$A_n' = -\frac{G_n(\alpha)}{F_n(\alpha)-iG_n(\alpha)} A_n \tag{8}$$

where $\alpha = ka_1$. The form of $F_n(\alpha)$ and $G_n(\alpha)$ was then determined in order to satisfy the boundary condition. $H_n(\alpha)$ and ϵ_n which are required later may now be defined from $F_n(\alpha)$ and $G_n(\alpha)$ by

$$F_n(\alpha)+i\,G_n(\alpha) = H_n(\alpha) \,.\, e^{i\epsilon_n}. \tag{9}$$

The surface harmonic $S_n(\mu, \Omega)$ may be expanded in a series of terms varying as $\cos m\Omega$ and $\sin m\Omega$ (Lamb 1932) and since the velocity potential at any point P is expressed in terms of S_n over the whole sphere, m may be considered an integer. The surface harmonic takes the form

$$S_n(\mu, \Omega) = P_n(\mu) + \sum_{m=1}^{n} (B_m \cos m\Omega + C_m \sin m\Omega)\, P_n^m(\mu), \tag{10}$$

where $P_n(\mu)$ is a Legendre polynomial and $P_n^m(\mu)$ are the associated functions. The sound field originating from a uniform line source lying in the zero plane of the angle Ω is symmetrical with respect to this plane and hence the non-symmetrical terms in Ω must vanish. Hence, the expansion (10) reduces to

$$S_n = P_n(\mu) + \sum_{m=1}^{n} B_m \cos m\Omega \,.\, P_n^m(\mu) \tag{11}$$

or

$$A_n S_n = \sum_{m=0}^{n} A_n^m \cos m\Omega \,.\, P_n^m(\mu).$$

Thus the incident sound field of Equation (7) becomes

$$\phi_i = \sum_{n=0}^{\infty} \sum_{m=0}^{n} A_n^m \,.\, \psi_n(k\rho) \,.\, (k\rho)^n \,.\, \cos m\Omega \,.\, P_n^m(\mu). \tag{12}$$

(*c*) *Analysis of the Radiation Force*

In general the coefficients A_n^m of the incident sound field are complex and may be written

$$A_n^m = |A_n^m| \exp[i(\omega t + \beta_n^m)]. \tag{13}$$

Using Equations (8), (9), (11), and (13), Equation (6) may be put in the form

$$\phi = \cos \omega t \sum_{n=0}^{\infty} \sum_{m=0}^{n} R_n^m \cos m\Omega \,.\, P_n^m(\mu) + \sin \omega t \sum_{n=0}^{\infty} \sum_{m=0}^{n} T_n^m \cos m\Omega \,.\, P_n^m(\mu), \tag{14}$$

where

$$R_n^m = \frac{|A_n^m| \cos(\beta_n^m + \epsilon_n)}{H_n(\alpha) \,.\, \alpha^{n+1}} \quad \text{and} \quad T_n^m = -\frac{|A_n^m| \sin(\beta_n^m + \epsilon_n)}{H_n(\alpha) \,.\, \alpha^{n+1}}. \tag{15}$$

When Equation (14) is substituted into Equation (2) an expression is obtained for the instantaneous pressure δp at any point on the surface of the sphere. This may then be averaged with respect to time to obtain the mean pressure at any point and integrated with respect to θ and Ω to obtain the net, mean force on the whole sphere, i.e. the radiation force.

The first-order pressure variation P_1 (from the first term of the right-hand side of Equation (2)) is

$$P_1 = \rho_0 c k \left\{ \cos \omega t \sum_{n=0}^{\infty} \sum_{m=0}^{n} T_n^m \cos m\Omega \,.\, P_n^m(\mu) - \sin \omega t \sum_{n=0}^{\infty} \sum_{m=0}^{n} R_n^m \cos m\Omega \,.\, P_n^m(\mu) \right\}. \tag{16}$$

The time average of this expression is zero, so P_1 contributes nothing to the mean pressure at any point on the sphere.

Let P_ϕ denote the contribution of the term $\frac{1}{2}(\rho_0/c^2)\dot{\phi}^2$ when integrated over the surface of the sphere and $\bar{P}_\phi$ its time average. From considerations of symmetry P_ϕ will act along the line joining O and L. We have

$$(17)\quad P_\phi = -\frac{a_1^2\rho_0}{c^2}\int_0^\pi\int_{-1}^1 \dot{\phi}^2\mu\,.\,d\mu\,.\,d\Omega$$

$$(18)\quad = -a_1^2\rho_0 k^2\int_0^\pi\int_{-1}^1\left\{\cos\omega t\sum_{n=0}^\infty\sum_{m=0}^n T_n^m\cos m\Omega\,.\,P_n^m(\mu) - \sin\omega t\sum_{n=0}^\infty\sum_{m=0}^n R_n^m\cos m\Omega\,.\,P_n^m(\mu)\right\}^2\mu\,.\,d\mu\,.\,d\Omega.$$

Taking the time average of this we obtain

$$(19)\quad \bar{P}_\phi = -\frac{a_1^2\rho_0 k^2}{2}\int_0^\pi\int_{-1}^1\left[\left\{\sum_{n=0}^\infty\sum_{m=0}^n R_n^m\cos m\Omega\,.\,P_n^m(\mu)\right\}^2 + \left\{\sum_{n=0}^\infty\sum_{m=0}^n T_n^m\cos m\Omega\,.\,P_n^m(\mu)\right\}^2\right]\mu\,.\,d\mu\,.\,d\Omega.$$

This expression may be evaluated by making use of the integrals (1) and (2) listed in the Appendix, and hence

$$(20)\quad \bar{P}_\phi = -2\pi\alpha^2\rho_0\sum_{n=0}^\infty\frac{(n+1)}{(2n+1)(2n+3)}(R_n^0R_{n+1}^0+T_n^0T_{n+1}^0) - \pi\alpha^2\rho_0\sum_{n=0}^\infty\sum_{m=1}^n\frac{(n+m+1)!}{(n-m)!\,(2n+1)(2n+3)}(R_n^mR_{n+1}^m+T_n^mT_{n+1}^m).$$

Similarly let P_q denote the contribution of the term $-\frac{1}{2}\rho_0(\nabla\phi)^2$ when integrated over the surface of the sphere and $\bar{P}_q$ its time average. As before we have

$$(21)\quad P_q = a_1^2\rho_0\int_0^\pi\int_{-1}^1(\nabla\phi)^2\mu\,.\,d\mu\,.\,d\Omega$$

$$(22)\quad = \rho_0\int_0^\pi\int_{-1}^1\left[\left(\frac{\partial\phi}{\partial\mu}\right)^2(1-\mu^2)+\left(\frac{\partial\phi}{\partial\Omega}\right)^2\frac{1}{(1-\mu^2)}\right]\mu\,.\,d\mu\,.\,d\Omega.$$

$(\partial\phi/\partial\mu)$ and $(\partial\phi/\partial\Omega)$ may be obtained from Equation (14). When Equation (22) is averaged with respect to time, it becomes

$$(23)\quad \bar{P}_q = \frac{\rho_0}{2}\int_0^\pi\int_{-1}^1\left[\left\{\sum_{n=0}^\infty\sum_{m=0}^n R_n^m\cos m\Omega\frac{\partial}{\partial\mu}P_n^m(\mu)\right\}^2 + \left\{\sum_{n=0}^\infty\sum_{m=0}^n T_n^m\cos m\Omega\frac{\partial}{\partial\mu}P_n^m(\mu)\right\}^2\right](1-\mu^2)\,\mu\,.\,d\mu\,.\,d\Omega$$
$$+\frac{\rho_0}{2}\int_0^\pi\int_{-1}^1\left[\left\{\sum_{n=0}^\infty\sum_{m=0}^n R_n^m\,m\,.\,\sin m\Omega\,.\,P_n^m(\mu)\right\}^2 + \left\{\sum_{n=0}^\infty\sum_{m=0}^n T_n^m\,m\,.\,\sin m\Omega\,.\,P_n^m(\mu)\right\}^2\right]\frac{\mu}{(1-\mu^2)}\,d\mu\,.\,d\Omega.$$

This expression (23) may be evaluated by using the integrals (1), (3), and (4) listed in the Appendix, giving

$$(24)\quad \bar{P}_q = 2\pi\rho_0\sum_{n=0}^\infty\frac{n(n+1)(n+2)}{(2n+1)(2n+3)}(R_n^0R_{n+1}^0+T_n^0T_{n+1}^0) + \frac{\pi\rho_0}{2}\sum_{n=0}^\infty\sum_{m=1}^n\frac{(n+m+1)!}{(n-m-1)!\,(2n+1)(2n+3)}\left\{2n+m+2+\frac{2n}{n-m}\right\} \times(R_n^mR_{n+1}^m+T_n^mT_{n+1}^m).$$

Finally let P_u denote the contribution of the term $-u \cdot \nabla\phi$ (which arises from the motion of the sphere under the action of the first-order sound field) when integrated over the surface of the sphere and $\bar{P}_u$ its time average,

$$P_u = -2a_1^2\rho_0 \int_0^{\pi} \int_{-1}^{1} \left[u^2\mu^2 - \frac{u(1-\mu^2)}{a_1}\left(\frac{\partial\phi}{\partial\mu} \right) \right] \mu \cdot d\mu \cdot d\Omega. \tag{25}$$

The first term of this integral obviously vanishes upon integration. From Equations (4) and (14) the velocity of the center of the sphere may be obtained as

$$u = -\{R_1^0 \cos\omega t + T_1^0 \sin\omega t\} \frac{k}{\alpha} \cdot \frac{\rho_0}{\rho_1}. \tag{26}$$

When this expression is substituted into Equation (25) and $(\partial\phi/\partial\mu)$ is found from Equation (14), we have for the time average $\bar{P}_u$

$$\bar{P}_u = -\frac{\rho_0^2}{\rho_1} \int_0^{\pi} \int_{-1}^{1} \sum_{n=0}^{\infty} \sum_{m=0}^{n} (R_1^0 R_n^m + T_1^0 T_n^m) \cos m\Omega \cdot (1-\mu^2) \cdot \frac{\partial}{\partial\mu} P_n^m(\mu) \cdot \mu \cdot d\mu \cdot d\Omega. \tag{27}$$

Now

$$\int_0^{\pi} \cos m\Omega \cdot d\Omega = 0 \quad \text{for } m > 0,$$
$$= \pi \quad \text{for } m = 0,$$

and making use of integral (4) listed in the Appendix, the expression for $\bar{P}_u$ becomes

$$\bar{P}_u = -\frac{4}{5}\pi \frac{\rho_0^2}{\rho_1} (R_1^0 R_2^0 + T_1^0 T_2^0). \tag{28}$$

The radiation force on the sphere is evidently given by the sum of Equations (20), (24), and (28) as

$$\bar{P} = -2\pi\rho_0 \left[\sum_{n=0}^{\infty} \frac{(n+1)}{(2n+1)(2n+3)} \{\alpha^2 - n(n+2)\} \cdot (R_n^0 R_{n+1}^0 + T_n^0 T_{n+1}^0) \right] - \pi\rho_0 \left[\sum_{n=0}^{\infty} \sum_{m=1}^{n} \frac{(n+m+1)!}{(n-m)!\,(2n+1)(2n+3)} \times \left\{ \alpha^2 - n(n+2) + m\left(\frac{n}{2} + \frac{m}{2} + 1 \right) \right\} (R_n^m R_{n+1}^m + T_n^m T_{n+1}^m) \right] \tag{29}$$

where

$$(R_n^m R_{n+1}^m + T_n^m T_{n+1}^m) = \frac{|A_n^m| \cdot |A_{n+1}^m|}{H_n^2(\alpha) \cdot H_{n+1}^2(\alpha) \cdot \alpha^{4n+6}} \left[\cos(\beta_{n+1}^m - \beta_n^m) \cdot \left(H_n^2(\alpha) \cdot H_{n+1}^2(\alpha) \cdot \alpha^{4n+6} - \{\alpha^2 - n(n+2)\}^2 \right)^{\frac{1}{2}} + \sin(\beta_{n+1}^m - \beta_n^m) \cdot \{\alpha^2 - n(n+2)\} \right]. \tag{30}$$

The Equation (30) is valid for all m. Its derivation involves certain properties of the $H_n(\alpha)$ functions which have not been given in this paper. In (29) and (30), $\{\alpha^2 - n(n+2)\}$ is to be replaced by $\{\alpha^2 - 3(1-\rho_0/\rho_1)\}$ when $n = 1$.

It should be noted that Equation (30) and the first half of Equation (29) are identical with the complete expressions for the radiation force which exist

for the two cases of plane and spherical waves (King 1934; Embleton 1954). The second half of Equation (29) has not vanished from this present analysis because of the lower degree of symmetry possessed by cylindrical waves.

(d) Evaluation of the Coefficients $|A_n^m|$ and β_n^m

It now remains to determine $|A_n^m|$ and β_n^m from Equation (13) after Equation (12) has been made to represent a field of diverging cylindrical waves originating from a line source whose nearest point to the origin is at a distance of r_0. Let the line source have a strength of s per unit length so that the velocity potential at P due to the element of line source at S is

$$\phi_{\delta l} = s\delta l \frac{e^{-ikx}}{kx} = s\delta l f_0(kx). \tag{31}$$

This may be written in terms of the spherical coordinates at O (Lamb 1932) as

$$\phi_{\delta l} = s\delta l \sum_{n=0}^{\infty} (2n+1) \,.\, (k\rho)^n \,.\, (kr)^n \,.\, f_n(kr) \,.\, \psi_n(k\rho) \,.\, P_n(\cos POS). \tag{32}$$

The velocity potential arising from the whole line source is obtained by integrating Equation (32). To simplify evaluation of the angle POS the point P is considered to be coplanar with O and the line source, i.e. $\Omega = 0$. Hence

$$\phi_t = \sum_{n=0}^{\infty} s(2n+1)(k\rho)^n \,.\, \psi_n(k\rho) \int_{-\infty}^{\infty} (kr)^n \,.\, f_n(kr) \,.\, P_n\left(\frac{r_0}{r}\cos\theta + \frac{l}{r}\sin\theta\right) dl. \tag{33}$$

Equation (33) is identical with Equation (12) for all values of θ (or μ) and ρ and this identity may be used to evaluate A_n^m. For each value of n

$$\sum_{m=0}^{n} A_n^m P_n^m(\mu) = s(2n+1) \int_{-\infty}^{\infty} (kr)^n \,.\, f_n(kr) \,.\, P_n\left(\frac{\mu r_0}{r} + \frac{(1-\mu^2)^{\frac{1}{2}} l}{r}\right) dl \tag{34}$$

where $r = (r_0^2 + l^2)^{\frac{1}{2}}$. The Legendre polynomial on the right-hand side of Equation (34) may be expanded by Taylor's theorem. Since $P_n(z)$ is a polynomial series in z up to z^n, the tth differential will be zero for $t > n$. If $P_n^m(u)$ is written in differential form, Equation (34) becomes

$$\begin{aligned} &\sum_{m=0}^{n} A_n^m (1-\mu^2)^{m/2} \left(\frac{d}{d\mu}\right)^m P_n(\mu) \\ &= s(2n+1) \int_{-\infty}^{\infty} (kr)^n \,.\, f_n(kr) \,.\, \left[P_n\left(\frac{\mu r_0}{r}\right) \right. \\ &\qquad \left. + \sum_{t=1}^{n} \frac{l^t}{r^t} \frac{(1-\mu^2)^{t/2}}{t!} \left(\frac{d}{d(\mu r_0/r)}\right)^t P_n\left(\frac{\mu r_0}{r}\right) \right] dl. \end{aligned} \tag{35}$$

If the coefficients of powers of μ greater than μ^n are considered, then it can be seen immediately that the terms of the left-hand side of Equation (35) for which m is odd are associated with, and only with, the terms of the right-hand side for which t is odd. Now consider the right-hand side of the equation when t is odd. The expansion of r is entirely in terms of even powers of l and hence the integral is of the form

(36) $$\int_{-\infty}^{\infty} (\text{odd powers of } l)\, dl$$

which is evidently zero. Thus all the coefficients A_n^m are zero when m is odd.

The Legendre functions of Equation (35) may each be expanded as finite polynomial series of their arguments. Then, giving μ a number of different values, a set of simultaneous equations is obtained (more correctly, one set for each value of n) from which the value of each A_n^m may be found. A typical coefficient of the incident sound field is

(37) $$A_6^2 = \frac{26s}{64}\int_0^{\infty} (kr)^6 \cdot f_6(kr) \cdot \frac{l^2}{r^2}\left[33\frac{r_0^4}{r^4} - 18\frac{r_0^2}{r^2} + 1\right] dl.$$

This integral may most easily be evaluated by converting to Bessel function notation. We have

(38) $$f_n(kr) = -\left(\frac{\pi}{2}\right)^{\frac{1}{2}} \frac{iH_{n+\frac{1}{2}}^{(2)}(kr)}{(kr)^{n+\frac{1}{2}}}$$

where H is a Bessel function of the third kind. From Equations (37) and (38) we have, writing $y = kl$,

(39) $$A_6^2 = -\frac{26s}{64k}\left(\frac{\pi}{2}\right)^{\frac{1}{2}} \int_0^{\infty} \frac{iH_{6\frac{1}{2}}^{(2)}[\sqrt{(y^2+k^2r_0^2)}]}{[\sqrt{(y^2+k^2r_0^2)}]^{6\frac{1}{2}}} \times[16(kr_0)^4y^2 - 16(kr_0)^2y^4 + y^6]\, dy.$$

Watson (1944) gives Sonine's formula for a similar integral of a Bessel function of the first kind and an identical formula may be derived for a Bessel function of the third kind. This is

(40) $$\int_0^{\infty} \frac{H_\nu^{(2)}[a\sqrt{(t^2+z^2)}]}{[\sqrt{(t^2+z^2)}]^\nu} t^{2b+1} dt = \frac{2^b\Gamma(b+1)}{a^{b+1}z^{\nu-b-1}} \cdot H_{\nu-b-1}^{(2)}(az)$$

provided that $a > 0$ and $\mathrm{Re}(\frac{1}{2}\nu - \frac{1}{4}) > \mathrm{Re}(b) > -1$. These conditions are satisfied by all the expressions similar to Equation (39) for every coefficient. The typical coefficient then becomes

(41) $$A_6^2 = -\frac{26s}{64k}\left(\frac{\pi}{2}\right)\left[16\frac{iH_6^{(2)}(kr_0)}{(kr_0)} - 48\frac{iH_4^{(2)}(kr_0)}{(kr_0)^2} + 15\frac{iH_3^{(2)}(kr_0)}{(kr_0)^3}\right].$$

A complete list of the first 20 non-zero coefficients A_n^m is given in Table I.

Since $iH_t^{(2)}(z) = Y_t(z) + iJ_t(z)$, every coefficient may easily be split into its modulus and argument, as required by Equation (13). It is obvious that if any coefficient in Table I is written as

(42) $$A_n^m = -\frac{S\pi}{k}(2n+1) \cdot \mathfrak{F}[iH_t^{(2)}(kr_0); m, n],$$

then $$|A_n^m| = -\frac{S\pi}{k}(2n+1)\{\mathfrak{F}^2[Y_t; m, n] + \mathfrak{F}^2[J_t; m, n]\}^{\frac{1}{2}},$$

(43) $$\cos\beta_n^m = \frac{\mathfrak{F}[Y_t; m, n]}{\{\mathfrak{F}^2[Y_t; m, n] + \mathfrak{F}^2(J_t; m, n]\}^{\frac{1}{2}}},$$

and $$\sin\beta_n^m = \frac{\mathfrak{F}[J_t; m, n]}{\{\mathfrak{F}^2[Y_t; m, n] + \mathfrak{F}^2[J_t; m, n]\}^{\frac{1}{2}}}.$$

TABLE I

$$A_0^0 = -\frac{s\pi}{k}[iH_0^{(2)}(kr_0)]$$

$$A_1^0 = -\frac{s\pi}{k}\ 3\ [iH_1^{(2)}(kr_0)]$$

$$A_2^0 = -\frac{s\pi}{k}\ 5\left[iH_2^{(2)}(kr_0) - \frac{1}{2}\frac{iH_1^{(2)}(kr_0)}{(kr_0)}\right]$$

$$A_2^2 = -\frac{s\pi}{k}\ 5\left[\frac{1}{4}\frac{iH_1^{(2)}(kr_0)}{(kr_0)}\right]$$

$$A_3^0 = -\frac{s\pi}{k}\ 7\left[iH_3^{(2)}(kr_0) - \frac{3}{2}\frac{iH_2^{(2)}(kr_0)}{(kr_0)}\right]$$

$$A_3^2 = -\frac{s\pi}{k}\ 7\left[\frac{1}{4}\frac{iH_2^{(2)}(kr_0)}{(kr_0)}\right]$$

$$A_4^0 = -\frac{s\pi}{k}\ 9\left[iH_4^{(2)}(kr_0) - 3\frac{iH_3^{(2)}(kr_0)}{(kr_0)} + \frac{9}{8}\frac{iH_2^{(2)}(kr_0)}{(kr_0)^2}\right]$$

$$A_4^2 = -\frac{s\pi}{k}\ 9\left[\frac{1}{4}\frac{iH_3^{(2)}(kr_0)}{(kr_0)} - \frac{1}{8}\frac{iH_2^{(2)}(kr_0)}{(kr_0)^2}\right]$$

$$A_4^4 = -\frac{s\pi}{k}\ 9\left[\frac{1}{64}\frac{iH_2^{(2)}(kr_0)}{(kr_0)^2}\right]$$

$$A_5^0 = -\frac{s\pi}{k}\ 11\left[iH_5^{(2)}(kr_0) - 5\frac{iH_4^{(2)}(kr_0)}{(kr_0)} + \frac{45}{8}\frac{iH_3^{(2)}(kr_0)}{(kr_0)^2}\right]$$

$$A_5^2 = -\frac{s\pi}{k}\ 11\left[\frac{1}{4}\frac{iH_4^{(2)}(kr_0)}{(kr_0)} - \frac{3}{8}\frac{iH_3^{(2)}(kr_0)}{(kr_0)^2}\right]$$

$$A_5^4 = -\frac{s\pi}{k}\ 11\left[\frac{1}{64}\frac{iH_3^{(2)}(kr_0)}{(kr_0)^2}\right]$$

$$A_6^0 = -\frac{s\pi}{k}\ 13\left[iH_6^{(2)}(kr_0) - \frac{15}{2}\frac{iH_5^{(2)}(kr_0)}{(kr_0)} + \frac{135}{8}\frac{iH_4^{(2)}(kr_0)}{(kr_0)^2} - \frac{75}{16}\frac{iH_3^{(2)}(kr_0)}{(kr_0)^3}\right]$$

$$A_6^2 = -\frac{s\pi}{k}\ 13\left[\frac{1}{4}\frac{iH_5^{(2)}(kr_0)}{(kr_0)} - \frac{3}{4}\frac{iH_4^{(2)}(kr_0)}{(kr_0)^2} + \frac{15}{64}\frac{iH_3^{(2)}(kr_0)}{(kr_0)^3}\right]$$

$$A_6^4 = -\frac{s\pi}{k}\ 13\left[\frac{1}{64}\frac{iH_4^{(2)}(kr_0)}{(kr_0)^2} - \frac{1}{128}\frac{iH_3^{(2)}(kr_0)}{(kr_0)^3}\right]$$

$$A_6^6 = -\frac{s\pi}{k}\ 13\left[\frac{1}{1536}\frac{iH_3^{(2)}(kr_0)}{(kr_0)^3}\right]$$

$$A_7^0 = -\frac{s\pi}{k}\ 15\left[iH_7^{(2)}(kr_0) - \frac{21}{2}\frac{iH_6^{(2)}(kr_0)}{(kr_0)} + \frac{315}{8}\frac{iH_5^{(2)}(kr_0)}{(kr_0)^2} - \frac{525}{16}\frac{iH_4^{(2)}(kr_0)}{(kr_0)^3}\right]$$

$$A_7^2 = -\frac{s\pi}{k}\ 15\left[\frac{1}{4}\frac{iH_6^{(2)}(kr_0)}{(kr_0)} - \frac{5}{4}\frac{iH_5^{(2)}(kr_0)}{(kr_0)^2} + \frac{75}{64}\frac{iH_4^{(2)}(kr_0)}{(kr_0)^3}\right]$$

$$A_7^4 = -\frac{s\pi}{k}\ 15\left[\frac{1}{64}\frac{iH_5^{(2)}(kr_0)}{(kr_0)^2} - \frac{3}{128}\frac{iH_4^{(2)}(kr_0)}{(kr_0)^3}\right]$$

$$A_7^6 = -\frac{s\pi}{k}\ 15\left[\frac{1}{1536}\frac{iH_4^{(2)}(kr_0)}{(kr_0)^3}\right]$$

The coefficients may then be taken in pairs as necessary to evaluate Equation (30). The factor $s\pi/k$ may be replaced by $|p|/kc\rho_0|H_0^{(2)}(kr_0)|$ where $|p|$ is the pressure amplitude of the sound field at the same distance r_0 from the line source as the spherical obstacle.

IV. CONCLUSION

Values of the radiation force $\bar{P}$ computed from Equation (29) are shown in Fig. 2 as a function of the distance of the spherical obstacle from the line source, origin of the diverging sound field. Curves are given for several sizes

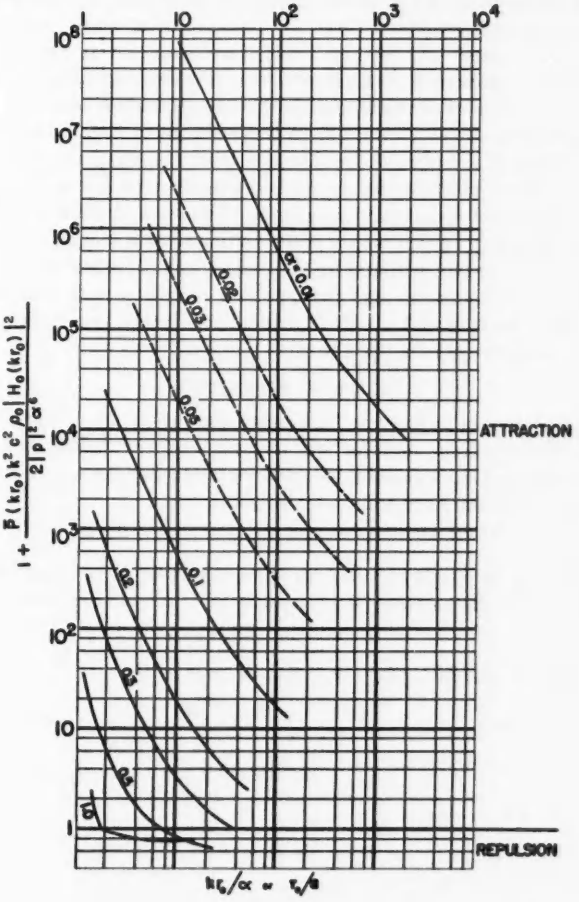

FIG. 2.

of spherical obstacle, $\alpha = ka$; both coordinates contain α as a normalizing factor in order that all the curves may be plotted more compactly on the same graph. In order that both positive and negative forces, attractions and repul-

sions respectively, may be shown on the same logarithmic scale a constant has been added to the ordinate so that all the values to be plotted are positive.

For all finite sizes of sphere the force at an infinite distance from the line source is one of repulsion, as expected since the wave fronts then tend to become plane. As the distance between the line source and the spherical obstacle is decreased so the radiation force of repulsion decreases until at some distance, which is a function of the size of the sphere and the frequency of the sound field, it becomes zero. At still smaller distances the radiation force becomes an ever-increasing attraction. As r_0/a approaches unity the force of attraction becomes infinitely great; this corresponds to the line source being tangential to the spherical obstacle.

In an earlier paper (Embleton 1954) curves are given for the radiation force acting on a spherical obstacle placed in a diverging spherical sound field as a function of size of obstacle and its distance from the center of the sound field. Qualitatively these are similar to those shown in Fig. 2. However in the case of a spherical sound field the distance from the center of the sound field to which the force of attraction extends is greater than for a cylindrical field providing the size of sphere and frequency of the sound field are the same in both cases. Also for a given size of sphere situated at a constant distance from the source of the sound field any force of attraction decreases as the frequency of the sound field increases and changes to a repulsion at a frequency which depends upon both r_0 and a—this frequency is lower in a cylindrical wave field than in a spherical field (for the same r_0 and a).

ACKNOWLEDGMENTS

The author wishes to express his sincere thanks to Dr. G. J. Thiessen for suggesting the problem and for his interest and invaluable criticism subsequently, also to Dr. S. Sueoka for showing a method by which the integrals (2), (3), and (4) of the Appendix could be obtained.

APPENDIX

The following integrals are used in the evaluation of the expressions (19), (23), and (27). In all cases only the values for $N \geqslant n$ were required.

$$(1)\quad \int_0^{\pi} \cos m\Omega \,.\, \cos M\Omega \,.\, d\Omega = \begin{cases} \pi/2 & \text{for } M = m \neq 0 \\ \pi & \text{for } M = m = 0 \\ 0 & \text{for } m \neq M \end{cases}$$

$$(2)\quad \int_{-1}^{1} \mu \,.\, P_n^m(\mu) \,.\, P_N^m(\mu) \,.\, d\mu = \begin{cases} \dfrac{2(n+m+1)!}{(n-m)!\,(2n+1)(2n+3)} & \text{for } N = n+1 \\ 0 & \text{for } N = n \text{ or } N > n+1 \end{cases}$$

$$(3)\quad \int_{-1}^{1} P_n^m(\mu) \,.\, P_N^m(\mu) \frac{\mu}{1-\mu^2}\, d\mu = \begin{cases} \dfrac{(n+2)}{m^2(2n+1)(2n+3)} \cdot \dfrac{(n+m+1)!}{(n-m-1)!} & \text{for } N = n+1 \\ 0 & \text{for } N = n \text{ or } N > n+1 \end{cases}$$

$$= \frac{(n^2-m^2+2n)\,.\,(n+m+1)!}{(n-m)!\,(2n+1)(2n+3)} \text{ for } N = n+1$$

$$(4) \quad \int_{-1}^{1} \frac{\partial}{\partial\mu} P_n^m(\mu)\,.\,\frac{\partial}{\partial\mu} P_N^m(\mu)\,.\,(1-\mu^2)\,.\,\mu\,.\,d\mu$$

$$= 0 \text{ for } N = n \text{ or } N > n+1$$

REFERENCES

AWATANI, J. 1955. J. Acoust. Soc. Amer. **27**: 282.
EMBLETON, T. F. W. 1954. J. Acoust. Soc. Amer. **26**: 40.
KING, L. V. 1934. Proc. Roy. Soc. (London), A, **147**: 212.
LAMB, H. 1932. Hydrodynamics. 6th ed. Cambridge University Press, London.
WATSON, G. N. 1944. Theory of Bessel functions. 2nd ed. Cambridge University Press, London. §13.47.

EVAPORATION NEUTRONS FROM COSMIC RAY NUCLEAR INTERACTIONS IN VARIOUS ELEMENTS[1]

By K. W. Geiger

ABSTRACT

Production of evaporation neutrons from nuclear interactions by cosmic rays is investigated in C, Al, Fe, Cu, Pb, and Bi. Boron trifluoride counters in a paraffin moderator in which the element under study is placed serve to detect the evaporation neutrons. A cosmic ray telescope allows the consideration of ionizing neutron-producing particles separately and it is found that of the total neutrons 14.6% are produced by ionizing particles. The mean neutron multiplicities are worked out and they show an increase with the two-thirds power of the atomic weight of the element in which the interactions take place. Also, the rate of interactions is calculated and this gives the relative interaction cross-sections which are found to increase slightly more with atomic weight than expected if the cross-section is geometric. An estimate of the intensity of the N-component is made and discussed in connection with measurements published by other authors.

I. INTRODUCTION

The component of cosmic radiation capable of producing nuclear interactions, the N-component, is known to consist mostly of fast neutrons and protons. At sea level only a small contribution is due to π-mesons, captured μ^--mesons, fast μ-mesons, and heavy mesons. For the study of the nuclear interactions several methods are available. For example, by the use of nuclear emulsion or cloud chamber the interactions can be observed directly as "stars" when the reaction products are ionizing particles. Another, more indirect, way is the use of neutron counters in a paraffin moderator where the interactions are studied by detection of evaporation neutrons. In particular, the multiplicity of neutrons can be evaluated. The advantage of this method is that it is based on a simple counting procedure and that the material in which the neutron production takes place (hereafter referred to as the producer) is easily interchangeable. The disadvantage is the relatively low neutron counting efficiency in such a recording arrangement which makes the results more difficult to interpret.

Neutron production in lead was first studied by Cocconi Tongiorgi (1949) by whom it was established that nuclear interactions were responsible. A very thorough investigation was made by Cocconi, Cocconi Tongiorgi, and Widgoff (1950) where the production and multiplicity of neutrons from energetic nuclear reactions, capable of emitting at least one penetrating ionizing particle, was studied in three different thicknesses of lead and in aluminum. The authors concluded that owing to the interaction of secondaries a cascade process develops because the average multiplicity of neutrons originating from a lead producer increases with increasing producer thickness. Therefore, it was estimated that the multiplicity for single interactions could only be evaluated when the thickness of the producer is not more than 1/10 of the interaction mean free path of the N-component. In a study of nuclear

[1]Manuscript received November 21, 1955.
Contribution from the Division of Pure Physics, National Research Council, Ottawa, Canada. Issued as N.R.C. No. 3872.

disintegrations by μ-mesons Cocconi and Cocconi Tongiorgi (1951) obtained an average neutron multiplicity in lead of 4.5 due to the entire N-component. Ortel (1954), using a liquid scintillator as well as neutron counters to detect the nuclear interactions directly, found an average neutron multiplicity of 1.3 for carbon. Absolute measurements of the neutron production at sea level were performed by Tobey and Montgomery (1951).

Thus far no systematic study had been made on the variation of multiplicities with different elements in which the disintegrations take place. This, therefore, was the main purpose of the present investigation. In addition, the relative production rates and hence the variation of interaction cross sections with atomic number are evaluated. The total N-component is considered as well as the ionizing part only. The experiment was performed during the period from February to August 1954 in Ottawa, 100 meters above sea level.

II. APPARATUS

The arrangement of neutron counters and of the producer in the paraffin moderator is shown in Fig. 1. The two neutron counters were 6.4 cm. in diameter and had a sensitive length of about 50 cm. They were filled with

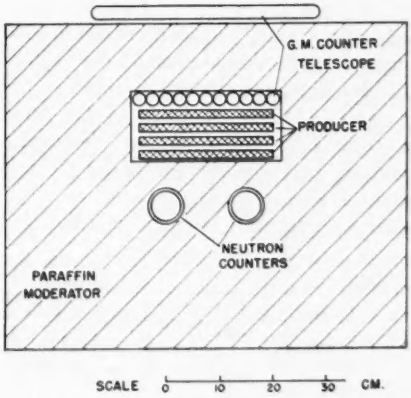

FIG. 1. Arrangement of producer, neutron counters, and cosmic ray telescope in the paraffin moderator.

boron trifluoride (enriched in B^{10}) at a pressure of 60 cm. Hg and the maximum energy of the recorded neutrons was estimated to be about 10 Mev. Therefore, practically, only evaporation neutrons are detected. These are emitted isotropically, as was shown in a similar type of experiment by Cocconi *et al.* (1950). It is known from nuclear emulsion work that evaporation protons are also emitted isotropically (e.g. Harding *et al.* 1949).

The producer area was 25 by 38 cm. and when the material did not take up the full available height of 8.8 cm. the producer was made up in the form of sheets and spaced evenly to avoid corrections due to a changing geometry.

A wide angle cosmic ray telescope placed on top of the producer, with the area of the lower tray slightly greater than the producer area, served as a means for distinguishing between the total and the ionizing neutron-producing component.

The neutron detection efficiency was determined by placing a calibrated 0.1 mc. Ra+Be neutron source at different locations within the producer so that the average efficiency

$$\epsilon = \frac{1}{V}\int_V \epsilon_{x,y,z}\, dxdydz$$

could be worked out. The energy spectra of the neutrons from a Ra+Be source and from the evaporation processes are similar enough to justify this method (Cocconi *et al.* 1950). For 8.3 cm. of lead in the producer space an integrated efficiency of $\epsilon = 1.7\%$ has been found, for all other producer materials and thicknesses an efficiency of 1.5% was determined. The error was estimated to be $\pm 20\%$. The neutron source was only known to $\pm 13\%$, the remainder of the error being due to experimental uncertainties.

The neutrons which come from a nuclear interaction in the producer are slowed down in the paraffin and have a mean life of about 150 μsec. before they are captured in the counters or in the paraffin. Hence neutrons which have a common origin do not reach the counters simultaneously and groups of neutrons arising from one interaction are spread over a time interval comparable with their mean life. The neutrons are detected successively and groups can be resolved. Because of the low efficiency of the arrangement generally only a very few neutrons from one event are detected, but a statistical analysis described later makes it possible to work out the multiplicity.

The electronic circuit is shown in Fig. 2. It can be divided into two parts; one records the neutrons produced by the ionizing and the other by the total

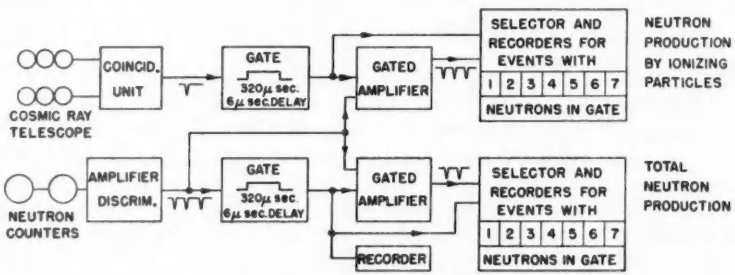

FIG. 2. Block diagram of electronic circuit.

N-component. The amplified neutron pulse after passing through a pulse height discriminator is fed into two gated amplifiers which are normally closed. A coincidence pulse from the telescope after a delay of 6 μsec. triggers a gate pulse, 320 μsec. long, about twice the half-life of neutrons in the paraffin moderator. The amplifier gate is opened for this time, one or more neutron

pulses can pass, and events are selected according to the number of pulses within the gate time. The gate of the second amplifier is opened by the first neutron pulse of any event and all events of more than one neutron detected are analyzed in the second selector. The number of events with one neutron detected can be calculated by subtracting the number of multiple events from the total number of gates which is recorded separately.

All information as well as rates from some auxiliary circuits was fed into message registers. A 20-pen operation recorder was also connected, and proper functioning of the equipment could be verified by analyzing the chart. In addition, the selectors were checked periodically by applying a square wave of known frequency admitted only during the gate opening. This should record an event with the corresponding number of square pulses. Further details on the circuit are given in a previous paper (Geiger and Rose 1954) where similar equipment was used to study the multiplicity of neutron production from the spontaneous fission of uranium.

The limited gate length reduces the neutron counting efficiency. With a mean life of thermal neutrons τ the gate efficiency is

$$f = \frac{1}{\tau}\int_{t_1}^{t_2} e^{-t/\tau}dt$$

where t_1 and t_2 represent the opening and closing time of the gate after the triggering event has taken place. The neutron mean life has been found experimentally to be 154 ± 13 μsec. by using three different gate lengths of 70, 120, and 320 μsec. and comparing the corresponding counting rates. The gate was triggered by an ionizing particle and lead was used as producer.

The slowing-down time of fast neutrons to thermal energies is of the order of the delay until the gate opens, i.e. 6 μsec. (Glasstone and Edlund 1952). Hence, slightly different gate efficiencies are to be expected, depending on whether the gate is opened by a first neutron pulse or a telescope coincidence pulse. In the first case, which applies to the part of the circuit recording total neutron production, t_1 and t_2 are 6 and 326 μsec. respectively and a gate efficiency of $f = 0.84$ was calculated. In the second case, that of the ionizing producing component, the time before the gate opens is used up to slow the neutron down. Therefore, t_1 and t_2 are 0 and 320 μsec. and the gate efficiency is $f' = 0.87$.

III. DATA AND CORRECTIONS

Only neutrons which originate in the producer are of interest and, hence, account has to be taken of neutrons from the paraffin wax and the surrounding material. The counting rate due to the producer alone is

$$R = R_p - R_b + (\Delta R_\infty + \Delta R_w)$$

where R_p is the rate with the producer inserted,

R_b is the background rate without producer,

and the term in brackets takes into account the effect of the presence of the producer on the background rate.

R_b is composed of three parts, namely

$$R_b = R_{Cd} + R_w + R_\infty.$$

R_{Cd} is the rate when the neutron counters are surrounded by cadmium; 23 ± 3 counts per hour have been found, and this was, as expected, practically constant whether a producer was present or not. R_∞ is the rate due to neutrons produced outside the arrangement and diffusing through the wax to the counters, and R_w is that due to neutrons produced by the N-component in the paraffin wax. Absorption or scattering is expected to decrease these contributions when the producer is present.

The influence of the producer on R_∞ is difficult to evaluate. An auxiliary experiment has been performed where a 1 mc. Ra+Be neutron source was placed on the top center of the pile to investigate scattering from the producer. It must, of course, be assumed that the neutron energy spectra from the source and from the surroundings are similar after they have been filtered through 12 cm. of paraffin, the amount on top of the producer space. The observed reduction due to producer scattering is shown in Table I.

TABLE I

SCATTERING OF NEUTRONS ON PRODUCER

Producer		Amount scattered s
C	8.5 cm.	0.37
Al	8.3 cm.	0.29
Fe	3.8 cm.	0.34
Cu	3.8 cm.	0.37
Sn	3.7 cm.	0.19
Pb	1.9 cm.	0.11
Pb	8.3 cm.	0.33
Paraffin	12.7 cm.	0.75

An idea of what fraction of R_∞ is due to diffusing neutrons passing through the producer space was obtained by determining the reduction in counting rate when the space is filled with paraffin. A decrease from 335 to 304 counts per hour was found. The minimum value for neutrons passing through the producer space, therefore, is 31 counts per hour. As the last line in Table I shows, this only represents 75% of the total, and furthermore, the figure is still too low because of neutron production in the carbon of the added paraffin which makes the above-mentioned decrease greater than measured. From these considerations 50 ± 10 counts per hour were estimated. The decrease of the background rate due to insertion of the producer is therefore

$$\Delta R_\infty = 50\, s \text{ (counts per hour)}$$

with s taken from Table I. This correction only applies to the rate of events with single neutrons, produced by the total N-component.

The remaining contribution to the background is R_w. Most of R_w would be due to production in the vicinity of the neutron counters where the detection efficiency is largest. Therefore, from geometrical considerations as well as by taking into account the other contributions to R_b, it was estimated that 40% of R_b or $0.4\times335 = 134$ counts per hour are due to the part of the N-component traversing the producer space. Hence, with the producer present:

$$\Delta R_w = 134(1-e^{-D/\lambda_0}) \text{ (counts per hour)}$$

TABLE II

OBSERVED HOURLY RATES OF EVENTS WITH m NEUTRONS AND CORRECTIONS

Producer		Total production						Production by ionizing particles					
		$m=1$	$m=2$	$m=3$	$m=4$	$m=5$	$m=6$	$m=1$	$m=2$	$m=3$	$m=4$	$m=5$	$m=6$
None	R_0	335±3	3.51±.06	0.14±.02				8.8±.2	0.25±.03				
8.5 cm. C	R_p	350±4	3.66±.18	0.11±.03				9.0±.4	0.23±.05				
(13.1 kgm.)	ΔR	29±6	0.11±.02					0.6±.1	0.02				
	R	44±8	0.26±.15	0				0.8±.5	0				
8.3 cm. Al	R_p	374±4	4.07±.12	0.12±.02				13.1±.5	0.36±.04				
(21.6 kgm.)	ΔR	28±6	0.14±.03	0.01				0.8±.2	0.02				
	R	67±8	0.70±.14	0				5.1±.6	0.13±.05				
3.8 cm. Fe	R_p	414±4	5.26±.23	0.28±.05				17.7±.4	0.46±.05	0.05±.02			
(29.0 kgm.)	ΔR	32±6	0.15±.03	0.01				0.9±.2	0.03	0			
	R	111±8	1.90±.25	0.15±.06				9.8±.5	0.24±.08	0.05±.02			
3.8 cm. Cu	R_p	433±5	6.75±.24	0.24±.05				20.5±.5	0.55±.07	0.06±.02			
(32.8 kgm.)	ΔR	36±7	0.18±.04	0.01				1.0±.2	0.03	0			
	R	134±9	3.42±.26	0.11±.06				12.7±.6	0.33±.08	0.06±.02			
3.7 cm. Sn	R_p	465±5	10.81±.38	0.56±.09	0.04			23.5±.5	1.45±.14	0.12±.04			
(26.2 kgm.)	ΔR	22±4	0.13±.03	0.01				0.7±.2	0.02	0			
	R	152±7	7.43±.40	0.43±.10	0.04			15.4±.6	1.22±.15	0.12±.04			
1.9 cm. Pb	R_p	471±5	13.1±.3	0.93±.08	0.09±.02			21.9±.4	1.56±.10	0.21±.04			
(20.9 kgm.)	ΔR	14±3	0.1	0.01	0			0.5±.1	0.01	0			
	R	150±7	9.7±.3	0.80±.09	0.09±.02			13.6±.5	1.32±.12	0.21±.04			
Bi in chips	R_p	540±6	19.7±.3	1.59±.09	0.16±.03	0.06±.02		31.0±.5	2.46±.10	0.40±.05	0.09±.02		
(33.2 kgm.)	ΔR	22±4	0.1	0.01	0	0		0.8±.2	0.02	0	0		
	R	227±8	16.3±.4	1.46±.10	0.16±.03	0.06±.02		23.0±.7	2.23±.12	0.40±.05	0.09±.02		
8.3 cm. Pb	R_p	806±8	53.7±.6	6.72±.15	1.26±.06	0.34±.04	0.10±.02	60.9±.7	7.80±.15	1.66±.07	0.49±.04	0.18±.03	0.048±.012
(90.4 kgm.)	ΔR	52±10	0.4±.1	0.02	0	0	0	2.1±.4	0.06±.02	0	0	0	0
	R	523±13	50.6±.7	6.60±.16	1.26±.06	0.34±.04	0.10±.02	54.2±.9	7.61±.16	1.66±.07	0.49±.04	0.18±.03	0.048±.012

$\Delta R = \Delta R_w + \Delta R_\infty$.

where D is the thickness of the producer and λ_a the absorption mean free path of the N-component.

Since the ionizing N-component is confined to the producer space by the cosmic ray telescope it was estimated that 90% of $R_{b,i}$ (production by ionizing particles) is affected by the presence of the producer:

$$\Delta R_{b,i} = 7.9(1-e^{-D/\lambda_a}) \text{ (counts per hour).}$$

Table II shows the observed hourly rates of events consisting of a group of m neutrons and also the background corrections. It can be seen that the influence of the producer on the background is small for producers of high atomic weight but is appreciable for carbon and aluminum.

R_p further includes small corrections for neutron pulses which fall into the gate accidentally. Barometric corrections were also included which, however, were small since the rates are averages over about seven days distributed over the whole time during which the experiment was performed. This brought the average pressure for those days near to the mean for the whole time.

The quoted errors are statistical, with a minimum error of $\pm 1\%$ to take account of variations of the intensity of the N-component. During the months this investigation was performed solar activity was low. Time variations of the N-component, as observed by Rose (private communication) at the same location, were small enough to justify such a small error.

IV. DIRECTIONAL INTENSITY OF IONIZING NEUTRON-PRODUCING RADIATION

When the total nuclear component is studied the producing particles can enter the producer from all directions. However, for particles which have to go through the cosmic ray telescope the angle is limited and the zenith angle distribution has to be known to apply the necessary correction. A simple method for obtaining the directional intensity is to take the counting rate as a function of the height of the top telescope tray. The cosmic ray intensity from the zenith angle θ is assumed to be $I = I_v \cos^n\theta$, using I_v for the vertical intensity. The total flux per unit sphere is then

$$(1) \qquad J_0 = 2\pi I_v \int_0^{\pi/2} \cos^n\theta \sin\theta \, d\theta = 2\pi I_v (n+1)^{-1}.$$

The vertical intensity can be determined:

$$I_v = \frac{d^2}{A_1 \times A_2} R, \qquad d \to \infty,$$

where d is the distance between the two telescope trays, A_1 and A_2 their areas, and R the observed neutron counting rate. In the present case, a lead producer, 5.7 cm. thick, has been used and the rate without producer subtracted. A lower limit for the total flux was determined by increasing the top tray area by a factor of two. This was done by moving the top tray to one side so that it covered half of the producer and multiplying the coincidence rate by two. The use of the lower tray only to trigger the gate is not suitable because of the possibility that fast neutrons change into protons within the paraffin

between the trays. After corrections for accidentals and barometric effect the following intensities were obtained:

$$I_v = 0.070 \text{ hr.}^{-1} \text{ cm.}^{-2} \text{ sterad.}^{-1}, \qquad J_0 = 0.069 \text{ hr.}^{-1} \text{ cm.}^{-2}.$$

These values do not represent the actual intensities of the ionizing part of the N-component because of multiple neutron production and the limited neutron counting efficiency. An exponent of $n = 5.4 \pm 0.6$ follows by inserting these values into formula (1).

A different approach, avoiding the use of the total flux, can be chosen. The integral in (1) extends over one half solid angle. When the rate is taken with the trays positioned as in Fig. 1, n can be found when I_v and the solid angle over which to integrate are known:

$$J_{0,t} = 2\pi I_v \int_0^{\theta'} \cos^n\theta \sin\theta \, d\theta \tag{2}$$

where $J_{0,t}$ represents the neutron rate in that geometry. θ' could be found from an auxiliary experiment on the total ionizing cosmic ray component capable of penetrating the paraffin within the telescope. For this component the exponent is known to be near $n = 2$ (Voisin 1950) and also has been determined experimentally using the method described in the previous paragraph to be $n = 2.1 \pm 0.2$. To obtain θ' the lower tray was placed in the center height of the producer space to simulate the angle in which the ionizing neutron-producing particles are admitted. $\theta' = 40°$ followed using a formula corresponding to (2) but for the intensity per unit area. Therefore

$$\frac{J_{0,t}}{2\pi I_v} = \int_0^{\theta'=40°} \cos^n\theta \sin\theta \, d\theta = \int_{\cos\theta'=0.766}^{1} \cos^n\theta \, d(\cos\theta) \tag{3}$$

$$= \frac{1}{n+1}(1 - 0.766^{n+1}).$$

With $J_{0,t} = 0.057$ hr.$^{-1}$ cm.$^{-2}$ the same result as before, namely $n = 5.3 \pm 0.6$, has been found.

The result can be compared with a value for protons of $n \sim 5$, given by Mylroi and Wilson (1951), which applies to protons having an energy of from 400 Mev. upwards. It is believed that most of the neutrons in the present experiment are produced by protons within that energy range. The exponent is energy dependent, being high, approximately 7, for very fast protons for which angular deviations after interactions are small, and n is based purely on the collimation due to absorption along different proton path lengths through the atmosphere.

To make the neutron production rate due to the ionizing component equivalent to that from the total, the former has to be multiplied by a factor

$$J_0/J_{0,t} = 1.21$$

to take account of the limited telescope angle.

V. ANALYSIS AND RESULTS

As pointed out under II the number of neutrons m in a recorded event, or recorded multiplicity, is not the actual neutron multiplicity from nuclear interaction, owing to the low neutron detection efficiency. Two slightly different approaches for the analysis have to be made according as the gate is opened by the first neutron pulse (total producing component) or by a telescope coincidence pulse (ionizing producing component).

(*a*) *Total producing component.*—The probability that k of ν neutrons released from one interaction are detected in the counters follows a binomial distribution

$$P(k, \nu) = \binom{\nu}{k} \epsilon^k (1-\epsilon)^{\nu-k}, \qquad \nu \geqslant k, \tag{4}$$

with ϵ being the neutron detection efficiency. Similarly, if a total of k neutrons is detected and the gate is opened by the first neutron, the probability that m of these k neutrons fall within the gate is

$$P(m, k) = \binom{k-1}{m-1} f^{m-1}(1-f)^{k-m}, \qquad k \geqslant m, \tag{5}$$

where f is the gate efficiency. The aim is to work out the average multiplicity $\bar{\nu}$ from the nuclear interactions. To simplify the analysis an assumption for the shape of the multiplicity spectrum has to be made. Following Cocconi *et al.* (1950, 1951) an exponential multiplicity spectrum has been used. The justification for its use in the present case will be seen later. Thus,

$$I(\nu) = (e^a - 1)\, e^{-a\nu} \text{ where } \sum_1^\infty I(\nu) = 1.$$

The average multiplicity is

$$\bar{\nu} = \sum_1^\infty \nu(e^a - 1)\, e^{-a\nu} = \frac{1}{1-e^{-a}}, \qquad \bar{\nu} = \frac{1}{a} + 0.5, \qquad a \ll 1.$$

The observed rate of events with m neutrons becomes therefore

$$R_m = Q \sum_{\nu=m}^\infty \sum_{k=m}^\infty I(\nu)\, P(k, \nu)\, P(m, k)$$

with Q being the rate of the interactions. This summation can be evaluated:

$$R_m = Q \frac{(e^a - 1)\epsilon^m f^{m-1} e^{-am}}{[1-(1-\epsilon)e^{-a}][1-(1-\epsilon f)e^{-a}]^m}.$$

To evaluate a and therefore $\bar{\nu}$ it is convenient to use the logarithmic form of this equation and to differentiate it with respect to m

$$\frac{d \log R_m}{dm} = \log \epsilon f - a \log e - \log[1-(1-\epsilon f)e^{-a}]. \tag{6}$$

This shows that R_m versus m should be a straight line when plotted on semi-logarithmic paper, the slope being a function of the mean neutron multiplicity.

(*b*) In the case of a charged particle opening the gate the limited gate length decreases the neutron detection efficiency and in (4) k can be replaced by m and ϵ by $\epsilon f'$. Equation (5) need not be used. Therefore

$$R_m = Q\sum_{\nu=m}^{\infty} I(\nu)\, P'(m, \nu),$$

which after summation gives

$$R_m = Q\frac{(e^a-1)(\epsilon f')^m e^{-am}}{[1-(1-\epsilon f')e^{-a}]^{m+1}}$$

or

$$\frac{d \log R_m}{dm} = \log \epsilon f' - a \log e - \log[1-(1-\epsilon f')e^{-a}]. \tag{7}$$

This also represents a straight line on a semilogarithmic plot. The slope is equal to that given in (6) apart from the differences between f and f'.

Further, it is of interest to know the actual rate of interactions taking place

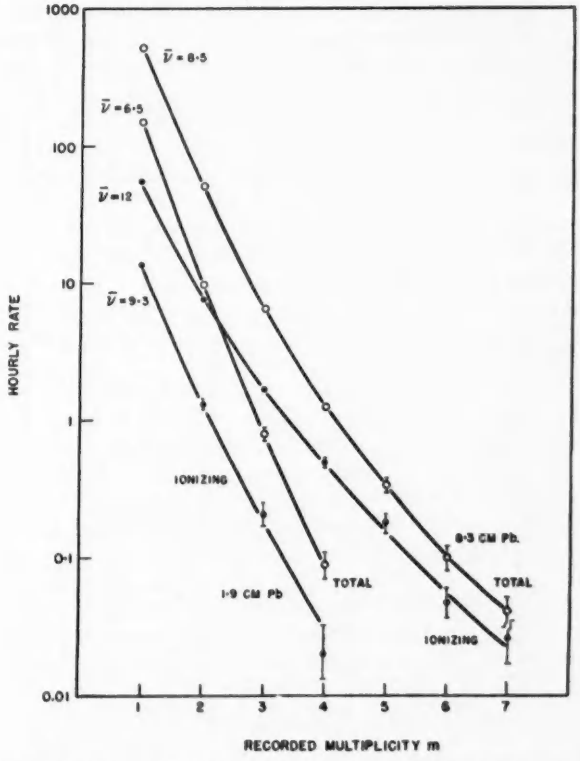

FIG. 3. Data on lead in semilogarithmic plot. The first two points of the curves have been used to work out the multiplicities.

in the producer. The rate can be taken from the formulae above or, more simply, is given by

$$Q = N/\bar{\nu}\epsilon$$

where N is the total neutron rate. N can be taken from the data by adding up the rates multiplied by m and correcting for the gate efficiency. In the case of neutrons produced by the ionizing cosmic ray component N has been multiplied by the factor 1.21 to take account of the limited telescope angle as described in Section IV.

Fig. 3 represents the experimental data of Table II for 1.9 and 8.3 cm. thickness of lead on a semilogarithmic plot. If the assumed exponential multiplicity spectrum is correct straight lines should appear on the graph. This is not the case for 8.3 cm. of lead where the curve flattens out, the expected effect due to cascades of nuclear interactions as concluded by Cocconi *et al.* (1950). A reasonably straight line is obtained with 1.9 cm. of lead. The remaining slight curvature is assumed to be due to non-uniformity of neutron detection efficiency over the whole of the producer. The number of cascades

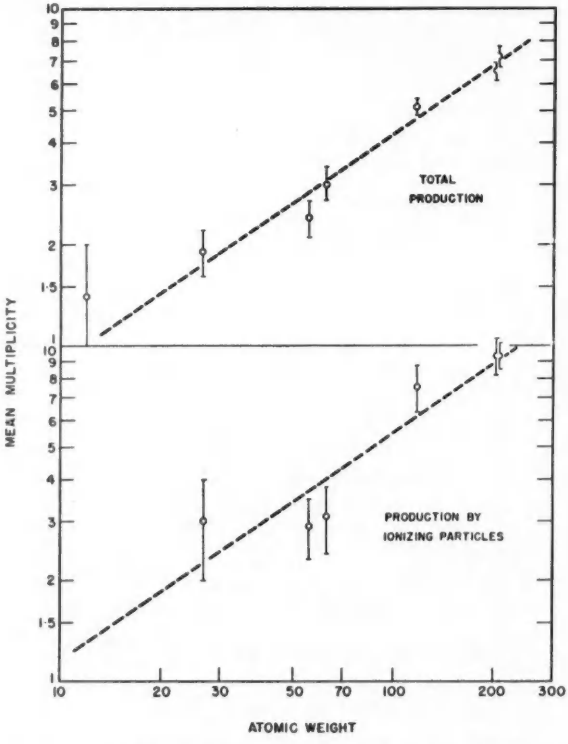

FIG. 4. Average multiplicity versus atomic weight of producer. The following elements ave been used: C, Al, Fe, Cu, Sn, Pb, and Bi. The dotted lines represent $A^{2/3}$.

must be very small, the lead thickness being one-eighth of the collision mean free path of about 160 gm./cm.^{2} Also, in contrast to the experiment of Cocconi *et al.* (1950) which discriminated against low energy events, all neutron-producing nuclear interactions are included, the low energy ones, not capable of producing cascades, being the most frequent. For the producer materials as listed in Table II, in order to eliminate cascades, reasonably small thicknesses were always used, thereby sacrificing some statistical accuracy due to lower neutron production. To calculate the mean multiplicities the slope through the two points R_1 and R_2 has been used which is thought to give the most realistic value for the multiplicities.

Fig. 4 shows two graphs in double-logarithmic form representing the mean multiplicities for total and for ionizing production as a function of the mass number of the producer. For lead, here as well as in the following graphs, only the values from 1.9 cm. thickness are included. The dotted lines have, tentatively, been drawn according to an $A^{2/3}$-dependence, and this fits the experimental points quite well.

The errors for $\bar{\nu}$ as given in Fig. 4 include only the statistical error from the measured rates and not the uncertainty for the neutron detection efficiency, the purpose of this work being not so much to obtain absolute figures as their comparison for a variety of elements. When account is taken of the additional error the mean multiplicity for neutrons produced by the total N-component in this lead ($\bar{\nu} = 6.5$) compares reasonably well with the value measured by Cocconi and Cocconi Tongiorgi (1951) of 4.5 or with Ortel's (1954) value of 6. Ortel also gave a value for carbon of 1.3 which is in good agreement with the present value of 1.4.

As expected, the average multiplicity was found to be higher for neutrons produced by the ionizing component than for neutrons produced by the neutral part of the N-component (or the total N-component), the figures for 1.9 cm. of lead being 9.3 (ionizing) and 6.5 (total). This difference is well known from nuclear emulsion work (Brown *et al.* 1949), the stars with only a few prongs being mostly produced by neutral particles. At higher particle energy (many-prong stars) the relative number of stars generated by ionizing and non-ionizing interacting particles is about equal. Similarly in the present experiment, the rates for the neutron groups R_1, R_2, etc. approach a ratio of 1: 2, for ionizing to total production, as the number of neutrons in the group becomes large (see Table II). The explanation for this is as follows: The nuclear interactions are mostly caused by fast neutrons and protons which are produced locally. The interaction mean free path for these particles in air is close to the geometric mean free path of 68 gm./cm.^{2} It can be assumed that the number of fast protons and neutrons produced in the air is equal. The protons undergo ionization losses which rise quickly when the proton energy falls below 500 Mev., the range then being comparable to the mean free path for nuclear interactions. Only the energetic protons survive and are capable of producing further nuclear interactions. The average energy of the protons, therefore, is higher than that of the fast neutrons.

For the same reason the number of neutrons produced by the total N-

component must be more than twice as high as the number of neutrons produced by the ionizing N-component only. This is shown in Fig. 5 which represents the rate for the total neutron production for both cases as a function of the atomic weight of the producer. Taking the mean of the data on neutron production for the heavier elements (from Sn up) where the accuracy is not too low, 14.6% of the total neutron production is due to the ionizing component. This compares well with 13%, a figure which can be taken from data as given by Hogrebe (1952) for lead. The figure quoted in that paper (18.5%) is not suitable for comparison because it is based on production at infinite

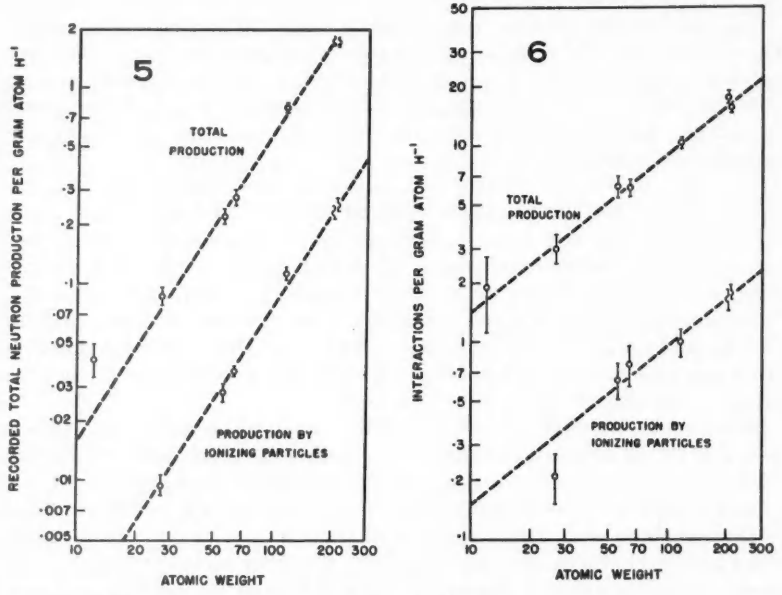

FIG. 5. Total number of neutrons versus atomic weight.
FIG. 6. Number of interactions per gram atom per hour versus atomic weight. This is proportional to the neutron production cross-section. The slope of the dotted line is taken from Fox *et al.* (1950).

lead thickness, there being appreciably different absorption mean free paths for total and ionizing N-component. For very energetic interactions Cocconi *et al.* (1950) have shown that the neutron production is about equally divided between neutral and ionizing particles. This is in agreement with the above considerations.

It is of interest to show the relative rates for the two types of interactions Q. Assuming the same interaction cross-sections for the neutral and ionizing N-components the ratio of their intensities must be equal to the ratio of the corresponding interactions. In Fig. 6 the rates of interactions per gram atom are drawn against atomic weight of the producer and 10.5% of the interactions

have been found to be due to the ionizing N-component. The interaction rate per gram atom is proportional to the interaction cross-section of the nuclei and hence Fig. 6 gives also the variation of cross-section with mass number. A geometric cross-section would require an $A^{2/3}$-dependence. Actually, the dashed lines have been drawn following the variation of total neutron cross sections as measured by Fox *et al.* (1950) for artificially produced neutrons of 280 Mev. They are somewhat steeper than $A^{2/3}$ which might be expected owing to transparency of nuclei of low atomic weight.

VI. SUMMARY AND DISCUSSION

The production of evaporation neutrons by cosmic rays in different materials has been studied and a distinction has been made between the ionizing and the total N-component. It has been shown that fast neutrons are the most abundant part of the N-component confirming observations with photographic plates.

The mean multiplicities of the evaporation neutrons and the rates of nuclear interactions were evaluated on the basis of an exponential neutron multiplicity spectrum. The mean multiplicities have been found to increase as the two-thirds power of the mass number of the producer material. For a theoretical consideration the conditions in the present experiment are rather complicated because of the fact that the incident neutron-producing particles are not monoenergetic. Jackson (private communication) computed the mean number of evaporation neutrons versus incident nucleon energy for mass numbers >100 using excitation energies (McManus, Sharp, and Gellman 1954) obtained with the Monte Carlo method. For energies of the incident particles between 90 and 160 Mev. these calculated values follow closely an $A^{2/3}$-law and are also in satisfactory agreement with the absolute values as given in Fig. 4 for the production by the total N-component. The average energy for incident neutrons is of this order as it can be taken from a graph given by Rossi (1952) for the computed energy spectrum of neutrons in air and considering only neutrons above 30 Mev. Not many interactions with neutron production could be expected below that energy.

The number of interactions per gram atom of producer material, which is proportional to the interaction cross-section, has been found to increase somewhat more steeply with the mass number of the producer material than expected if the cross-section is geometric. This indicates a certain transparency for lighter nuclei.

Using the data from the 1.9 cm. lead producer the intensity of the part of the N-component capable of producing nuclear interactions with emission of evaporation neutrons can be estimated. The omnidirectional intensity is:

$$J_{\square} = \frac{n+1}{n+2}\frac{Q}{W}\lambda_{\text{int}}.$$

The factor $(n+1):(n+2)$ converts the intensity per unit sphere to intensity per unit area. The value of n is not known but has been assumed to be 5. λ_{int} is the interaction mean free path for the N-component in lead. Lacking other information λ_{int} has been assumed to be geometric (160 gm./cm.^{2}).

Q/W is the number of interactions per gram of lead and is 0.24×10^{-4} gm.$^{-1}$ sec.$^{-1}$. Therefore, the omnidirectional intensity becomes

$$J_{\square} = 33\times10^{-4}\ \text{sec.}^{-1}\,\text{cm.}^{-2}$$

with an estimated error of $\pm30\%$. This represents the intensity at sea level since the roof and the paraffin on top of the producer consist of about 15 gm./cm.^{2} of light material, and cancels with the difference in atmospheric depth to sea level (13 gm./cm.^{2}). The figure agrees with $J_{\square} = 40\times10^{-4}$ sec.$^{-1}$ cm.$^{-2}$ as given by Cocconi and Cocconi Tongiorgi (1951) who use the same value for the interaction mean free path. As pointed out in their paper this value is also consistent with estimates for the intensity of the N-component as deduced from star production in nuclear emulsions and from measurements of neutron production in the free atmosphere.

A similar calculation can be applied to the ionizing part of the N-component. Not all of the interactions are caused by protons. The main additional contribution is due to nuclear absorption of μ^--mesons which is followed by neutron emission. The number of stopped μ^--mesons in the 1.9 cm. lead producer can be worked out. According to the differential range spectrum of mesons at sea level as given by Rossi (1948) the number of μ^--mesons stopped in air is $I_{v,\mu^-} = 2\times10^{-6}$ gm.$^{-1}$ sec.$^{-1}$ sterad.$^{-1}$. Then, the number of μ^--mesons stopped in the lead producer and passing through the cosmic ray telescope, the effect of which is given by equation (3), is

$$J_{0,\mu^-} = \frac{2\pi}{n+1}(1-0.766^{n+1})\,\frac{I_{v,\mu^-}}{\rho}\,W$$

where $\rho = 1.7$ is the equivalent absorber thickness of lead relative to air, W the weight of the producer (20.9 kgm.), and $n = 3$ has been assumed for slow mesons (Voisin 1951). Practically all of these stopped μ^--mesons are captured in a lead nucleus followed on the average by the emission of 2.14 neutrons (Widgoff 1953). Assuming again an exponential multiplicity spectrum, this would give a rate $R_1 = 2.6$ and $R_2 = 0.04$ which would change the values for 1.9 cm. of lead to $R_1 = 11.0$ and $R_2 = 1.28$ in the row for production by ionizing particles in Table II. This brings the average multiplicity up to $\bar{\nu} = 11$ and the interaction rate down from $Q = 166$ to $Q = 116$ per hour.

The number of interactions due to fast μ-mesons is very small. A rate of $Q = 7$ hr.$^{-1}$ is due to them, using an interaction cross section of 1×10^{-29} cm.^{2}/nucleon and the above multiplicity.

Neglecting interactions due to π-mesons the number of which in air at sea level is very small and neglecting also interactions due to photons accompanied by an electron which triggers the cosmic ray telescope, the rate of interactions which are thought to be initiated by protons is $Q = 109$ hr.$^{-1}$. With $\lambda_{\text{Int}} = 160$ gm./cm.^{2} and $n = 5$ the vertical proton intensity is

$$I_{v,p} = \frac{n+1}{2\pi}\,\frac{Q}{W}\,\lambda_{\text{Int}} = 2.3\times10^{-4}\ \text{sec.}^{-1}\,\text{cm.}^{-2}\,\text{sterad.}^{-1}.$$

This figure applies to protons with a lower momentum limit of 550 Mev./c which is given by absorption in the paraffin on top of the producer and in the

roof. The same considerations as in the case of the total N-component apply making the above figure the sea level intensity.

The figure can be compared with the vertical intensity as derived from experimental determinations of the differential proton spectrum. Up to 10^3 Mev./c Ogilvie (1955) draws a spectrum through his own measured points and gives those of previous authors. From 550 Mev./c to 10^3 Mev./c the value $I_{v,p} = 0.65 \times 10^{-4}$ sec.$^{-1}$ cm.$^{-2}$ sterad.$^{-1}$ can be taken from his graph. Mylroi and Wilson (1951) give the intensity for momenta above 10^3 Mev./c with $I_{v,p} = 0.55 \times 10^{-4}$ sec.$^{-1}$ cm.$^{-2}$ sterad.$^{-1}$. Therefore, at sea level, the vertical intensity of protons above the energy limit set by the absorber on top of the producer is $I_{v,p} = 1.20 \times 10^{-4}$ sec.$^{-1}$ cm.$^{-2}$ sterad.$^{-1}$.

Although good agreement with the figure derived from the present experiment can not be claimed, it must be considered that experimental errors are quite high. It is felt that because of the various, not too well known, factors entering the calculation, the present determination can be out by as much as $\pm 50\%$. Also, there is a considerable spread in the intensity determinations by different authors as shown by Ogilvie in his graph.

It is generally assumed that nearly all nuclear interactions which are produced by non-ionizing particles are due to neutrons. Therefore, Q(total) represents reasonably well the interaction rate when Q(ion.) is subtracted. But Q(ion.) is not entirely due to protons and an appreciable proportion is due to other ionizing particles of which the N-component is composed. For heavier elements, where nuclear absorption of μ^--mesons is important, this is the main additional contribution. One therefore has to bear in mind that the results which are given in Section V for the ionizing N-component do not apply to the cosmic ray protons only but to a mixture of various ionizing particles.

ACKNOWLEDGMENT

The author wishes to thank Dr. D. C. Rose for his encouragement and helpful advice.

REFERENCES

BROWN, R. H., CAMERINI, U., FOWLER, P. H., HEITLER, W., KING, D. T., and POWELL, C. F. 1949. Phil. Mag. **40**: 862.
COCCONI, G. and COCCONI TONGIORGI, V. 1951. Phys. Rev. **84**: 29.
COCCONI, G., COCCONI TONGIORGI, V., and WIDGOFF, M. 1950. Phys. Rev. **79**: 768.
COCCONI TONGIORGI, V. 1949. Phys. Rev. **76**: 517.
FOX, R., LEITH, C., WOUTERS, L., and MACKENZIE, K. R. 1950. Phys. Rev. **80**: 23.
GEIGER, K. W. and ROSE, D. C. 1954. Can. J. Phys. **32**: 498.
GLASSTONE, S. and EDLUND, M. C. 1952. The elements of nuclear reactor theory. D. Van Nostrand Company, Inc., Toronto, New York, London. p. 184.
HARDING, J. B., LATTIMORE, S., and PERKINS, D. H. 1949. Proc. Roy. Soc. (London), A, **196**: 325.
HOGREBE, K. 1952. Z. Naturforsch. **7a**: 772.
JACKSON, J. D. Private communication.
MCMANUS, H., SHARP, W. T., and GELLMAN, H. 1954. Phys. Rev. **93**: 924. Abstr. K2.
MYLROI, M. G. and WILSON, J. G. 1951. Proc. Phys. Soc. A, **64**: 404.
OGILVIE, K. W. 1955. Can. J. Phys. **33**: 746.
ORTEL, W. C. G. 1954. Phys. Rev. **93**: 561.
ROSE, D. C. Private communication.
ROSSI, B. 1948. Revs. Mod. Phys. **20**: 537.
——— 1952. High energy particles. Prentice-Hall, Inc., New York. p. 489.
TOBEY, A. R. and MONTGOMERY, C. G. 1951. Phys. Rev. **81**: 517.
VOISIN, A. G. 1950. Compt. rend. **230**: 1396.
——— 1951. Can. J. Phys. **29**: 505.
WIDGOFF, M. 1953. Phys. Rev. **90**: 891.

THE BEHAVIOR OF FERROMAGNETICS UNDER STRONG COMPRESSION[1]

By F. D. Stacey

ABSTRACT

Specimens in the form of thin disks have been subjected to strong compression simultaneously with high magnetic fields by means of a new design of permeameter, with which their magnetizations have been measured. Magnetization curves extending to saturation have been plotted for a number of materials at (non-hydrostatic) pressures up to 10,000 atmospheres. The most interesting result is the strong increase in saturation magnetization shown by nickel and the nickel–copper alloys.

1. INTRODUCTION

The application of high magnetic fields to materials under hydrostatic pressure presents technical difficulties which have led to several compromises. The measurements of Yeh (1925) and Steinberger (1933) were not extended above 100 oersteds, while the method used by Ebert and Kussmann (1937) can be shown to be invalid because they measured the changes in the total flux caused by interchanging specimens in the field gap of an electromagnet with saturated pole-pieces.

Another approach was suggested by Bridgman's (1950) method of applying high pressures to foils compressed between massive anvils. This does not produce hydrostatic pressures, but the present work has shown that there is an important hydrostatic component to the compression of soft specimens.

The surprising increase in the saturation magnetization of nickel, compressed in this manner, has been reported previously by Jones and Stacey (1953). Measurements have now been made on the ferromagnetic nickel–copper alloys and a number of other metals, showing that this effect is a characteristic both of pure nickel and of nickel–copper alloys.

2. EXPERIMENTATION

The permeameter was a low reluctance magnetic circuit, machined from black mild steel, and shown assembled in Fig. 1. Specimens were disks of foil inserted between the pole-pieces through one of two circular openings in the outer case, and pressure was applied to them by placing the whole system between the anvils of a hydraulic press. The compression of the specimens was estimated from the oil pressure in the press, assuming that the total force on the piston was transferred to the specimens. A correction for friction of the piston was avoided by allowing a small leak of oil past it, the oil pressure being maintained by a backing of nitrogen.

Magnetizing direct currents between 2 and 60 ma. were passed through the primary windings, totalling 3000 turns, in series with the primary coil of a standard variable mutual inductance. The mutual inductances M_1 and M_2

[1]Manuscript received November 4, 1955.
Contribution from the Department of Physics, University of British Columbia, Vancouver, B.C.

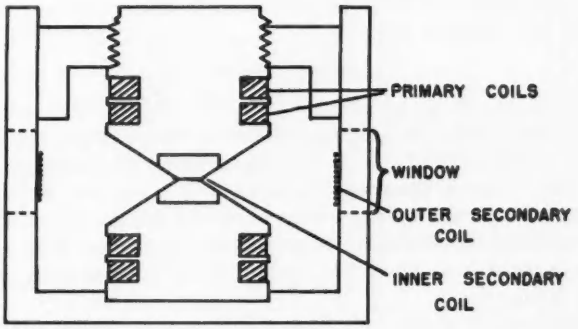

FIG. 1.

between the primary and each of the secondary coils of the permeameter were measured by the automatic reversal of the primary current with each of the secondary coils connected in series opposition to the secondary of the inductometer and to a ballistic galvanometer of fairly long time constant. These measurements were used to calculate the flux through the specimens and through the whole permeameter. The magnetizing current, i, was measured by balancing the voltage across a resistance box in the primary circuit against a standard cell.

Each secondary coil on the permeameter had 10 turns, giving a low resistance to the secondary circuit and strong damping to the galvanometer. This facilitated the direct measurement of the impure (iron-cored) inductances between the permeameter coils by balancing them against the pure (air-cored) inductance of the inductometer. At each reversal of the primary current the galvanometer first showed a sharp deflection which was reversed and returned to a sudden stop, the final deflection indicating the extent to which the bridge was off balance.

Complete reproducibility was obtained by beginning measurements on each specimen with the highest pressure, and, at each pressure, subjecting the system to a cycling demagnetization process before taking readings.

3. ANALYSIS OF READINGS

The magnetic intensity in a specimen is given by

$$B = iM_1/n_2a, \tag{1}$$

where i is the primary current, M_1 is the mutual inductance between the primary coil and the inner secondary of n_2 turns, and a is the specimen area. There is a small correction for the flux outside the specimen but enclosed by the inner secondary coil.

A consideration of the reluctances of the different parts of the magnetic circuit gives an expression for the relation between the flux through the specimen, which is measured by M_1, and the flux through the whole permeameter, measured by M_2, the mutual inductance between the primary and

the outer secondary. It is convenient to make the specimen reluctance the subject of the resulting equation:

$$\frac{t}{\mu a} = A\,\frac{(M_2/M_1)-(M_2/M_1)_0}{1-\alpha[(M_2/M_1)-(M_2/M_1)_0]}. \tag{2}$$

t and μ are the thickness and permeability of the specimen, $(M_2/M_1)_0$ is the value of the ratio M_2/M_1 observed with no specimen (at the same value of (iM_1) or flux through the pole-piece tips), and A is a constant. α is a small correcting factor which takes account of the air flux measured with M_1 and of the fact that the pole-piece reluctances vary slightly with specimen reluctance. Since A is a calibration constant of the apparatus a is conveniently included in it.

The constants A, α, and $(M_2/M_1)_0$ of equation 2 are characteristics of the permeameter, being functions of both pressure and flux. Calibration tests were made with standard thicknesses of copper so that graphs of these constants against (iM_1) were plotted for each of nine pressures. Tests at constant magnetic flux and pressure with seven thicknesses of copper gave exact fitting to equation 2.

Equations 1 and 2 are sufficient to determine the intensity of magnetization, I, and field, H, in a specimen, since:

$$H = B\frac{1}{\mu}, \text{ and} \tag{3}$$

$$I = \frac{B}{4\pi}\left(1-\frac{1}{\mu}\right). \tag{4}$$

Specimen thicknesses were between 0.002 cm. and 0.02 cm. and were measured with a micrometer, with an accuracy very much less than that of the other measured quantities i, M_1, and M_2, which were determined to one part in 10^4 or better. A method was devised of correcting for the errors introduced to the results by inaccuracies in the measurements of specimen thicknesses, so that the micrometer values were needed only as a first approximation.

For the non-magnetic specimens no measurement of t was needed since a direct comparison of specimen reluctances with and without pressure showed that the susceptibilities were unaltered, within the limits of the experiment (Jones and Stacey 1953).

If the micrometer value, t', for the thickness of a magnetic specimen was related to the accurate value, t, by:

$$t = t'(1+\epsilon),$$

then all of the values of permeability calculated from this were also in error:

$$\frac{t'}{\mu'} = \frac{t}{\mu} = \frac{t'(1+\epsilon)}{\mu}, \qquad \frac{1}{\mu'} = \frac{1+\epsilon}{\mu}.$$

In high fields the specimen was saturated, so that from equations 1 and 4:

$$\frac{d}{d(iM_1)}\left\{iM_1\left(1-\frac{1}{\mu}\right)\right\} \to 0$$

whereas:

$$\frac{d}{d(iM_1)}\left\{iM_1\left(1-\frac{1}{\mu'}\right)\right\} \rightarrow -\epsilon \tag{5}$$

so that if, instead of saturating in high fields, the specimen appeared to give a linear increase in I with (iM_1), according to equation 5, the correcting factor $(1+\epsilon)$ for t' was immediately obtained.

Frequent rupture of the inner secondary coil caused a slight revision of the method, so that once calibrations had been completed measurements with this coil were no longer necessary. A further consideration of the reluctances of the magnetic circuit yielded:

$$M_1 = CM_2 - D \tag{6}$$

where C and D are constants for which calibrations were obtained in the same way as for A and α in equation 2. Tests with permalloy, nickel, and copper specimens showed that equation 6 was adequate for the determination of M_1 from M_2.

Calibration of the apparatus was found to be constant after the first few applications of pressure. As a check on the method, measurements of specimen flux and magnetomotive force were made with a fluxmeter and a magnetic potentiometer, which gave the same results within the limits of their accuracy.

4. NICKEL AND NICKEL-COPPER ALLOYS

The magnetizations of nickel–copper alloys with 0 to 25% copper were increased by pressure at all pressures and in all fields. Fig. 2, which shows the effect of pressure on the maximum permeability of nickel, gives an indication of the nature of the compression imposed upon the specimens. The graphs show the effects of three types of compression, linear (Ewing 1900), hydrostatic (Yeh 1925), and the clearly intermediate type of the present work.

Further evidence about the nature of the compression was obtained from the non-magnetic specimens, which were shown to remain non-magnetic up to 10,000 atm. (Jones and Stacey 1953). The values of t/μ obtained with specimens of different hardnesses reflected the elastic compression of the specimens, which appeared to be governed by an elastic modulus intermediate between Young's modulus and bulk modulus. Correction for this effect has been made to the results obtained with all the magnetic specimens.

The saturation magnetizations of nickel–copper alloys have been found to increase markedly with compression, the increase depending upon the copper content, as indicated in Fig. 3, where the proportions of copper are given in atomic percentages.

Measurements were also made on a series of six nickel–copper alloys with 29.1 to 33.5 atomic per cent copper. These alloys showed very little ferromagnetism at room temperature, which is comparable with their Curie temperatures. A small increase with pressure was observed in the saturation magnetization of the 29.1% alloy, but in the others the effect was small enough to be masked by experimental error. This means that within the limits of the experiment, $\pm 5°$ C., pressure was not observed to affect the Curie

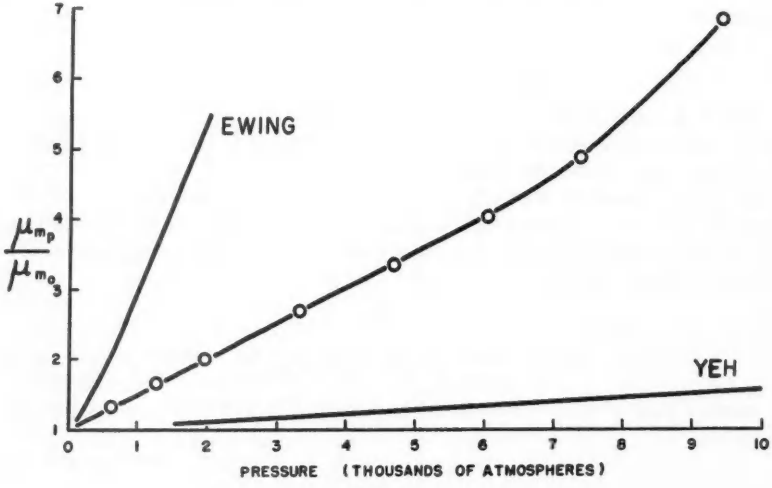

FIG. 2.

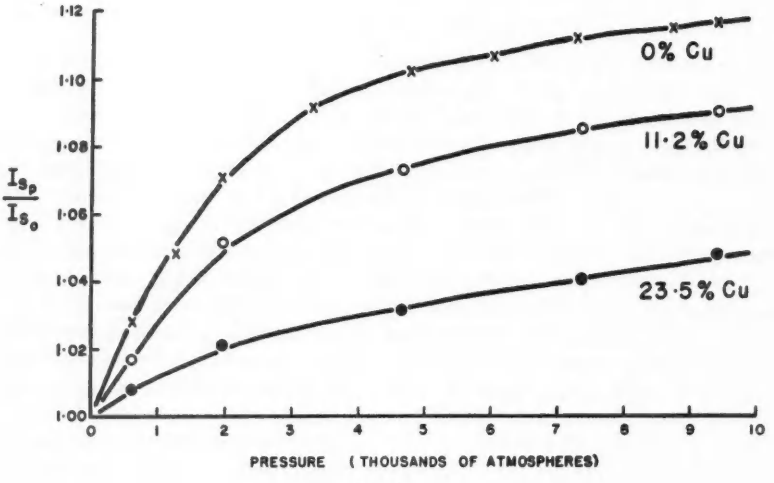

FIG. 3.

temperatures of copper–nickel alloys with about 30% copper. Curie temperatures of nickel and Monel (basically 70Ni–30Cu) under hydrostatic pressure have been observed directly by Patrick (1954), who found a very small effect with Monel, in agreement with Michels *et al.* (1937, 1941), but a much larger effect with nickel.

From measurements of volume magnetostriction, ω, at saturation, the

variation of saturated intensity of magnetization, I_s, with pressure, p, can be calculated, using the thermodynamic relation:

$$(\partial\omega/\partial H)_p = -(\partial I/\partial p)_H.$$

Calculations from values of the volume magnetostriction of nickel reported by Kornetski (1935) and Azumi and Goldman (1954) give -1.6×10^{-4} e.m.u./atm. and $+0.55\times10^{-4}$ e.m.u./atm. respectively. The present work gave $+180\times10^{-4}$ e.m.u./atm. at 1000 atm. and $+25\times10^{-4}$ e.m.u./atm. at 10,000 atm. This must have been due to a substantial increase in the occupation of the 3*d* band, although the shape of the curves of Fig. 3 may represent a gradual transition from purely longitudinal to largely hydrostatic compression. The results obtained with the Nilo alloys eliminated the possibility that this behavior was a characteristic of the apparatus.

5. IRON AND COBALT

These metals revealed one of the limitations of the present method. The use of magnetic intensities greater than about 18,000 gauss was prevented by saturation of the pole-piece tips, so that adequate saturation of iron and cobalt specimens was not possible.

The effect of compression on iron in low fields is strongly dependent upon carbon content and thermal history. A specimen of Swedish iron subjected to a prolonged hydrogen anneal at 900° C. gave a positive pressure coefficient of magnetization in all fields and at all pressures, whereas the same specimen only partly annealed had given a negative coefficient in low fields at low pressures. Mild steel gave a negative coefficient except for the initial compression at moderate fields, but a Swedish iron specimen which had been case-hardened to the maximum carbon content gave a positive coefficient under all conditions.

It appears that pressure increases the magnetizations of pure iron and high carbon steels but that at intermediate compositions, corresponding roughly to mild steel, the opposite effect is observed. Work-hardening has the same effect as increasing carbon content. This probably explains the disagreements between the results of early workers (Nagaoka and Honda 1898; Frisbie 1904).

Cobalt is very little affected by pressure and measurements up to 5000 oersteds indicate that its saturation magnetization is independent of pressure within the limits of the present method ($\pm2\%$). In moderate fields magnetization is increased slightly by compression and in low fields it is decreased, the Villari reversal of behavior being a function of pressure and occurring at 130 oersteds at low pressures. The agreement of this result with that of Chree (1889) may be fortuitous; the disagreement with Yeh (1925) is due to the hardened state of the specimen, and possibly also to the method of compression.

6. SOME COMMERCIAL ALLOYS

Monel and Brightray C (80Ni–20Co) (Mond Nickel Co.) are negligibly affected by pressure, but Nilo 36 (36Ni–64Fe) gives a strong decrease in magnetization in all fields, the saturation magnetization being given by:

$$I_s = (1060\pm20) - (1.14\pm0.05)\times10^{-2}p \text{ e.m.u.},$$

p being in atmospheres. I_s increases slightly with pressure for Nilo 50 (50Ni–50Fe).

Three austenitic stainless steels based on the composition 18Cr–6Ni–76Fe have been tested. They are only slightly magnetic, with a tendency for magnetization to decrease with pressure.

7. CONCLUSION

The method has only been used for measurements up to 10,000 atm., but it has been shown to be capable of giving a considerable extension of the range. Tests on copper specimens with the pole-piece tips replaced by cobalt steel ones have shown that pressures up to 80,000 atm. can be reached without rupturing the specimens, but the magnetic hardness of these tips greatly reduces the accuracy of measurements.

Correlation of the results of this experiment with measurements on magnetostriction presents some difficulty since the compression which has been applied is neither hydrostatic nor linear. Agreement with volume magnetostriction is poor (Lee 1955). For comparison with longitudinal magnetostriction we may consider the results of Kirchner (1936), who measured the magnetostriction of materials under pressure. He found a strong decrease in the longitudinal magnetostriction of nickel with increasing pressure, which is in general agreement with the decrease in $\partial I_s/\partial p$ observed in the present experiment. However, direct correlation cannot be attempted, firstly because Kirchner measured the changes in length caused by saturating his specimens and not the effect of increasing the field on already saturated specimens, and secondly because the effects of longitudinal compression on both longitudinal and volume magnetostriction were not included. The possibility of repeating measurements up to 10,000 atm. in a hydrostatic pressure chamber, using a similar permeameter method of attaining high fields, is therefore of considerable interest.

Apart from the thermodynamic connection of magnetostriction and the effects of stress, one must explain the increase in saturation magnetization of nickel–copper alloys in terms of decreased occupation of the $3d$ electron bands. It is possible to invent band shapes to give this effect when broadened by compression, but the nature of the broadening is sufficiently unknown to prevent a useful conclusion being drawn. Some light would be thrown on this by repeating the nickel–copper experiments at liquid air temperatures, at which the 30% copper alloys are strongly magnetic.

ACKNOWLEDGMENTS

This work was carried out at Queen Mary College, London, during the tenure of a grant from the Department of Scientific and Industrial Research. Major components of the apparatus were provided by the Central Research Fund of the University of London. The special nickel–copper alloys were given by the Mond Nickel Co. and Dr. B. R. Coles of Imperial College. The problem was suggested by Professor G. O. Jones, whose help throughout I gratefully acknowledge.

REFERENCES

AZUMI, K. and GOLDMAN, J. E. 1954. Phys. Rev. **93**: 630.
BRIDGMAN, P. W. 1950. Proc. Roy. Soc. A, **203**: 1.
CHREE, C. 1889. Proc. Roy. Soc. **47**: 41.
EBERT, H. and KUSSMANN, A. 1937. Physik. Z. **38**: 437.
EWING, J. A. 1900. Magnetic induction in iron and other metals. The Electrician Publishing Co., London.
FRISBIE, F. C. 1904. Phys. Rev. **18**: 432.
JONES, G. O. and STACEY, F. D. 1953. Proc. Phys. Soc. (London), B, **66**: 255.
KIRCHNER, H. 1936. Ann. Physik, **27**: 49.
KORNETSKI, M. 1935. Z. Physik, **97**: 662.
LEE, E. W. 1955. Repts. Progr. in Phys. **18**: 184.
MICHELS, A., JASPERS, A., DEBOER, J., and STRYLAND, J. 1937. Physica, **4**: 1007.
MICHELS, A. and STRYLAND, J. 1941. Physica, **8**: 53.
NAGAOKA, H. and HONDA, K. 1898. Phil. Mag. **46**: 261.
PATRICK, L. 1954. Phys. Rev. **93**: 384.
STEINBERGER, R. L. 1933. Physica, **4**: 153.
YEH, CHI-SUN. 1925. Proc. Am. Acad. Arts Sci. **60**: 503.

SELECTION RULES AND TEMPERATURE DEPENDENCE OF THE FIRST-ORDER RAMAN EFFECT IN CRYSTALS[1]

By O. Theimer

ABSTRACT

Starting from the most general scattering formulae, the current theory of the Raman effect in crystals is modified in such a way as to remove the well-known discrepancies between theory and experiment concerning the selection rules for calcite and similar crystals. A distinction is made between electrons in delocalized crystal orbitals and electrons in localized atomic or molecular orbitals and it is shown that only the latter produce a Raman scattering in agreement with the unmodified theory. The general formula for the scattering by delocalized electrons is analyzed and it is found that the magnitude of the components $[(\partial\alpha_{\rho\sigma}/\partial q_j)_0 q_j]^{v_j}_{v_j+1}$ of the first-order polarizability (q_j normal coordinate of the scattering lattice vibration) depends on the wave vectors $\mathbf{Q}'$ and $\mathbf{Q}''$ of incident and scattered light. The wave vector dependence of the first-order polarizability requires selection rules for the first-order Raman effect which do not correspond to the full symmetry of the scattering crystal but only to the symmetry operations of the group of $\mathbf{Q} = \mathbf{Q}' - \mathbf{Q}''$ which leave $\mathbf{Q}$ unchanged. These modified selection rules are shown to be compatible with experiment. The influence of mechanical anharmonicity and of polarizability derivatives of higher order on the first-order Raman effect is also discussed. It is found that these non-linear effects offer no satisfactory explanation for the great intensity of forbidden lines in the Raman spectrum of some crystals. Concerning temperature effects the non-linear terms in the intensity formulae are found to be of greater importance and are tentatively suggested as being responsible for the anomalous temperature dependence of low frequency external lattice vibrations.

1. INTRODUCTION

It has been known for several years that there are certain discrepancies between the theory of the Raman effect in crystals and some experimental results (see p. 314) which, so far, have not been explained.[2] It is the purpose of this paper to modify the current theory such as to remove this deficiency. We first try to find a starting point for possible modifications by a critical analysis of the current theory and the relevant experimental results.

In its most elaborate form, the theory of the Raman effect in crystals has been given by Born and his collaborators (Born and Bradburn 1947; Smith 1948; Theimer 1951, 1952). The theory is a straightforward extension of Placzek's theory for atoms and molecules (1934) and it leads in most essential points to the same results as the semiclassical theory used by J. Cabannes and other authors who are quoted extensively in a paper by Couture (1947, 1948). Born's theory, referred to as the linear, atomic polarizability theory in this paper, is based upon the following assumptions:

(*a*) The scattered intensity corresponding to the transition between two vibrational states v', v'' is proportional to the square of the matrix element

[1]Manuscript received July 15, 1955.
Contribution from the Physics Department of the University of British Columbia, Vancouver, British Columbia, and Summer Research Institute, Queen's University, Kingston, Ontario.

[2]Some explanations have been tentatively suggested by several authors (Barriol and Fruhling 1948; Matossi and Mayer 1948; Kastler 1948; Couture-Mathieu 1950*a*, *b*, 1952; Hornig 1948) which are, however, not quite satisfactory.

$[\mathbf{M}]_{\nu''}^{\nu'}$, where $\mathbf{M} = \alpha\mathbf{E}$ is the electric moment induced by the electric field $\mathbf{E}$ of the incident light wave and α is the polarizability tensor of the scattering crystal.

(*b*) $\mathbf{M}$ and α are considered to be the sum of the contributions of the individual atoms: $\alpha = \sum_{n=1}^{N}\alpha(n)$; N is the number of atoms in the crystal.

(*c*) The frequencies ν' and ν'' of the incident and scattered light are far removed from all the resonance eigenfrequencies ν_r^k of the scattering system, such that the condition $|\nu_r^k - \nu'| \gg \nu_{\nu''}^{\nu'}$ is fulfilled. $\nu_{\nu''}^{\nu'}$ is the vibrational frequency corresponding to the transition $v' \rightarrow v''$.

(*a*), (*b*), and (*c*) form a set of independent assumptions; they impose some further conditions upon the scattering theory which are listed as items (*d*) to (*g*):

(*d*) α is a symmetric tensor.

(*e*) α is a characteristic property of the electronic ground state of the scattering crystal and depends on the incident light only via a resonance denominator. In particular, it is assumed that α becomes asymptotically independent of the wave vectors $\mathbf{Q}'$ and $\mathbf{Q}''$ of the incident and scattered light, if $|Q'|$ tends towards zero.

(*f*) The wave vectors $\mathbf{Q}'$ and $\mathbf{Q}''$ enter the scattering formulae only in the form of phase factors which take care of the retardation of the induced moments at a distant point of observation:
$\mathbf{M} = \mathbf{E}\sum_n \alpha(n) \exp[2\pi i\mathbf{Q} \cdot \mathbf{r}(n)]$, $\mathbf{Q} = \mathbf{Q}' - \mathbf{Q}''$, $\mathbf{r}(n)$ = position vector of the nth atom.

(*g*) Only those lattice vibrations are active in the first-order Raman effect for which $\mathbf{q}_j = -\mathbf{Q} \cdot \mathbf{q}_j$ represents the wave vectors of the normal vibrations of a crystal lattice which may be represented as running or stationary plane waves. It is generally assumed that, for visible light, the scattering by waves with $\mathbf{q}_j = -\mathbf{Q}$ is practically identical to the scattering by the fundamental lattice vibrations with $\mathbf{q}_j = 0$.

There are still two additional, independent assumptions contained in Born's theory which are responsible for the label *linear* polarizability theory:

(*h*) If α is expanded in terms of the normal coordinates* q_j, only the first-order polarizability $(\partial\alpha/\partial q_j)_0 q_j$ contributes substantially to the first-order Raman effect ($v_j'' = v_j' \pm 1$).

(*i*) The lattice vibrations are harmonic.

The selection rules are derived on the basis of the preceding assumptions. It follows from (*e*) and (*g*) that they correspond to the full symmetry of the scattering crystal and that they do not depend on the direction of the incident and scattered light; according to the assumptions (*h*) and (*i*), they are exclusively determined by the transformation properties of $(\partial\alpha/\partial q_j)_0 q_j$.

*The notation q_j and $\mathbf{q}_j$ for normal coordinates and the associated wave vectors has been chosen as most closely resembling the different notations introduced by Placzek and Born.

The formula for the temperature dependence of the intensity of first-order Raman lines is based upon the assumptions (*c*), (*h*), and (*i*). One finds

$$I^{v_j}_{v_j+1} \sim \frac{1}{1-\exp(-h\nu_j/kT)} \quad \text{(Stokes lines)},$$

$$I^{v_j+1}_{v_j} \sim \frac{1}{\exp(h\nu_j/kT)-1} \quad \text{(anti-Stokes lines)}.$$

$\nu_j = \nu^{v_j}_{v_j+1}$ is the vibrational frequency of the scattering lattice vibration.

The selection rules and the temperature dependence of Raman lines can be observed experimentally. Hence, the validity of the assumptions (*a*) to (*i*) may be checked, at least indirectly, by comparing the experimental results with the predictions of the linear, atomic polarizability theory. It is found in this way that at least some of the premisses of this theory must be abandoned.

Perhaps the most important and most interesting argument leading to this conclusion is the breakdown of selection rules for calcite and similar ionic crystals and for organic crystals like benzene and diphenyl (Michalke 1938; Couture 1947, 1948; Aynard 1952; Fruhling 1951). It appears to be well established by the work of different authors that some of the tensor components $[\alpha_{\rho\sigma}]^{v}_{v+1}$ which should vanish according to the predictions of the polarizability theory have finite values such that the magnitude of the forbidden components is of the same order as the magnitude of the allowed ones. Furthermore, it is found that the magnitude of the forbidden components depends strongly on the direction of propagation $\mathbf{Q}'$ and $\mathbf{Q}''$ of the incident and scattered radiation. Kastler (1948) has suggested that both anomalies have the same physical origin.

Another discrepancy between the theory and experiment is observed for the temperature dependence of the scattered intensity. According to the *linear* polarizability theory the intensity of Stokes lines should increase with increasing temperature or, for high vibrational frequencies, remain practically constant; actually it decreases strongly in many observed cases (Landsberg and Mandelstam 1930; Nedungadi 1940, 1941; Ornstein and Went 1935*b*; Venkatesvarlu 1941, 1942). This will be referred to as the inverse temperature effect in this paper.

It will be shown in the next sections that these experimental results can be understood in terms of the general scattering theory for arbitrary systems of nuclei and electrons in which the simplifying assumptions (*a*) to (*i*) are abandoned. In particular, it will be found that the premisses (*b*) and (*e*) are mainly responsible for the apparent breakdown of selection rules and the assumptions (*h*) and (*i*) for the inverse temperature effect. The arguments leading to these conclusions are developed in the following sequence:

Section 2.—Assuming the resonance condition (*c*) to be valid, the general scattering tensor (2.2) is transformed into the polarizability, i.e. a tensor, which is a characteristic property of the electronic states of the crystal and which depends on the positions only but not on the vibrational states (energies) of the nuclei. It is shown that the polarizability may be represented by the conventional formula (2.20) only if the electrons of the crystal move in

localized atomic or molecular orbitals while equation (2.17) is required if they move along delocalized crystal orbitals. In this latter case the wave vectors $\mathbf{Q}'$ and $\mathbf{Q}''$ appear in integrals over delocalized electronic wave functions and, hence, determine the magnitude of the polarizability components.

Section 3.—The difference in the behavior of localized and delocalized electrons shows up most clearly in the selection rules which are extensively discussed in Section 5. The basis for this discussion is the expansion of the polarizability in terms of normal coordinates given by the equations (3.3) to (3.8) of Section 3. The influence of the *second-order* and *third-order* terms in this expansion on the *first-order* Raman effect ($v_j'' = v_j' \pm 1$) is analyzed in some detail and an upper limit for the magnitude of the non-linear effects is estimated (subsections (*a*) to (*d*)); the upper limit is found to be big enough to offer a possible explanation for the inverse temperature effect which is discussed in Section 4.

Section 5 deals with the selection rules. The general principles of the method used for their derivation are outlined in subsections (*a*) and (*b*), and applied to electrons in localized orbitals in subsection (*c*). It is shown that the selection rules for the fundamental ($\mathbf{q}_j = 0$) and Raman active ($\mathbf{q}_j = -\mathbf{Q}$) lattice vibrations are practically identical in the case of localized electrons and that the higher order terms discussed in Section 3 are very unlikely to cause a pronounced breakdown of selection rules. This leaves the electrons in delocalized orbitals as the most probable origin of forbidden Raman lines. The latter hypothesis is discussed in subsection (*d*) where the selection rules for the Raman scattering by delocalized electrons are derived (equations (5.8), (5.9), (5.11)).

Section 6.—The Raman scattering of calcite is discussed in great detail and is shown to confirm the hypothesis that electrons in delocalized crystal orbitals are responsible for the observed anomalies.

2. GENERAL THEORY OF THE RAMAN EFFECT IN CRYSTALS

According to Dirac's theory of radiation the scattered intensity $I_n^k(\mathbf{Q}', \mathbf{Q}'')$ corresponding to a transition between two states k, n of any arbitrary system of nuclei and electrons can be represented in the form (Dirac 1927; Fermi 1932; Kramers 1938; Heitler 1954)

$$(2.1)\quad I_n^k(\mathbf{Q}', \mathbf{Q}'')d\omega = \frac{8\pi^3 c}{\lambda''^4 r^2}\left|\sum_{\rho\sigma}[C_{\rho\sigma}]_n^k e_\rho^{*\prime\prime} e_\sigma'\right|^2 I_0\, d\omega, \qquad (\rho, \sigma = 1, 2, 3)$$

where

$\mathbf{e}', \mathbf{e}''$ = polarization vectors,
λ', λ'' = wave-lengths,
ν', ν'' = frequencies,
$\mathbf{Q}', \mathbf{Q}''$ = wave vectors,
} of the incident and scattered radiation,

r = distance between the scattering system and a distant observer,
$d\omega$ = small solid angle in direction $\mathbf{Q}''$,
I_0 = intensity of the incident light.

As indicated by the notation $I_n^k(\mathbf{Q}', \mathbf{Q}'')d\omega$, equation (2.1) refers to the case that incident plane waves with wave vector $\mathbf{Q}'$ are scattered and that radiation with wave vector $\mathbf{Q}''$ is observed within a small solid angle $d\omega$.

The component $[C_{\rho\sigma}]_n^k$ of the scattering tensor has the form

$$(2.2) \qquad [C_{\rho\sigma}]_n^k = \frac{1}{4\pi^2\nu'\nu''\hbar}\left[R_{\lambda''n}^{\lambda'k}\delta_{\rho\sigma} - \sum_r \left\{\frac{(I_\rho^{\lambda''})_r^k (I_\sigma^{\lambda'})_n^r}{\nu_r^k - \nu'} + \frac{(I_\sigma^{\lambda'})_r^k (I_\rho^{\lambda''})_n^r}{\nu_r^n + \nu'}\right\}\right],$$

where

$$(2.3) \qquad h\nu_r^k = E_r - E_k \text{ is the energy difference between state } r \text{ and } k,$$

$$(2.4) \qquad (\mathbf{I}^{\lambda''})_r^k = \int \exp(-2\pi i \mathbf{Q}'' \cdot \mathbf{r})(\rho\mathbf{v})_r^k \, dv, \qquad dv = dxdydz,$$

$$(2.5) \qquad (\mathbf{I}^{\lambda'})_n^r = \int \exp(2\pi i \mathbf{Q}' \cdot \mathbf{r})(\rho\mathbf{v})_n^r \, dv,$$

$$(2.6) \qquad R_{\lambda''n}^{\lambda'k} = \hbar \int \exp(2\pi i \mathbf{Q} \cdot \mathbf{r})(\rho^2/m)_n^k \, dv, \qquad \mathbf{Q} = \mathbf{Q}' - \mathbf{Q}'',$$

$$(2.7) \qquad (\rho\mathbf{v})_r^k = \sum_i \left[\int \tfrac{1}{2}(\psi_k^* \epsilon_i \mathbf{v}_i \psi_r + \psi_r \epsilon_i \mathbf{v}_i^* \psi_k^*) \prod_{\substack{j \\ j\neq i}} dx_j dy_j dz_j\right]_{x_i=x, y_i=y, z_i=z},$$

$$(2.8) \qquad (\rho^2/m)_n^k = \sum_i \left[\int \tfrac{1}{2}(\psi_k^* \frac{\epsilon_i^2}{m_i} \psi_n + \psi_n \frac{\epsilon_i^2}{m_i} \psi_k^*) \prod_{\substack{j \\ j\neq i}} dx_j dy_j dz_j\right]_{x_i=x, y_i=y, z_i=z},$$

$\epsilon_i, m_i, \mathbf{v}_i$ = charge, mass, and velocity of the ith particle of the scattering system; only the electrons need to be considered in the case of visible light.

According to the equations (2.2) to (2.8), the scattering tensor is, in general, complex and non-Hermitian ($C_{\rho\sigma} \neq C_{\sigma\rho}$) and a complicated function of $\mathbf{Q}'$ and $\mathbf{Q}''$. Furthermore it is a property of the whole crystal and can not immediately be resolved into a sum of atomic contributions. This indicates that the assumptions (*a*) to (*e*) implied in the polarizability theory can be valid only under certain conditions which will be analyzed in the following discussion.

We try first to replace the general scattering tensor $C_{\rho\sigma}$ by a tensor which is a property of the electronic ground state and depends on the positions of the nuclei only but neither on their velocities nor on the vibrational states of the crystal. We shall call this tensor the polarizability α of the crystal although it will be a function of the wave vectors $\mathbf{Q}'$ and $\mathbf{Q}''$. In order to introduce $\alpha_{\rho\sigma}$ into the scattering formulae we write for the total eigenfunction ψ_k of the system of nuclei and electrons the product

$$(2.9) \qquad \psi_k = \Phi_e(x, q) U_{e,v}(q), \qquad \left.\begin{matrix} e = \text{electronic} \\ v = \text{vibrational} \end{matrix}\right\} \text{quantum number},$$

where $\Phi_e(x, q)$ represents the electronic and $U_{e,v}(q)$ the vibrational eigenfunction of the system. (We need not consider rotations in most cases of crystals.) x and q stand for all the electronic and nuclear coordinates and the notation indicates that $\Phi_e(x, q)$ is assumed to depend on the nuclear normal coordinates q which act as parameters in the Hamiltonian for the electrons.

With the product notation (2.9) the matrix elements of equation (2.2) can be written

$$(2.10)\quad (I_\rho^{\lambda''})_\tau^k = [\{I_\rho^{\lambda''}(q)\}_{e'''}^{e'}]_{v'''}^{v'} = \int U^*_{e''',v'''}(q)\{I_\rho^{\lambda''}(q)\}_{e'''}^{e'} U_{e',v'}(q)dq,$$

where $\{I_\rho^{\lambda''}(q)\}_{e'''}^{e'}$ is obtained from the formulae (2.4) and (2.7) after replacing ψ_k and ψ_τ by $\Phi_{e'}(x, q)$ and $\Phi_{e'''}(x, q)$. Similar expressions result for $(I_\sigma^{\lambda'})_n^\tau$ and for $R_{\lambda'',n}^{\lambda',k}$.

We now consider the denominators of equation (2.2) and write with an obvious notation

$$(2.11)\quad \frac{1}{\nu_\tau^k \pm \nu'} = \frac{1}{\nu_{e'''}^{e'} + \nu_{v'''}^{v'} \pm \nu'} = \frac{1}{\nu_{e'''}^{e'} \pm \nu'} - \frac{\nu_{v'''}^{v'}}{(\nu_{e'''}^{e'} \pm \nu')^2} + \cdots.$$

This allows one to split the scattering tensor in the polarizability*

$$(2.12)\quad [\alpha_{\rho\sigma}(q)]_{v''}^{v'} = \frac{1}{4\pi^2\nu'\nu''h}\Bigg[R_{\lambda'',e'v''}^{\lambda',e'v'}\delta_{\rho\sigma} - \sum_{e'''}\Bigg\{\frac{\sum_{v'''}[\{I_\rho^{\lambda''}(q)\}_{e'''}^{e'}]_{v''}^{v'}[\{I_\sigma^{\lambda'}(q)\}_{e''}^{e'''}]_{v''}^{v'''}}{\nu_{e'''}^{e'} - \nu'} + \frac{\sum_{v'''}[\{I_\sigma^{\lambda'}(q)\}_{e'''}^{e'}]_{v''}^{v'}[\{I_\rho^{\lambda''}(q)\}_{e''}^{e'''}]_{v''}^{v'''}}{\nu_{e'''}^{e'} + \nu'}\Bigg\}\Bigg]$$

and in the tensor

$$(2.13)\quad [\beta_{\rho\sigma}(q, v)]_{v''}^{v'} = \frac{1}{4\pi\nu'\nu''h}\Bigg[\sum_{e''',v'''}\Bigg\{\frac{\nu_{v'''}^{v'}(I_\rho^{\lambda''})_{e'''v''}^{e'v'}(I_\sigma^{\lambda'})_{e'v''}^{e'''v'''}}{(\nu_{e'''}^{e'} - \nu')^2} + \frac{\nu_{v'''}^{v'}(I_\sigma^{\lambda'})_{e'''v''}^{e'v'}(I_\rho^{\lambda''})_{e'v''}^{e'''v'''}}{(\nu_{e'''}^{e'} + \nu')^2}\Bigg\}\Bigg],$$

which depends on the vibrational frequencies $\nu_{v'''}^{v'}$ as well. This dependence leads to rather complicated formulae for the temperature dependence of Raman intensities if the condition 1(*c*), i.e. the condition $\alpha(q) \gg \beta(q, v)$, is not fulfilled.

The summation over v''' in equation (2.12) can be removed by means of the rules of matrix multiplication ($[P(q)]_{v''}^{v'} = \sum_{v'''}[A(q)]_{v'''}^{v'}[B(q)]_{v''}^{v'''}$, $P = AB$) and one obtains

$$(2.14)\quad [\alpha_{\rho\sigma}(q)]_{v''}^{v'} = \frac{1}{4\pi^2\nu'\nu''h}\Bigg[R_{\lambda'',e'v''}^{\lambda',e'v'}\delta_{\rho\sigma} - \sum_{e'''}\Bigg\{\frac{[I_\rho^{\lambda''}(q)]_{e'''}^{e'}[I_\sigma^{\lambda'}(q)]_{e''}^{e'''}}{\nu_{e'''}^{e'} - \nu'} + \frac{[I_\sigma^{\lambda'}(q)]_{e'''}^{e'}[I_\rho^{\lambda''}(q)]_{e''}^{e'''}}{\nu_{e'''}^{e'} + \nu'}\Bigg\}\Bigg]_{v''}^{v'}.$$

$\alpha(q)$ is a function of the nuclear coordinates q and depends, even in this simplified form, on the wave vectors $\mathbf{Q}'$ and $\mathbf{Q}''$ in a way which is more complicated than postulated by the assumption 1(*f*) of the polarizability theory. This assumption is based upon the possibility of representing $\alpha(q)$ as a sum of

*In equation (2.12) and in all the following formulae, it is assumed that the electronic eigenfunctions $\Phi_{e'}$ and $\Phi_{e''}$ of the initial and final state of the scattering system are identical: $e' = e''$. At reasonable temperatures they will refer to the electronic ground state.

atomic contributions. Hence, we shall now analyze the conditions under which such a representation is possible.

We shall show that these conditions are related to the question whether the electrons of crystals are restricted to move in localized atomic or molecular orbitals, or whether they may travel, more or less freely, in crystal orbitals spread over the whole crystal. Since the idea of localized atomic and delocalized crystal orbitals refers to two extreme limiting cases which are hardly found in nature, one can not generally assume that some orbitals are completely localized and others are not. We shall therefore represent all orbitals as linear superpositions of localized, non-overlapping, atomic orbitals and plane waves, the latter having coefficients which measure the degree of delocalization.* Not much is known of the magnitude of these coefficients for ionic crystals of the type $CaCO_3$ but the widely accepted assumption that the ionic bond is never perfectly realized, not even in NaCl, indicates that they can not, a priori, be neglected in a general theory of the Raman effect in crystals.†

In order to introduce the concept of localized and delocalized orbitals into the scattering theory we represent the electronic eigenfunction $\Phi_e(x, q)$ by an antisymmetric sum of products of one-electron eigenfunctions:

$$(2.15)\quad \Phi_e(x, q) = \frac{1}{\sqrt{N_e!}} \sum (-1)^{in} P w_1^1(x, q) w_2^2(x, q) \ldots w_l^i(x, q) \ldots w_{N_e}^{N_e}(x, q),$$

with

N_e = total number of electrons in the scattering system,

in = number of inversions in the permutation P,

$w_l^i(x, q)$ = orbital l occupied by the electron i; the $w_l^i(x, q)$ are orthogonal and normalized and depend on q.

Since the number of available orbitals is much larger than the number N_e of electrons, different functions $\Phi_e(x, q)$ are characterized by a different set of occupied orbitals w_l.

We now introduce, in place of ψ_k and ψ_r, electronic eigenfunctions $\Phi_{e'}(x, q)$ and $\Phi_{e'''}(x, q)$ of the form (2.15) into the matrix element (2.7). This matrix element is a sum of terms, each of which depends on the velocity of one single electron only. Hence, this matrix element vanishes unless $\Phi_{e'''}(x, q)$ and $\Phi_{e'}(x, q)$ differ by not more than one of the occupied orthogonal orbitals w_l. More explicitly, one finds that

$$(2.16)\quad (\rho \mathbf{v})_{e'e'''} = (\rho \mathbf{v})_{l'l'''} = \tfrac{1}{2}[w_{l'}^*(x, q) \epsilon \mathbf{v} w_{l'''}(x, q) + w_{l'''}(x, q) \epsilon \mathbf{v}^* w_{l'}^*(x, q)],$$

where $w_{l'}(x, q)$ and $w_{l'''}(x, q)$ are those occupied orbitals which are different in the initial (e') and intermediate (e''') state.

Equations (2.16) and (2.14) combined give an expression for the polariza-

*It is always possible to represent the electronic eigenfunctions of a periodic crystal exclusively in the form of plane waves. In this case, the mobility or delocalization of the electrons may be measured by the group velocity $dE/d(h/\lambda)$. It is, however, more convenient for our purpose to reserve the plane wave representation for delocalized orbitals with group velocity different from zero.

†The absence of electronic conductivity does not contradict the assumption of delocalized orbitals which is a necessary, but not a sufficient, condition for metallic conductivity.

bility in which the summation over electrons is replaced by a summation over the initially occupied orbitals $w_{l'}(x, q)$:

$$(2.17)\quad [\alpha_{\rho\sigma}(q)]^{\nu'}_{\nu''} = \frac{1}{4\pi^2\nu'\nu''\hbar}\Bigg[\sum_{l'}\left\{\hbar\int\exp(2\pi i\mathbf{Q}\cdot\mathbf{r})\left(\frac{\rho^2}{m}\right)^{l'}_{l'}dv\right\}\delta_{\rho\sigma}$$
$$-\sum_{l'}\sum_{l'''}\left\{\frac{\int\exp(-2\pi i\mathbf{Q}''\cdot\mathbf{r})(\rho v_\rho)^{l'}_{l'''}dv\int\exp(2\pi i\mathbf{Q}'\cdot\mathbf{r})(\rho v_\sigma)^{l'''}_{l'}}{\nu^{l'}_{l'''}-\nu'}\right.$$
$$\left.+\frac{\int\exp(2\pi i\mathbf{Q}'\cdot\mathbf{r})(\rho v_\sigma)^{l'}_{l'''}dv\int\exp(-2\pi i\mathbf{Q}''\cdot\mathbf{r})(\rho v_\rho)^{l'''}_{l'}dv}{\nu^{l'}_{l'''}+\nu'}\right\}\Bigg]^{\nu'}_{\nu''}.$$

Equations (2.16) and (2.17) have a form which allows one immediately to visualize the different behavior of localized orbitals ($w_l{}^l$) and delocalized orbitals ($w_l{}^d$). According to the discussion on page 318 we write for each orbital

$$(2.18)\qquad w_l(x, q) = w_l{}^l(x, q)+cw_l{}^d(x, q),$$

and substitute (2.18) in (2.16); this gives a sum of terms containing three different types of products of eigenfunctions, namely: w^lw^l, w^lw^d, and w^dw^d. The last product is a space function spread over the whole crystal while the first two products vanish everywhere outside the charge cloud of the localized orbital. It is essential to note that the mixed products represent localized space functions; hence, $(\rho\mathbf{v})^{l'}_{l'''}$ will contain localized terms due to the initially occupied orbitals $w^l_{l'}$, even if all the exited orbitals $w_{l'''}$ should be essentially delocalized.

The contributions of the localized terms to the polarizability can be formally simplified by grouping together all the localized orbitals $w_{l(n)}$ belonging to the same atom (n) and by introducing the position vectors $\mathbf{r}(n)$ of the atomic nuclei with the help of the relation

$$(2.19)\qquad \mathbf{r} = \mathbf{r}(^n_l)+\mathbf{r}(n),$$

where $\mathbf{r}(^n_l)$ is the vector from a nucleus to an electron in the localized orbital $w_{l(n)}(x, q)$. Since the linear dimensions of atomic charge clouds are negligibly small compared to the wave-length of visible light the phase factor $\exp[2\pi i\mathbf{Q}'\cdot\mathbf{r}(^n_l)]$ in (2.17) is practically equal to one, over the whole range of integration; while the factor $\exp[2\pi i\mathbf{Q}'\cdot\mathbf{r}(n)]$ may be taken before the integral, $\mathbf{r}(n)$ being constant by definition. We obtain in this way the following expression for the polarizability $\alpha^l(q)$ of electrons in localized orbitals:

$$(2.20)\qquad [\alpha^l_{\rho\sigma}(q)]^{\nu'}_{\nu''} = \sum_n \exp[2\pi i\mathbf{Q}\cdot\mathbf{r}(n)][\alpha_{\rho\sigma}(n)]^{\nu'}_{\nu''}$$

with

$$(2.21)^*\quad [\alpha_{\rho\sigma}(n)]^{\nu'}_{\nu''} = \frac{1}{4\pi^2\nu'\nu''\hbar}\Bigg[\sum_{l'(n)}\hbar\left\{\int(\rho^2/m)^{l'(n)}_{l'(n)}dv\right\}\delta_{\rho\sigma}$$
$$-2\sum_{l'(n)}\sum_{l'''}\left\{\frac{\nu^{l'(n)}_{l'''}}{(\nu^{l'(n)}_{l'''})^2-(\nu')^2}\int(\rho v_\sigma)^{l'(n)}_{l'''}dv\int(\rho v_\rho)^{l'''}_{l'(n)}dv\right\}\Bigg]^{\nu'}_{\nu''}.$$

This may be finally transformed (Kramers 1938; Placzek 1934) into an expression resembling Placzek's formula for free molecules:

*The imaginary part of $\alpha_{\rho\sigma}(n)$ which is usually negligible has been omitted.

$$(2.22)\quad [\alpha_{\rho\sigma}(n)]_{\nu''}^{\nu'} = \frac{2}{h}\left[\sum_{l'(n)}\sum_{l'''}\left\{\frac{\nu_{l'''}^{l'(n)}}{(\nu_{l'''}^{l'(n)})^2-(\nu')^2}\int (M_\rho)_{l'''}^{l'(n)}dv\int (M_\sigma)_{l'(n)}^{l'''}dv\right\}\right]_{\nu''}^{\nu'}. \quad (\mathbf{M}=\epsilon\mathbf{r})$$

The equations (2.20), (2.21), and (2.22) correspond exactly to the assumptions $1(a)$ to $1(g)$ of the polarizability theory. However, they are valid only as far as the electrons in localized orbitals and their contributions to the polarizability are concerned.

The situation is quite different for the contributions $\alpha^{\mathrm{d}}(q)$ of electrons in delocalized crystal orbitals to the total polarizability α. For these contributions the general formula (2.17) can not be further simplified. In particular, the phase factors can not be written outside the integrals over electronic orbitals and the wave vectors $\mathbf{Q}'$ and $\mathbf{Q}''$ influence the scattering intensity even if $|Q'|$ tends towards zero. This means that the tensor components $[\alpha_{\rho\sigma}^{\mathrm{d}}(q)]_{\nu''}^{\nu'}$ depend on the direction of propagation of the incident and scattered light even if the wave-length is long compared to the linear dimensions of the elementary lattice cell.

From the preceding discussion of the general scattering formula (2.1) it appears that it is the polarizability $\alpha^{\mathrm{d}}(q)$ of electrons in delocalized crystal orbitals which is most probably responsible for the breakdown of selection rules mentioned in the introduction. We shall elaborate this hypothesis in some more detail in Section 5.

3. EXPANSION OF THE SCATTERING TENSOR IN TERMS OF NORMAL COORDINATES

The problems of light scattering are most readily understood by expanding the scattering tensor $\alpha_{\rho\sigma}(q)$ in terms of the normal coordinates q_j of the scattering system.

We write

$$(3.1)\quad U_v = u_{v_1}(q_1)u_{v_2}(q_2)\ldots u_{v_j}(q_j)\ldots u_{v_{3N}}(q_{3N}) \qquad (N = \text{number of nuclei})$$

for the vibrational eigenfunction, and

$$(3.2)\qquad E_v = \sum_j (v_j+\tfrac{1}{2})h\nu_j$$

for the vibrational energy of a crystal in its electronic ground state, and we expand $\alpha_{\rho\sigma}(q)$ in terms of the q_j:

$$(3.3)\quad \alpha_{\rho\sigma}(q) = (\alpha_{\rho\sigma})_0+\sum_j\left(\frac{\partial\alpha_{\rho\sigma}}{\partial q_j}\right)_0 q_j+\frac{1}{2}\sum_{jj'}\left(\frac{\partial^2\alpha_{\rho\sigma}}{\partial q_j\partial q_{j'}}\right)_0 q_j\,q_{j'} + \frac{1}{6}\sum_{jj'j''}\left(\frac{\partial^3\alpha_{\rho\sigma}}{\partial q_j\partial q_{j'}\partial q_{j''}}\right)_0 q_j\,q_{j'}\,q_{j''}+\ldots.$$

(The subscript zero refers to the equilibrium position of the nuclei.)

In the case of crystals with localized electrons the terms in the expansion (3.3) have the following form (Born and Bradburn 1947; Theimer 1951):

$$(3.4)\quad {}^{(1)}\alpha_{\rho\sigma}(j) = \left(\frac{\partial\alpha_{\rho\sigma}}{\partial q_j}\right)_0 q_j = \left(\sum_{\bar{l}}\sum_k\sum_\mu \alpha_{\rho\sigma,\mu}(k)e_{\mu j}(k)\exp[2\pi i(\mathbf{q}_j+\mathbf{Q})\cdot\mathbf{r}(\bar{l})]\right)q_j,$$

$$(3.5)\quad \overset{(2)}{\alpha}_{\rho\sigma}(j,j') = \left(\frac{\partial^2\alpha_{\rho\sigma}}{\partial q_j \partial q_{j'}}\right) q_j\, q_{j'} = \Bigg(\sum_{\bar{l}(\bar{l}-\bar{l}')} \sum_{kk'} \sum_{\mu\mu'} \alpha_{\rho\sigma,\mu\mu'}\left(\tfrac{\bar{l}-\bar{l}'}{kk'}\right) e_{\mu j}(k) e_{\mu' j'}(k') \times \exp\{2\pi i[(\mathbf{q}_j+\mathbf{q}_{j'}+\mathbf{Q})\,.\,\mathbf{r}(\bar{l}) - (\mathbf{q}_{j'}-\mathbf{Q})\,.\,\mathbf{r}(\bar{l}-\bar{l}')]\}\Bigg) q_j\, q_{j'}.$$

The index $\bar{l}$ enumerates the different lattice cells and the index k the different nuclei in one cell. $e_{\mu j}(k)\exp[2\pi i \mathbf{q}_j\,.\,\mathbf{r}(\bar{l})]$ is the normalized μ-component of the displacement of the nucleus (k) in the cell $(\bar{l})$ with position vector $\mathbf{r}(\bar{l})$, corresponding to the normal vibration q_j with wave vector $\mathbf{q}_j$. The $\alpha_{\rho\sigma,\mu}(k)$ and $\alpha_{\rho\sigma,\mu\mu'}\left(\tfrac{\bar{l}-\bar{l}'}{kk'}\right)$ are the first and second tensor derivatives with respect to these nuclear displacements. The $\alpha_{\rho\sigma,\mu}(k)$ do not depend on the cell index $\bar{l}$ and the $\alpha_{\rho\sigma,\mu\mu'}\left(\tfrac{\bar{l}-\bar{l}'}{kk'}\right)$ depend only on the difference $(\bar{l}-\bar{l}')$. Hence the $\overset{(1)}{\alpha}_{\rho\sigma}(j)$ and $\overset{(2)}{\alpha}_{\rho\sigma}(j,j')$ vanish unless $\mathbf{q}_j+\mathbf{Q}=0$ or $\mathbf{q}_j+\mathbf{q}_{j'}+\mathbf{Q}=0$. This is a consequence of the summation over $\bar{l}$. (For more details see Born and Bradburn 1947; Smith 1948; Theimer 1951, 1952.)

The scattering intensity is determined by the matrix elements of the scattering tensor. For the case of harmonic vibrations one finds:

$$(3.6)\quad [\alpha_{\rho\sigma}]^{v_j}_{v_j} = \alpha_0 + \tfrac{1}{2}\sum_{j'} (v_{j'}+1)\left(\frac{\partial^2\alpha_{\rho\sigma}}{\partial q_{j'}^2}\right)_0 b_{j'}^2 + \ldots, \qquad b_j = \sqrt{\frac{h}{8\pi^2\nu_j}},$$

$$(3.7)\quad [\alpha_{\rho\sigma}]^{v_j}_{v_j+1} = \sqrt{(v_j+1)}\left\{\left(\frac{\partial\alpha_{\rho\sigma}}{\partial q_j}\right)_0 b_j + \sum_{j'}\frac{1}{6}(v_{j'}+1)\left(\frac{\partial^3\alpha_{\rho\sigma}}{\partial q_j \partial q_{j'}^2}\right)_0 b_j b_{j'}^2 + \ldots\right\},$$

$$(3.8)\quad [\alpha_{\rho\sigma}]^{v_j, v_{j'}}_{v_j+i,\, v_{j'}+i'} = \frac{1}{(i+i')!}\sqrt{\prod_{i=1}^{i}(v_j+i)\prod_{i'=1}^{i'}(v_{j'}+i')}\left(\frac{\partial^{i+i'}\alpha_{\rho\sigma}}{\partial q_j^{\,i}\partial q_{j'}^{\,i'}}\right) b_j^{\,i} b_{j'}^{\,i'} + \ldots.$$

We shall now shortly discuss some problems related to the formulae (3.6), (3.7), and (3.8) which are of interest for the understanding of selection rules and of the temperature dependence of Raman intensities.

(*a*) The influence of the third-order terms in the first-order matrix element (3.7).

One can try to find an upper limit for the contributions of the third-order terms to the intensity of first-order Raman lines from the fact that the same terms determine the intensity of the third-order Raman effect ($v_j'' = v_j'+3$ and $v_j'' = v_j'+1, v_{j'}'' = v_{j'}'+2$).

We write for the intensity of one first-order Raman line

$$(3.9)\quad \overset{(1)}{I}(j) = I^{v_j}_{v_j+1} \sim \{[\alpha_{\rho\sigma}]^{v_j}_{v_j+1}\}^2 \sim a^2(1+\gamma)^2; \qquad a = \left(\frac{\partial\alpha_{\rho\sigma}}{\partial q_j}\right) b_j,$$

$$\gamma = \frac{1}{a}\sum_{j'}\frac{1}{6}(v_{j'}+1)\left(\frac{\partial^3\alpha_{\rho\sigma}}{\partial q_j \partial q_{j'}^2}\right)_0 b_j b_{j'}^2,$$

(γ measures the relative contribution of third-order terms to $\overset{(1)}{I}(j)$)
and for the intensity of the whole third-order Raman spectrum

$$(3.10)\quad \overset{(3)}{I} \sim a^2\gamma^2,$$

and obtain

$$\overset{(3)}{I} / \overset{(1)}{I}(j) \simeq \frac{\gamma^2}{(1+\gamma)^2}. \tag{3.11}$$

One should now distinguish between the case of molecules where the third-order spectrum is a line spectrum and the case of crystals where it is a continuum. The absence of third-order Raman lines in molecular spectra indicates that $\gamma \ll 1$ and justifies the assumption $1(h)$ of the linear polarizability theory. In crystals, however, one can not definitely exclude the possibility that the total intensity $\overset{(3)}{I}$ of the *continuous* third-order spectrum is of the order of some per cent of the intensity of one first-order line. Such a small effect, spread over a wide frequency region, could hardly be separated from a weak continuous background due to other causes. Thus, assuming $\overset{(3)}{I}/\overset{(1)}{I}(j) < 0.03$, we find: $\gamma^2/(1+\gamma)^2 < 1/30$ or $\gamma < 0.2$. This high value is an upper limit and, hence, offers no decisive argument against the assumption $1(h)$. But it is of interest as a *possible* explanation for the inverse temperature effect, as it allows for strong higher order effects with complicated temperature dependence. It should, however, be stressed that the third-order terms in equation (3.7) can be hardly responsible for a great intensity of forbidden Raman lines, even if γ has as high a value as 0.2. The reason is that the first-order term a of equation (3.9) is zero in this case and the intensity $\overset{(1)}{I}(j)$ of the forbidden Raman line is of the order γ^2, i.e. at the most 4% of the allowed first-order lines. Only if $a \neq 0$ are the third-order contributions enhanced to the value 2γ by forming the square of $(1+\gamma)$.

(*b*) For the understanding of temperature effects it is also useful to note that the formulae (3.6) to (3.8) are not valid for the matrix elements $[\beta_{\rho\sigma}(q, v)]^{v'}_{v''}$ (see equation (2.13)) of this part of the scattering tensor which is negligible if the resonance condition $1(c)$ is fulfilled. Those matrix elements depend on the vibrational quantum numbers v_j in a rather complicated way which is different in each individual case and which strongly modifies the formula for the temperature dependence of Raman lines. Hence, breakdown of the condition $1(c)$ may produce an inverse temperature effect.

(*c*) The equations (3.6) to (3.8) refer only to the case of harmonic vibrations. The mechanical anharmonicity of the lattice vibrations introduces the following modifications:

(i) The formulae for the matrix elements of anharmonic oscillators are different from those for the harmonic oscillator. As far as the matrix element $[\alpha_{\rho\sigma}]^{v_j}_{v_j+1}$ is concerned one finds quite generally that the odd derivatives which are contained in (3.7) decrease and that the even derivatives, for example $[(\partial^2\alpha_{\rho\sigma}/\partial q_j \partial q_{j'})_0 q_j q_{j'}]^{v_j}_{v_j+1}$, which are zero in (3.7) appear and increase with increasing anharmonicity. They have probably the same magnitude as the odd terms of next higher order.

(ii) $[\alpha_{\rho\sigma}]^{v_j}_{v_j+1}$ is a function of the vibrational quantum number v_j. As far as only the term $[(\partial\alpha_{\rho\sigma}/\partial q_j)_0 q_j]^{v_j}_{v_j+1}$ is concerned, this function is monotonously increasing with v_j and tends asymptotically towards a limiting value (Buckmaster 1952). One has here an analogy to the classical behavior of the vibra-

tional amplitude which increases with increasing vibrational energy until dissociation occurs. This special property of the function $[(\partial\alpha_{\rho\sigma}/\partial q_j)_0 q_j]^{v_j}_{v_j+1} = f(v_j)$ is important for a discussion of temperature effects; it warrants that only the higher terms in the expansion of $\alpha(q)$ can be responsible for a decrease of $[\alpha_{\rho\sigma}]^{v_j}_{v_j+1}$ with growing v_j.

(iii) As a result of the mechanical anharmonicity the transition frequencies $\nu^{v_j}_{v_j+1}$ of a certain lattice vibration (q_j) depend on the quantum number v_j and tend towards zero with increasing v_j. This produces a strong broadening of Raman lines, particularly of those corresponding to highly excited, low frequency vibrations of ionic lattices, where the ions are known to move in strongly anharmonic potential wells. The broadening, again, reduces the peak intensity of Raman lines and may even produce an *apparent* loss of the integral intensity if the wings of broad Raman lines escape observation or are confounded with a continuous background.

(iv) A rather important deviation from the case of harmonic normal vibrations is the hindered rotation of certain atomic groups, e.g. the CO_3^{--}-ion in calcite, which is a consequence of the existence of several different potential minima. We discuss shortly this case as it may have an influence on the selection rules for the vibrational Raman effect.

The problems of hindered rotation can be understood from a discussion of the two limiting cases: anharmonic torsional vibration and free rotation. Only the latter case introduces some new aspects into the theory of the Raman effect.

We write for the eigenfunction of the rotating group the product

$$\psi(q, \phi) = U(q)\, R(\phi), \qquad (\phi \text{ is angle of rotation about the } z\text{-axes}) \tag{3.12}$$

where the rotational eigenfunction is given by

$$R(\phi) = Ce^{\pm i m\phi}, \qquad (C = \text{normalization factor}) \tag{3.13}$$

and we replace the Taylor series (3.3) by the Fourier series

$$\alpha_{\rho'\sigma'}(q, \phi) = \sum_s \alpha_{\rho'\sigma'}(q, s)e^{is\phi}, \qquad (s = \text{integer}). \tag{3.14}$$

Some of the $\alpha_{\rho'\sigma'}(q, s)$ may be zero because of symmetry. The subscripts ρ', σ' in (3.14) refer to a coordinate system attached to the rotating group; hence, equation (3.14) describes an intrinsic ϕ-dependence of the polarizability α which is due to the influence of the neighboring atoms and ions surrounding the rotating group.* For the understanding of the selection rules it is important to note that $\alpha_{\rho'\sigma'}(q, 0)$ corresponds to the equilibrium position of the nuclei and to the full symmetry of the crystal lattice. Most of the other $\alpha_{\rho'\sigma'}(q, s)$ with $s \neq 0$ are used to represent the polarizability of the rotating group in non-equilibrium positions with lower symmetry. This is quite different in the expansion (3.3) where all the terms refer to the equilibrium position. We come back to the problem of rotating groups in crystals in Section 5 dealing with the selection rules.

*This influence, clearly, excludes a completely free rotation; but the simple assumption of a free rotation is sufficient for a qualitative discussion.

(*d*) It is well known that the higher polarizability derivatives and mechanical anharmonicity of lattice vibrations give rise to a continuous second-order Raman scattering which contains overtones and combination tones of all lattice vibrations irrespective of their wave-length. This opens up the possibility of interpreting a forbidden first-order Raman line with frequency ν_j as a second-order continuum with a sharp intensity peak at ν_j. Excluding accidental coincidence the line-like second-order peak must correspond to a combination band involving the branch of lattice vibrations with limiting frequency ν_j and elastic vibrations with limiting frequencies ν_e near zero. Several authors (Barriol and Fruhling 1948; Hornig 1948) have tentatively adopted this interpretation of forbidden Raman lines without closer inspection, thereby overlooking the fact that no sharp intensity peak can be found with a combination band in the frequency region $\nu_j+\nu_e(\nu_e \to 0)$.

This can be shown in the following way: We assume that ν_j refers to a branch of internal lattice vibrations with frequencies practically independent of the wave-vectors and that the intensity of one single second-order transition $v_j, v_e \to v_j+1, v_e\pm1$ involving long elastic waves (index e) as one partner depends only on the direction but not on the length of the wave vectors $\mathbf{q}_e$ tending towards zero; this latter assumption can be rigorously proved to be correct by means of the detailed formulae for the second-order Raman effect derived by Born and collaborators (Born and Bradburn 1947; Smith 1948). With these assumptions the total intensity $I(\nu_j+\nu_e)$ of the combination band in the frequency region round $(\nu_j+\nu_e)$ is proportional to the number $N(\nu_e)d\nu_e$ of elastic vibrations with frequencies between ν_e and $\nu_e+d\nu_e$. In general the frequency distribution in $\mathbf{q}$-space is not known and the theoretical determination of intensity peaks is a very difficult problem (Van Hove 1953). However, for the simple case of long elastic waves, $N(\nu_e)$ is well known to be

$$N(\nu_e)d\nu_e = \frac{\nu_e^2}{\bar{v}^3}\,d\nu_e, \tag{3.15}$$

$\bar{v}$ = mean velocity of sound. $N(\nu_e)$ vanishes for $\nu_e = 0$; hence, the intensity of the combination band $\nu_j+\nu_e$ $(\nu_e \to 0)$ is zero in the frequency region ν_j. No intensity peak of the combination band is to be expected there.

4. THE TEMPERATURE DEPENDENCE OF THE FIRST-ORDER RAMAN EFFECT

Owing to time dependent thermal perturbations, a crystal in thermal equilibrium is in a non-stationary state which may be represented as a linear superposition of stationary vibrational states. The squares of the expansion coefficients oscillate irregularly around average values which are given by the Boltzmann distribution. As far as light scattering is concerned and if a small interdependence of thermal and electromagnetic perturbations is neglected, a crystal in such a state behaves essentially like an ensemble of individual scattering normal vibrations q_j with a Boltzmann energy distribution. The intensity scattered by this ensemble may be obtained from equation (3.7) with the following, rather obvious modifications.

(*a*) We consider a Raman line with frequency ν_j scattered by the normal

vibration q_j. The total intensity $I(\nu_j)$ of this line may be represented as a sum $I(\nu_j) = \sum_{v_j} I^{v_j}_{v_j+1}$, where $I^{v_j}_{v_j+1}$ is the intensity scattered by the transitions with initial vibrational level v_j. $I^{v_j}_{v_j+1}$ is proportional to the square of the matrix element (3.7)* if $(v_{j'}+1)$ is replaced by the thermal average

$$(4.1) \qquad \overline{(v_{j'}+1)} = \frac{\sum_{v_{j'}}(v_{j'}+1)\exp(-v_{j'}h\nu_{j'}/kT)}{\exp(-v_{j'}h\nu_{j'}/kT)} = \frac{1}{1-\exp(-h\nu_{j'}/kT)}.$$

(*b*) The intensity $I(\nu_j)$ of a Raman line with frequency ν_j corresponding to all the different transitions $v_j \to v_{j+1}$ $(v_j = 0, 1, 2, \ldots)$ is obtained from the intensity $I^{v_j}_{v_j+1}$ by introducing the thermal average $\overline{(v_j+1)}$ instead of one special number (v_j+1). This gives

$$(4.2) \quad I(\nu_j) \simeq \frac{1}{1-\exp(-h\nu_j/kT)}\left\{\left(\frac{\partial\alpha_{\rho\sigma}}{\partial q_j}\right)_0 b_j + \sum_{j'}\frac{1}{6[1-\exp(-h\nu_{j'}/kT)]}\left(\frac{\partial^3\alpha_{\rho\sigma}}{\partial q_j \partial q_{j'}^2}\right)b_j b_{j'}^2 + \ldots\right\}^2.$$

The exponential outside the curly brackets produces an increase of the intensity with increasing temperature which can only be inverted if the third-order terms in the curly brackets have negative signs and are not negligible compared to the first-order term. In order to estimate the influence of the third-order terms we introduce an average frequency $\overline{\nu_{j'}} = 3\times10^{12}$ sec.$^{-1}$ corresponding to a wave number $\nu^*_{j'}$ of 100 cm.$^{-1}$. This choice implies the assumption that the highly excited, low frequency vibrations of the elastic branches of the crystal spectrum contribute essentially to the third-order terms. We now investigate the cases where $\nu^*_j = 500$ cm.$^{-1}$ and 1000 cm.$^{-1}$ and γ (see equation (3.9)) = 0.1, 0.05, 0.02, and 0.01 at very low temperatures $(\bar{v}_{j'} = 1)$. The resulting temperature dependence of $I(\nu_j)$ in arbitrary units is given in Fig. 1; it shows that under extreme conditions the third-order terms may be responsible for an inverse temperature effect. The effect could be further enhanced by reducing the value of $\overline{\nu_{j'}}$.

According to equation (4.2) and the numerical results of Fig. 1 the high frequency lattice vibrations are more likely to show an inverse temperature effect than the low frequency vibrations for which the exponential outside the curly brackets is decisive. This theoretical prediction is not confirmed by experiments (Nedungadi 1940, 1941; Ornstein and Went 1935*b*; Venkatesvarlu 1941, 1942). One may, therefore, hesitate to ascribe the inverse temperature effect to the contributions of third-order terms which, for unknown reasons, should always be opposed in sign to the derivative $(\partial\alpha_{\rho\sigma}/\partial q_0)_0$; but one can not completely exclude this possibility. The situation remains essentially unchanged if the mechanical anharmonicity of the lattice vibrations is taken into account; this follows immediately from the discussion in subsection 3(*c*).

In addition to the contributions of the higher-order terms, line broadening

*$[\alpha_{\rho\sigma}]^{v_j}_{v_j+1}$ determines the intensity of polarized Raman lines produced by polarized incident light. In the case of natural light summation over ρ, σ is required.

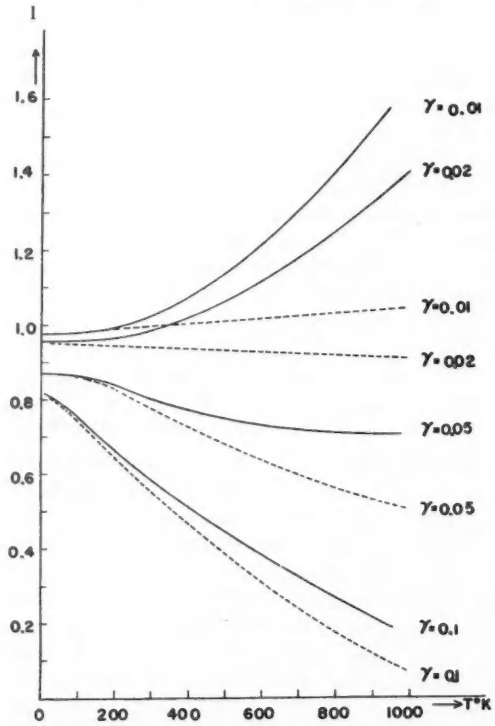

FIG. 1. The temperature dependence of the intensity of first-order Raman lines for different values of ν_i^* and γ. $\nu_i^* = 500\ \text{cm.}^{-1}$ (full curves); $\nu^* = 1000\ \text{cm.}^{-1}$ (dotted curves).

and resonance may be responsible for the inverse temperature effect. Concerning the influence of resonance the following considerations are helpful for an estimate of its magnitude.

(i) The relative magnitude of the tensor component $[\beta_{\rho\sigma}(q, v)]_{e''}^{e'}$ which, in principle, could produce an inverse temperature effect, can be estimated from the approximate relation (compare equations (2.11) and (2.13))

$$\left\{\frac{[\beta_{\rho\sigma}(q, v)]_{e''}^{e'}}{[\alpha_{\rho\sigma}(q)]_{e''}^{e'}}\right\}^2 \approx \left\{\frac{\nu_{e''}^{e'}}{\nu_{e''}^{e'} - \nu'}\right\}^2 = \eta \tag{4.3}$$

where $\nu_{e''}^{e'}$ and $\nu_{e''}^{e'}$ are vibrational and electronic absorption frequencies of the crystal. A contribution of $\beta(q, v)$ to the intensity of first-order Raman lines which is strong enough for producing an inverse temperature effect requires η to be at least of the order 0.1. The consequences of this condition can be seen from the following example: We assume that $\nu_{e''}^{e'} = 3\times10^{13}\ \text{sec.}^{-1}$ and $\nu' = 70\times10^{13}\ \text{sec.}^{-1}$ ($\lambda' = 4300$ Å), and obtain from the condition $\eta \leqslant 0.1$ that $\nu_{e''}^{e'}$ is about $80\times10^{13}\ \text{sec.}^{-1}$ ($\lambda_{e''}^{e'} = 3800$ Å). This estimate shows that for the scattering of blue light absorption in the near ultraviolet region between 3800

and 4000 Å implies a breakdown of the resonance condition 1(*c*) which may be partly responsible for the inverse temperature effect.

(ii) If the absorption frequencies of a crystal are unknown, the validity of the resonance condition 1(*c*) can be checked indirectly in different ways. Most useful for this purpose is the relation $\alpha_{\rho\sigma} = \alpha_{\sigma\rho}$ expressing the symmetry of the scattering tensor and the formula for the intensity ratio of Stokes and anti-Stokes Raman lines:

$$\frac{I(\nu_j)\text{Stokes}}{I(\nu_j)\text{anti-Stokes}} = \frac{(\nu'-\nu_j)^4}{(\nu'+\nu_j)^4} \exp(-h\nu_j/kT). \tag{4.4}$$

Both relations are a consequence of the resonance condition 1(*c*) and become invalid if the light frequency approaches an absorption frequency of the crystal (Placzek 1934).

5. SELECTION RULES FOR THE FIRST-ORDER RAMAN EFFECT IN CRYSTALS

(*a*) *General Principles*

Selection rules are rules derived from the symmetry of the scattering system according to which certain components of the tensor $[\alpha_{\rho\sigma}]^{\nu'}_{\nu}$ are zero and, hence, do not contribute to the intensity of the Raman scattering. The vanishing of certain tensor components can be understood and predicted from the following argument: The matrix elements $[\alpha_{\rho\sigma}]^{\nu'}_{\nu}$ are completely determined by the Hamiltonian function of the scattering system and must, therefore, have the same numerical values in all equivalent coordinate systems; i.e. in all those coordinate systems which may be transformed into each other by the covering operations which leave the Hamiltonian of the scattering system unchanged. In terms of group theory this may be expressed as follows: We consider, for convenience, those matrix elements $[\alpha_{\rho\sigma}]^{\nu'}_{\nu}$ and those of their linear combinations which have simple transformation properties, e.g. $(\alpha_{xx}+\alpha_{yy})$, $(\alpha_{xx}-\alpha_{yy})$, α_{zz}, α_{xy}, α_{yz}, α_{zx}, in the case of rotations about the z-axis.* They must vanish, if they do not transform according to the totally symmetric, irreducible representation of the space group of the scattering system. More generally this is true if they belong to a reducible representation in which the totally symmetric irreducible representation is not contained. The question whether or not a representation is totally symmetric in this general sense can be answered by means of the standard rules for reducing reducible representations and by applying the rule that the character of the representation of a direct product is equal to the product of the characters of the individual representations. Furthermore, one has to use the rule that the derivative $(\partial^n\alpha_{\rho\sigma}/\partial q^n)_0$ transforms like the product $x_\rho x_\sigma q^n$ (x_ρ, x_σ, . . . are the coordinates).

(*b*) *The Representation of Space Groups* (*Bouckaert, Smoluchowsky, and Wigner 1936; Seitz 1936*)

We consider first the Abelian subgroup of the translations. Suitable repre-

*In this case the linear combinations could be avoided by introducing the circular coordinates z, $x+iy$, $x-iy$, which will be denoted by the subscripts 0, +1, and −1. It can be shown that the circular tensor components $\alpha_{\mu\nu}$ ($\mu, \nu = 0, \pm 1$) are multiplied by the factor $\exp[i(\mu-\nu)\phi]$, if the coordinate system is rotated through the angle ϕ about the z-axis. It can be further shown that $(\alpha_{xx}+\alpha_{yy}) = 2\alpha_{11}$ and $(\alpha_{xx}-\alpha_{yy}) = -(\alpha_{12}+\alpha_{21})$.

sentations of this group are the matrices corresponding to the displacement by the identity period $\mathbf{a}_i$ $(i = 1, 2, 3)$; they are diagonal and have the diagonal elements $M_{jj} = \exp(2\pi i \mathbf{q} \cdot \mathbf{a}_i)$. Since the eigenfunctions of a mechanical system form bases for the representations of the group of operations which leave the Hamiltonian of the system unchanged, it follows, for instance, that the electronic eigenfunctions of a crystal with nuclei fixed in lattice points may be characterized by a wave vector $\mathbf{q}$. The same is true for the vibrational eigenfunctions as long as the equilibrium positions of the nuclei form essentially a periodic lattice.

We come now to the non-translatory elements of the space groups. These elements may be classified according to their effect on the wave vectors $\mathbf{q}$ which characterize the eigenfunctions $\psi_{\mathbf{q}}$ of a system. For each $\psi_{\mathbf{q}}$ one can distinguish between those operations which change $\mathbf{q}$ and those which transform $\mathbf{q}$ in itself (or change only its sign).* The latter operations form a group which is called the group of the wave vector $\mathbf{q}$ or $\mathbf{q}$-group. $\psi_{\mathbf{q}}$ transforms under the operations of the group of $\mathbf{q}$ by an irreducible representation of this group which is called a small representation of the space group.

If $\mathbf{q} = 0$, the group of $\mathbf{q}$ is isomorphous with the crystallographic point group of the crystal and the full symmetry of this point group determines the displacement vectors of the normal vibrations and the optical selection rules. For general directions of $\mathbf{q}$, however, the group of $\mathbf{q}$ contains only the identity, and the displacement vectors are arbitrary, i.e. only determined by force constants and masses. No selection rules can, in principle, be obtained from the non-translatory symmetry elements for these cases. Practically, of course, it may be that the selection rules valid for $\mathbf{q} = 0$ are still a good approximation for cases where $|q| \ll 1/|a_i|$. Whether or not this is true is a physical problem which will be discussed later.

(*c*) *Selection Rules for the Scattering by Electrons in Localized Orbitals*

(i) *Selection Rules for the Wave Vectors*

Any component $(\partial\alpha_{\rho\sigma}/\partial q_j)_0 q_j$ of the first-order polarizability contributes to the matrix element $[\alpha_{\rho\sigma}]^{n'}_{n'+1}$ a term which transforms by a representation with character $\exp[2\pi i(\mathbf{q}_j+\mathbf{Q}) \cdot \mathbf{a}_i]$. This follows quite generally from the transformation properties of direct products (see the rule at the end of Section 5(*a*)), if one considers that $\alpha_{\rho\sigma}$ has the character $\exp(2\pi i \mathbf{Q} \cdot \mathbf{a}_i)$ (see equation (2.20)) and that q_j has the character $\exp(2\pi i \mathbf{q}_j \cdot \mathbf{a}_i)$. The same result may be obtained without reference to group theory from the equation (3.4). This first-order term is invariant against all possible translations only if

$$\mathbf{q}_j+\mathbf{Q} = 0 \text{ or } \mathbf{q}_j = -\mathbf{Q}. \tag{5.1}$$

This selection rule is often interpreted as representing the law of conservation of momentum for a collision between a photon and a free phonon. Concerning the contributions of the third-order terms in equation (3.7) the same selection rule can be obtained in the following way:

The third-order terms transform by a representation with character $\exp[2\pi i(\mathbf{Q}+\mathbf{q}_j+\mathbf{q}_{j'} \pm \mathbf{q}_{j'})]$. This requires the selection rule

*The transformation $\mathbf{q} \rightarrow -\mathbf{q}$ does not change the geometry of the system; for scattering problems it is equivalent to a reversal of the optical path of the incident and scattered light.

(5.2) $$\mathbf{Q}+\mathbf{q}_j+\mathbf{q}_{j'}\pm\mathbf{q}_{j'} = 0.$$

The ambiguity in the sign of the last term can be removed by the condition that selection rules must be invariant against the transformation $\mathbf{Q} \rightarrow -\mathbf{Q}$. This condition requires the negative sign in the last term and leads again to the selection rule (5.1).*

The selection rule (5.1) is stringent only for harmonic lattice vibrations. In the case of mechanical anharmonicity one has to consider the behavior of polarizability derivatives of even order, e.g. $(\partial^2\alpha_{\rho\sigma}/\partial q_j\partial q_{j'})_0 q_j q_{j'}$. It is readily found that they are subject to the selection rule

(5.3) $$\mathbf{q}_j = -\mathbf{Q}+\mathbf{q}_{j'},$$

according to which lattice vibrations with any possible wave vector $\mathbf{q}_j$ can be active in the first-order Raman effect. The contributions of the anharmonic terms $(\partial^2\alpha_{\rho\sigma}/\partial q_j\partial q_{j'})_0 q_j q_{j'}$ produce a very weak Raman spectrum of the first order which is continuous, since the frequency of the lattice vibrations q_j belonging to one certain branch of the lattice spectrum depends more or less strongly on the wave vector $\mathbf{q}_j$. Only if this continuous first-order spectrum is concentrated within a very small line-like frequency interval may it become intense enough for observation. This condition shows that the internal vibrations of molecules or polyatomic ions in crystals which have practically the same frequency for all wave vectors are the only ones which, in case of extreme mechanical anharmonicity, may produce a line-like first-order Raman effect for which deviations from the selection rule (5.1) and others become observable. This effect is equivalent to the anharmonic coupling of "individual molecules" in a crystal with the surrounding crystal field which has been discussed by Hornig (1948).

It should be pointed out that the selection rule (5.3) violates the law of conservation of momentum for collisions between photons and individual phonons. This difficulty can be easily overcome, if anharmonic lattice vibrations are pictured as phonons which are not free but coupled to the lattice by the anharmonic terms in the potential energy. In this case the law of conservation of momentum is only valid for the scattering system as a whole but not for collisions between photons and individual "bound" phonons.

(ii) *Selection Rules for the Matrix Elements* $[\alpha_{\rho\sigma}]^{q_j}_{v_j+1}$

The selection rules for the wave vectors are valid for all the tensor components $[\alpha_{\rho\sigma}]^{q_j}_{v_j+1}$ independent of the subscripts $\rho\sigma$. The symmetry elements of the group of $\mathbf{q}_j$ give rise to additional selection rules which are based on the different behavior of different components $[\alpha_{\rho\sigma}]^{q_j}_{v_j+1}$ under the transformations of the group of $\mathbf{q}_j$. The problem of physical interest is to find the group of $\mathbf{q}_j$.

We consider first harmonic lattice vibrations for which the q-selection rule (5.1) is valid. In this case the question arises whether, for the purpose of deriving selection rules, the vibrations with $\mathbf{q}_j = -\mathbf{Q}$ may be practically

*The positive sign in the last term gives for positive Q: $\mathbf{q}_j(+) = -(\mathbf{Q}+2\mathbf{q}_{j'})$ and for negative Q: $\mathbf{q}_j(-) = (\mathbf{Q}-2\mathbf{q}_{j'})$. The resulting inequality $|q_j(+)| \neq |q_j(-)|$ is forbidden by the above condition.

identified with the fundamental lattice vibrations with $\mathbf{q}_j = 0$. The following arguments seem to justify this approximation.

It is generally assumed that all properties of crystal vibrations approach asymptotically the properties of the fundamental lattice vibrations if $|q|$ tends towards zero. Particularly, it is assumed that different lattice vibrations have very nearly identical optical properties if they belong to the same branch of the lattice spectrum and if their wave-lengths are larger than the wave-length of visible light. The theory of lattice vibrations justifies this assumption as long as only short-range interactions between vibrating lattice points are taken into account. However, calculations of Blackman (1952) indicate that the long-range electrostatic forces in ionic crystals of lower than cubic symmetry may strongly perturb the asymptotic behavior of lattice vibrations such that the restoring forces $\partial^2 P/\partial q_j^2$ (P is potential energy) of electrostatic origin depend on the direction of $\mathbf{q}_j$ even if $|q_j|$ tends towards zero.* It appears that this effect has been discovered experimentally by Mathieu and Couture-Mathieu (1950) who mention cases where the frequencies of Raman lines depend on the direction of the incident and scattered light, and hence, according to equation (5.1), on $\mathbf{q}_j$. It should, however, be mentioned that such frequency variations do not occur in calcite and most of those crystals which have forbidden lines in their Raman spectrum.

We come now to the asymptotic behavior of $\partial\alpha/\partial q_j$ which is important for the derivation of selection rules. As long as only electrons in localized orbitals are concerned the polarizability of an atom or polyatomic molecule depends mainly on the position of the immediate neighbors and is insensitive against the electric field due to the displacement of distant ions; this follows from the fact that the polarizability of molecular systems is practically independent of weak external electric fields. We conclude therefore that $\partial\alpha/\partial q_j$ is less sensitive against variations of $\mathbf{q}_j$ ($|q_j| \to 0$) than $\partial^2 P/\partial q_j^2$ and that it should be a constant independent of $\mathbf{q}_j$ if the same is observed for the frequency $\nu(q_j)$. To make this point quite clear we consider the totally symmetric vibration of the CO_3^{--}-ion in calcite which offers a good testing ground for the theory of the Raman effect in crystals. This vibration is a typical "internal" vibration such that the vibrational distortion of the individual CO_3^{--}-ions and their neighborhood is completely independent of $\mathbf{q}_j$ if $|q_j|$ tends towards zero. The same follows necessarily for the polarizability derivative $(\partial\alpha/\partial q_j)_0 q_j$ if only electrons in localized orbitals are involved. In this case, the selection rules for the scattering by lattice vibrations with $\mathbf{q}_j = -\mathbf{Q}$ are practically equivalent to the selection rules for the fundamental lattice vibrations in the sense that Raman lines which are strictly forbidden by the latter are extremely weak according to the former.

As far as the first-order term of equation (3.7) is concerned the selection rules for the fundamental vibrations have been worked out by several authors

*Blackman's results refer to wave-lengths long compared to the lattice cell but small compared to the macroscopic crystal. They have nothing to do with the fact, well known since the work of Lyddane and Herzfeld (1938), that the shape of an ionic crystal determines the frequencies of those lattice vibrations the wave-lengths of which are of the order of the crystal dimensions.

(Brester 1923; Cabannes 1940; Mathieu 1945; Hornig 1948) and need no further discussion; they are contained in the selection rule (5.11). Regarding the contributions of the third-order terms the selection rules are determined by the symmetry character of the third-order derivatives $(\partial^3\alpha_{xy}/\partial q_j \partial q_{j'}^2)$, which transform like the product $xyq_jq_{j'}^2$. If $q_{j'}$ is a non-degenerate normal coordinate, then $q_{j'}^2$ transforms always by a totally symmetric representation with character 1 and the product $xyq_jq_{j'}^2$ transforms like the product xyq_j; this means that the selection rules for $(\partial\alpha_{\rho\sigma}/\partial q_j)_0$ and $(\partial^3\alpha_{\rho\sigma}/\partial q_j\partial q_{j'}^2)_0$ are identical. However, if $q_{j'}$ is a degenerate normal coordinate, $q_{j'}^2$ belongs to a reducible representation which, generally, does not reduce to a totally symmetric representation alone (Rosenthal and Murphy 1936). Hence, symmetry character and selection rules are different for $(\partial\alpha_{\rho\sigma}/\partial q_j)_0$ and $(\partial^3\alpha_{\rho\sigma}/\partial q_j\partial q_{j'}^2)_0$ if $q_{j'}$ is degenerate; accordingly, first-order Raman lines which are forbidden by the *linear* polarizability theory may have a non-vanishing intensity produced by the third-order terms in equation (3.7).

We shall now investigate how the selection rules are modified by the mechanical anharmonicity of the lattice vibrations. The vibrational eigenfunctions of a crystal form bases for the representations of the space group of the crystal independent of their harmonic or anharmonic nature. Hence, the selection rules for the *fundamental lattice* vibrations are valid for harmonic and anharmonic vibrations alike. The only new features introduced by the mechanical anharmonicity are the contributions of the terms $(\partial^2\alpha_{\rho\sigma}/\partial q_j\partial q_{j'})_0$ to the first-order Raman effect. Since the **q**-selection rules for these terms do not exclude any possible wave vector they belong mostly to a group of **q** corresponding to a general direction of **q**. No selection rules can, therefore, be obtained which require the vanishing of these terms for reasons of symmetry.

The situation is similar for the case of a hindered rotation of certain atomic groups in the crystal. For the extreme case of practically free rotation the selection rules can be readily obtained by introducing the circular coordinates described in the footnote on page 327. Using this new system of coordinates the tensor components $\alpha_{\mu\nu}(q, \phi)$ of equation (3.14) $(\mu, \nu = 0, \pm 1)$ transform under rotations about the z-axis by representations with character $\exp[i(\mu-\nu+s)\phi]$ and the matrix element $[\alpha_{\mu\nu}(q, \phi)]^{\nu', m'}_{\nu'', m''}$ has the character $\exp[i(\mu-\nu+s+m'-m'')\phi]$. This gives the rotational selection rule

$$m''-m' = \mu-\nu+s, \tag{5.4}$$

according to which all tensor components $\alpha_{\mu\nu}(q, s)$ may contribute to the first-order Raman effect. The components $\alpha_{\mu\nu}(q, s)$ do not correspond to the full symmetry of the crystal if $s \neq 0$ and the same is true for the selection rules to which they are subject.

Summarizing one can say that the selection rules obtained from the *linear* polarizability theory may be violated by the third-order terms of equation (3.7) in crystals with degenerate normal vibrations, by second-order terms in crystals with strong mechanical anharmonicity, and by rotating groups. All these higher order effects strongly increase with increasing temperature.

Their magnitude should, however, be independent of the direction of the incident light.*

(*d*) *Selection Rules for the Scattering by Electrons in Delocalized Crystal Orbitals*

(i) *Selection Rules for the Wave Vectors*

The selection rules for the scattering by electrons in delocalized crystal orbitals are determined by the transformation properties of the general scattering tensor $[\alpha_{\rho\sigma}(q)]^{\nu'}_{\nu''}$ of equation (2.17). We investigate first the integrals

$$\{I^{\lambda'}_{\sigma}(q)\}^{\nu'}_{\nu''} = \int \exp(2\pi i \mathbf{Q}' \cdot \mathbf{r})(\rho v_{\sigma})^{\nu'}_{\nu''} dv \tag{5.5a}$$

and

$$\{I^{\lambda''}_{\rho}(q)\}^{\nu''}_{\nu'} = \int \exp(-2\pi i \mathbf{Q}'' \cdot \mathbf{r})(\rho v_{\rho})^{\nu''}_{\nu'} dv, \tag{5.5b}$$

by expanding the space function $(\rho\mathbf{v})^{\nu'}_{\nu''}$:

$$(\rho\mathbf{v})^{\nu'}_{\nu''} = [(\rho\mathbf{v})^{\nu'}_{\nu''}]_0 + \sum_j \left[\frac{\partial}{\partial q_j}(\rho\mathbf{v})^{\nu'}_{\nu''}\right]_0 q_j + \ldots . \tag{5.6}$$

According to equation (2.16) $[(\rho\mathbf{v})^{\nu'}_{\nu''}]_0$ transforms like the product of two electronic wave functions of the crystal with nuclei fixed in the equilibrium positions; hence, $[(\rho\mathbf{v})^{\nu'}_{\nu''}]_0$ transforms by a representation with character $\exp(2\pi i \mathbf{q}_i \cdot \mathbf{a}_i) \cdot (\mathbf{q}_i = \mathbf{q}_{\nu''} - \mathbf{q}_{\nu'})$. Similarly, the first-order terms of the expansion (5.6) have the character $\exp[2\pi i(\mathbf{q}_i + \mathbf{q}_j) \cdot \mathbf{a}_i]$. This has the effect that the product of the integrals (5.5*a*) and (5.5*b*) which appears in equation (2.17) vanishes unless at least one of the following pairs of conditions (*a*) and (*b*) is simultaneously fulfilled:

(5.7) $\mathbf{Q}' + \mathbf{q}_i = 0$ (*a*), $\mathbf{Q}'' + \mathbf{q}_i = 0$ (*b*), — condition required for the non-vanishing of the product of the zeroth-order terms, i.e. selection rule for the Rayleigh scattering;

(5.8) $\mathbf{Q}' + \mathbf{q}_i = 0$ (*a*), $\mathbf{Q}'' + \mathbf{q}_i + \mathbf{q}_j = 0$ (*b*),

(5.9) $\mathbf{Q}' + \mathbf{q}_i + \mathbf{q}_j = 0$ (*a*), $\mathbf{Q}'' + \mathbf{q}_i = 0$ (*b*), — condition required for the non-vanishing of the mixed product of a zeroth-order and a first-order term, i.e. selection rule for the first-order Raman effect;

(5.10) $\mathbf{Q}' + \mathbf{q}_i + \mathbf{q}_j = 0$ (*a*), $\mathbf{Q}'' + \mathbf{q}_i + \mathbf{q}_j = 0$ (*b*), — condition required for the non-vanishing of the product of the first-order terms, i.e. selection rule for the second-order Raman effect.

By eliminating $\mathbf{q}_i$, the conditions (5.8) and (5.9) are transformed into the selection rules (5.1).

*The latter statement may be wrong if the thermal equilibrium of the crystal is disturbed by the irradiation with an intense beam of light. This irradiation produces strong heating effects and possibly a selective excitation of lattice vibrations which may easily depend on the direction of the incident light beam.

(ii) *Selection Rules for the Matrix Elements* $[\alpha_{\rho\sigma}]^{\nu_j}_{\nu_{j+1}}$

One question of physical interest is whether or not the selection rules depend on the wave vectors $\mathbf{Q}'$ and $\mathbf{Q}''$ of the incident and scattered visible light. In order to answer this question we consider the conditions (5.8) and (5.9) to be selection rules for the electronic wave vectors $\mathbf{q}_l$. We find in this way that the summation over l' and l''' in equation (2.17) contains only terms for which $\mathbf{q}_l = -\mathbf{Q}'$ and $\mathbf{q}_l = -\mathbf{Q}''$. This means that the wave vectors $\mathbf{Q}'$ and $\mathbf{Q}''$ determine the electronic orbitals which contribute to the polarizability $[\alpha_{\rho\sigma}]^{\nu'}_{\nu''}$ in such a way that different orbitals are involved for different directions of the incident and scattered light; this may cause a strong anisotropy of the tensor components $[\alpha_{\rho\sigma}]^{\nu'}_{\nu''}$ even if the wave vectors $\mathbf{Q}'$ and $\mathbf{Q}''$ tend towards zero.

We come now to the special selection rules for the $[\alpha_{\rho\sigma}]^{\nu'}_{\nu''}$. According to the selection rules (5.8) and (5.9), the product of the two matrix elements (5.5*a*) and (5.5*b*) is only different from zero if (5.5*a*) contributes to it the zeroth-order matrix element $[(\rho v_\sigma)^{\nu'}_{\nu''}]_0$ and (5.5*b*) the first-order matrix element $[\partial/\partial q_j(\rho v_\rho)^{\nu'''}_{\nu'}]_0 q_j$ or the other way round. Hence, the product $\{I^{\lambda'}_{\sigma}(q)\}^{\nu'}_{\nu''} \times \{I^{\lambda'''}_{\rho}(q)\}^{\nu'''}_{\nu'}$ does not vanish only if $[(\rho v_\sigma)^{\nu'}_{\nu''}]_0$ and $[\partial/\partial q_j(\rho v_\rho)^{\nu'''}_{\nu'}]_0$ are simultaneously different from zero. This condition leads to the required selection rules on the basis of the following argument: Both $[(\rho v_\sigma)^{\nu'}_{\nu''}]_0$ and $[\partial/\partial q_j(\rho v_\rho)^{\nu'''}_{\nu'}]_0$ refer to the equilibrium position of the nuclei and, hence, transform by a representation of the space group of the crystal. In particular the zeroth-order term transforms like the product $w_{l''}v_\sigma w_{l'}$ and the first-order term transforms like the product $w_{l''}v_\rho q_j w_{l'}$ and both products must be totally symmetric. ($w_{l''}$ and $w_{l'}$ are electronic orbitals.) Since the velocity components v_σ ($\sigma = 1, 2, 3$) transform like the coordinates x_σ ($\sigma = 1, 2, 3$), this condition gives the selection rule*

$$
\begin{aligned}
&[\alpha_{\rho\sigma}]^{\nu_j}_{\nu_{j+1}} = 0 \text{ unless } \chi(x_\rho q_j) = \chi(x_\sigma), \\
&\chi(x_\sigma) = \text{symmetry character of } x_\sigma, \\
&\chi(x_\rho q_j) = \text{symmetry character of the product } x_\rho q_j.
\end{aligned} \tag{5.11}
$$

This selection rule for the first-order Raman scattering by electrons in delocalized crystal orbitals is formally identical with the selection rule for the scattering by localized electrons. There is, however, the essential difference that, as far as the properties of the delocalized space functions $[(\partial\alpha_{\rho\sigma}/\partial q_j)_0 q_j]^{\nu_j}_{\nu_{j+1}}$ are concerned, the normal vibrations q_j can not be approximately identified with fundamental lattice vibrations. This may be formally derived from the $\mathbf{q}$-selection rules (5.8) and (5.9) which associate different electronic orbitals with different lattice vibrations depending on their respective wave vectors. More physically speaking, localized atomic or molecular orbitals in crystals depend only on the nuclear arrangement in their immediate neighborhood; hence, the polarizability of electrons in such orbitals depends only on the *local* distortions produced by lattice vibrations, which are, in the case of

*This selection rule is only valid for the first-order derivative and neglects higher terms in the expansion (5.6) or (3.3).

internal vibrations, practically equal for all $\mathbf{q}_j$ ($\mathbf{q}_j \to 0$). The polarizability of electrons in delocalized orbitals, however, depends on the arrangement of *all* the nuclei in the lattice and this introduces a difference between long waves and the fundamentals. It follows that the selection rules for a vibration with wave vector $\mathbf{q}_j = -\mathbf{Q}$ are determined by the group of $\mathbf{q}_j$ and not even approximately by the full crystallographic point group.

6. THE CASE OF CALCITE

We conclude the theoretical investigation of the Raman effect in crystals with an analysis of the Raman scattering of calcite which has been investigated most thoroughly and is typical for all cases where deviations from the predictions of the linear, atomic polarizability theory occur. We give first a summary of the relevant experimental results and discuss them later in terms of the preceding theory.

(*a*) *Experimental Results*

(i) *The Resonance Condition* 1(*c*)

The absorption spectrum of calcite (Table I) has been measured by Pflüger and Ornstein (Ornstein and Went 1935*a*; Pflüger 1904). It is difficult to predict whether or not the weak absorption in the region near 4000 Å is compatible with the resonance condition 1(*c*); hence, additional arguments will be used to clarify this question.

TABLE I

THE ABSORPTION SPECTRUM OF CALCITE

λ in Å	2310	2400	2800	3910	4910
Absorption coefficient	1.00	0.58	0.16	0.092	0.078

Perhaps the most convincing argument is obtained from an analysis of the intensities of Raman lines corresponding to different frequencies ν' of the incident light. Ornstein and Went (1935*b*) find that the experimental results can be explained by the assumption that only one of the different resonance denominators $[(\nu^{l'}_{l''})^2 - (\nu')^2]$ in equation (2.17) is decisive; it corresponds to a strong absorption in the wave-length region around 1600 Å. This absorption does not violate the condition 1(*c*). The same may be concluded from the intensity ratio of Stokes and anti-Stokes Raman lines (Ornstein and Went 1935*b*) and from the experimental fact that the scattering tensor is symmetric (Michalke 1938).

(ii) *The Temperature Dependence of the First-order Raman Effect*

Ornstein and Went (1935*b*) find an increase in line width and a decrease of frequency and intensity of all the first-order Raman lines if the temperature is raised. All these effects are most pronounced with the low frequency lattice vibrations and practically disappear in the case of the internal vibration of the CO_3^{--}-ion with frequency 1088 cm.$^{-1}$. Most interesting for our discussion is the pronounced inverse temperature effect which is quantitatively given in

Table II by the ratio $R_\nu = I_{cal}/I_{obs}$ (I_{obs} = observed intensity, I_{cal} = intensity calculated from the formula of the linear polarizability theory; the subscript ν gives the frequency of the Raman line).

TABLE II

THE INVERSE TEMPERATURE EFFECT IN CALCITE

T, °K.	R_{155}	R_{282}	R_{714}	R_{1088}
90	—	0.75	—	0.99
293	1.00	1.00	1.00	1.00
376	1.30	1.12	1.20	0.99
426	2.12	1.22	1.60	1.02

(iii) *The Selection Rules*

The experimental results concerning the selection rules for the first-order Raman effect in calcite have been most thoroughly discussed by Couture (1947, 1948). We repeat some of her results which are necessary for our analysis. The experimental situation is described by a coordinate system x (direction of incident light), y (direction of scattered light), z which is fixed in space and a coordinate system X, Y, Z fixed in the crystal, such that Z is the direction of the optical axis. This allows one to distinguish between three different relative orientations of crystal and radiation which may be characterized by the direction Z of the optical axis:

$$Z||x,\ Z||y,\ Z||z\ (|| = \text{parallel}).$$

For each of these three cases one can measure the degree of depolarization $\rho = I_z/I_z$ and the total intensity of Raman lines $I = I_z + I_z$. (I_z and I_z are the components of the scattered light with polarization vector in direction x and z.) ρ and I are proportional to the squares of the matrix elements $[\alpha_{\rho\sigma}(q)]^{\nu_j}_{\nu_{j+1}}$ for which we write, in short, $\epsilon_{\rho\sigma}$. If the $\epsilon_{\rho\sigma}$ are represented in the coordinate system fixed in the crystal and if natural incident light is used one finds the following relations:

$$(6.1)\qquad \begin{array}{lccc} & Z||x & Z||y & Z||z \\ \rho = & \dfrac{\epsilon_{ZX}^2+\epsilon_{YZ}^2}{\epsilon_{XY}^2+\epsilon_{YY}^2}, & \dfrac{\epsilon_{XY}^2+\epsilon_{ZX}^2}{\epsilon_{YY}^2+\epsilon_{YZ}^2}, & \dfrac{\epsilon_{XY}^2+\epsilon_{ZX}^2}{\epsilon_{YZ}^2+\epsilon_{ZZ}^2}, \\ I = & \epsilon_{YY}^2+A, & \epsilon_{YY}^2+A, & \epsilon_{ZZ}^2+A, \end{array}$$

$$A = \epsilon_{XY}^2+\epsilon_{YZ}^2+\epsilon_{ZX}^2.$$

This scheme allows one to calculate the tensor components $\epsilon_{\rho\sigma}$ from the experimental values of ρ and I. We discuss only the Raman line corresponding to the totally symmetric internal vibration of the CO_3^{--}-ion with frequency 1088 cm.$^{-1}$ since it is the only one in the calcite spectrum which shows pronounced deviations from the predictions of the linear, atomic polarizability theory. The experimental results are contained in the scheme

$$(6.2)\qquad \begin{array}{lccc} & Z||x & Z||y & Z||z \\ \rho = & 0.0, & 0.4, & 0.2, \\ I = & 1.4, & 1.4, & 0.3. \end{array}$$

This gives

$$\left.\begin{aligned} &\epsilon^2_{XY} = 0.4, \qquad \epsilon^2_{YZ} = \epsilon^2_{ZX} = 0 \\ &\epsilon^2_{YY} = 1, \end{aligned}\right\} \text{for the cases } Z||x \text{ and } Z||y, \tag{6.3}$$

and

$$\left.\begin{aligned} &\epsilon^2_{XY} = 0.048, \qquad \epsilon^2_{YZ} = \epsilon^2_{ZX} = 0 \\ &\epsilon^2_{ZZ} = 0.25, \end{aligned}\right\} \text{for the case } Z||z. \tag{6.4}$$

These results show that the magnitude of some of the components of the scattering tensor depends strongly on the direction of the incident and scattered light and that ϵ_{XY} is different from zero in contrast to the ordinary selection rules. It is, however, important to note that the cases $Z||x$ and $Z||y$ are compatible with one single set of tensor components.

(*b*) *Interpretation of Experimental Results*

In order to explain the behavior of calcite in a convincing way, we exclude first all possible interpretations which are not really satisfactory and show later that the only remaining explanation is compatible with all the observable facts.

The resonance condition 1(*c*) has been already dealt with in subsection 6(*a*), (i) and has been shown to be reasonably well fulfilled.

We come now to the higher order effects of subsection 5(*c*), (ii). These effects could, in principle, be responsible for the appearance of Raman lines which are forbidden by selection rules derived from the *linear* polarizability theory. But the intensity of these forbidden lines should be strongly dependent on the temperature and independent of the direction of the incident light.* The contrary is true according to the experiments.

The only remaining effect is the scattering by electrons in delocalized crystal orbitals which is most conspicuous if the scattering by electrons in localized orbitals is forbidden by the ordinary selection rules. It has been shown in the preceding sections that the magnitude of the components of the scattering tensor corresponding to electrons in delocalized crystal orbitals depends on the directions of the incident and scattered light. This explains qualitatively the most striking feature of the experiments. Furthermore, it can be shown that the results tabled in the equations (6.3) and (6.4) are compatible with the selection rule (5.11). The group of $\mathbf{q} = -\mathbf{Q}$ is in all three cases the point group S which is formed by the two symmetry elements' identity and center of symmetry. The normal coordinate q_{1088} is totally symmetric and transforms by a small representation with character 1; the cartesian coordinates transform all by the same antisymmetric representation with character -1. Hence, no single tensor component $\epsilon_{\rho\sigma}$ is forbidden and the finite experimental value of ϵ_{XY} is compatible with the selection rules. The vanishing of ϵ_{YZ} and ϵ_{ZX} is not required by a rigorous selection rule, but is an

*It has been mentioned in the footnote on page 332 that a selective excitation of lattice vibrations due to the strong irradiation with an incident light beam could be responsible for the anisotropy of the tensor components $\epsilon_{\rho\sigma}$. This possibility must be excluded for calcite, since the cases $Z||y$ and $Z||z$ are equivalent with respect to the direction of the incident light.

accidental property of the scattering system. The reason for the smallness of ϵ_{YZ} and ϵ_{ZX} is most probably the fact that the nuclear displacements corresponding to the totally symmetric vibration with frequency 1088 cm.$^{-1}$ are perpendicular to the z-axis; this leaves the matrix elements $[\alpha_{YZ}]^0_{i+1}$ and $[\alpha_{ZX}]^0_{i+1}$ apparently unchanged and affects mainly the matrix element $[\alpha_{XY}]^0_{i+1}$. It appears that simple relations between nuclear displacements and the corresponding polarizability changes of the type suggested above are most pronounced in the case of delocalized crystal orbitals; in fact, the experimental results of Couture-Mathieu (1950*b*, 1952) indicate that they are in general true also for the polarizability of localized electrons.

The equivalence of the cases $Z||x$ and $Z||y$ is also readily explained. These two cases can be formally transformed into each other by exchanging $\mathbf{Q}'$ with $\mathbf{Q}''$. This corresponds to the transformation $\mathbf{Q} \rightarrow -\mathbf{Q}$ which leaves the scattering system unchanged.

Concerning the inverse temperature effect of the low frequency Raman lines of calcite, the electrons in localized and delocalized orbitals need not be considered separately. We believe that strong line broadening is the essential cause of this effect but we do not exclude contributions of the higher-order polarizability derivatives as a possible explanation.

ACKNOWLEDGMENTS

The author is indebted to the Summer Research Institute for Mathematics and Theoretical Physics in Queen's University for the award of a Fellowship and to Prof. Dr. W. Opechowski for valuable discussions.

REFERENCES

AYNARD, R. 1952. Compt. rend. **234**: 2352.
BARRIOL, J. and FRUHLING, A. 1948. J. phys. **9**: 98.
BLACKMAN, M. 1952. Proc. Phys. Soc. A, **65**: 394.
BORN, M. and BRADBURN, M. 1947. Proc. Roy. Soc. A, **89**: 277.
BOUCKAERT, L. P., SMOLUCHOWSKY, R., and WIGNER, E. 1936. Phys. Rev. **50**: 58.
BRESTER, C. J. 1923. Kristallsymmetrie und Reststrahlen. Dissertation, Utrecht.
BUCKMASTER, H. A. 1952. Can. J. Phys. **30**: 314.
CABANNES, J. 1940. Compt. rend. **211**: 625, 750.
COUTURE, L. 1947. Ann. phys. **2**: 5.
——— 1948. Ann. phys. **3**: 520.
COUTURE-MATHIEU, L. 1950*a*. J. phys. **11**: 511.
——— 1950*b*. Compt. rend. **231**: 839.
——— 1952. Compt. rend. **234**: 1761.
DIRAC, P. A. M. 1927. Proc. Roy. Soc. A, **114**: 243, 710.
FERMI, E. 1932. Revs. Mod. Phys. **4**: 87.
FRUHLING, A. 1951. Ann. phys. **6**: 401.
HEITLER, W. 1954. The quantum theory of radiation. 3rd ed. The Clarendon Press, Oxford.
HORNIG, D. F. 1948. J. Chem. Phys. **16**: 1063.
KASTLER, A. 1948. Communication au Congres de Bordeaux.
KRAMERS, H. A. 1938. Handb. und Jahrb. Chem. Physik, **I**: 2.
LANDSBERG, G. and MANDELSTAM, L. 1930. Z. Physik, **60**: 334, 364.
LYDDANE, R. H. and HERZFELD, K. F. 1938. Phys. Rev. **54**: 846.
MATHIEU, J. P. 1945. Spectres de vibration et symmetrie. Hermann, Paris.
MATHIEU, J. P. and COUTURE-MATHIEU, L. 1952. Compt. rend. **234**: 1961.
MATOSSI, B. F. and MAYER, R. 1948. Phys. Rev. **74**: 449.
MICHALKE, H. 1938. Z. Physik, **108**: 748.
NEDUNGADI, T. M. K. 1940. Proc. Indian Acad. Sci. **11**: 86.
——— 1941. Proc. Indian Acad. Sci. **14**: 242.
ORNSTEIN, L. S. and WENT, J. J. 1935*a*. Physica, **2**: 391.
——— 1935*b*. Physica, **2**: 503.

PFLÜGER, A. 1904. Physik. Z. **5**: 215.
PLACZEK, G. 1934. Handb. Radiologie, **VI**: 2.
ROSENTHAL, J. E. and MURPHY, G. M. 1936. Revs. Mod. Phys. **8**: 317.
SEITZ, F. 1936. Ann. Math. **37**: 17.
SMITH, H. M. J. 1948. Trans. Roy. Soc. A, **241**: 105.
THEIMER, O. 1951. Proc. Phys. Soc. A, **64**: 1012.
——— 1952. Proc. Phys. Soc. A, **65**: 38.
VAN HOVE, L. 1953. Phys. Rev. **89**: 1189.
VENKATESVARLU, K. 1941. Proc. Indian Acad. Sci. **13**: 64; **14**: 529.
——— 1942. Proc. Indian Acad. Sci. **16**: 45.

LETTERS TO THE EDITOR

Under this heading brief reports of important discoveries in physics may be published. These reports should not exceed 600 words and, for any issue, should be submitted not later than six weeks previous to the first day of the month of issue. No proof will be sent to the authors.

The Resonant Absorption of γ-Rays by N^{14}

The $C^{13}(p, \gamma)N^{14}$ reaction has a broad resonance ($\Gamma = 32$ kev.) for 554 kev. protons (Seagrave 1952) which forms N^{14} in a $1-$, $T = 1$ state of 8.06 Mev. excitation (Clegg and Wilkinson 1953). This state decays 90% by transitions direct to the ground state (Woodbury, Day, and Tollestrup 1953). The possibility of exciting N^{14} nuclei to the 8.06 Mev. state by absorption of these 8.06 Mev. γ-rays is suggested by two facts: first, the great width of the level means that shifts in the γ-ray energy, occurring between production and subsequent resonant absorption, due to Doppler and recoil effects are not as serious as in the resonant scattering work of Moon (1951); second the recoil losses occurring on emission and absorption and amounting to about 5 kev. total can be compensated for by the Doppler shift which in effect transfers some of the incident proton energy to the γ-rays which are emitted in a forward direction.

The resonant absorption has been observed in the present experiment. A thick C^{13} target containing 65% C^{13} (supplied by Dr. M. L. Smith, A.E.R.E., Harwell, England) was bombarded with 700 kev. protons. The target was sufficiently thick that the protons did not leave it until reduced to about 420 kev. or less, so that with little error the γ-ray yield corresponded to the full integral over the 554 kev. resonance.

The inverse resonant absorption of the 8.06 Mev. γ-rays in N^{14} was detected using a glass proportional counter, with an active volume 27 cm. long by 4 cm. in diameter, filled to a pressure of one atmosphere with nitrogen gas and operated with a gas amplification of 10. A metallic layer of sodium evaporated into one end of the counter maintained the purity of the gas. The energy scale was calibrated by means of the $N^{14}(n, p)C^{14}$ reaction produced in the counter gas by thermal neutrons and by injecting α-particles into the counter via a thin mica window.

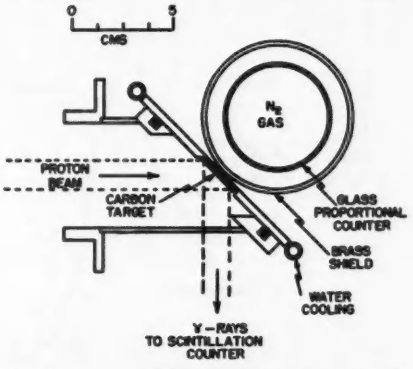

FIG. 1. The proportional counter and target used to observe the resonant $N^{14}(\gamma, p)C^{13}$ reaction.

The counter was placed adjacent to the C^{13} target as shown in Fig. 1 and the pulses from it were recorded on a 100 channel kicksorter (Wilkinson 1950). Simultaneously the γ-ray flux was measured with a NaI scintillation counter in conjunction with a 60 channel kicksorter (Hutchinson and Scarrott 1951). The efficiency of this counter for 6 Mev. γ-rays had been determined by simultaneous α and γ counting on $F^{19}(p, \alpha\gamma)O^{16}$ (Van Allen and Smith 1941). The efficiency for 8 Mev. γ-rays was obtained by extrapolation using the theoretical absorption cross sections. Typical proton and γ-ray spectra are shown in Figs. 2 and 3. That the 550 kev. peak was due to resonant absorption of γ-rays by the reaction $N^{14}(\gamma, p)C^{13}$ was confirmed by the absence of a peak in the spectrum when the counter was bombarded with 6, 12, or 17 Mev. γ-rays. Calculations are in progress to determine the $N^{14}(\gamma, p)C^{13}$ cross section from the data; results and experimental details will be published later.

I would like to thank Dr. D. H. Wilkinson who suggested this experiment to me and Prof. O. R. Frisch who extended to me the hospitality of the Cavendish laboratory where this work was done. I am also indebted to Mr. D. D. Stewart who operated the Cavendish high tension

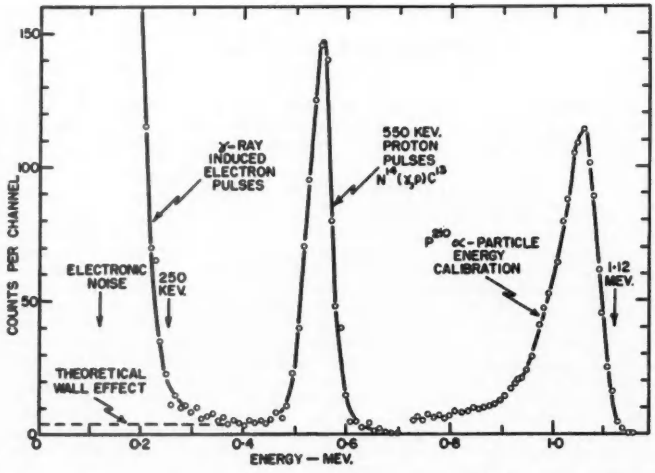

FIG. 2. Proportional counter spectra produced by 1.12 Mev. test α-particles (right-hand curve) and by the $N^{14}(\gamma, p)C^{13}$ reaction.

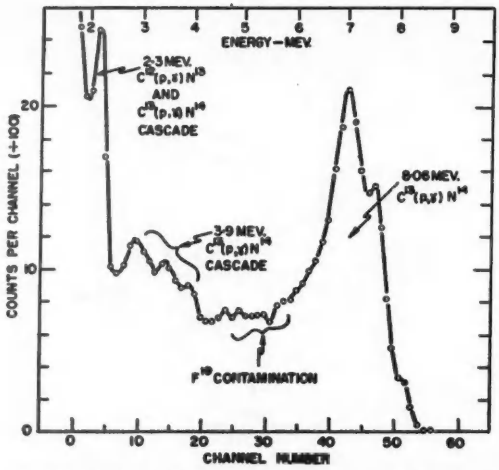

FIG. 3. Typical pulse height spectrum produced by the $C^{13}(p, \gamma)N^{14}$ γ-rays.

set. The work was carried out while the author held a Royal Society of Canada Rutherford Memorial Fellowship and a National Research Council of Canada Fellowship, for which he is grateful.

CLEGG, A. B. and WILKINSON, D. H. 1953. Phil. Mag. **44**: 1269.
HUTCHINSON, G. W. and SCARROTT, G. G. 1951. Phil. Mag. **42**: 792.
MOON, P. B. 1951. Proc. Phys. Soc. A, **64**: 76.
SEAGRAVE, J. D. 1952. Phys. Rev. **85**: 197.
VAN ALLEN, J. and SMITH N. 1941. Phys. Rev. **59**: 618.
WILKINSON, D. H. 1950. Proc. Camb. Phil. Soc. **46**: 508.
WOODBURY, H. H., DAY, R. B., and TOLLESTRUP, A. V. 1953. Phys. Rev. **92**: 1199.

RECEIVED JANUARY 26, 1956.
GEO. M. GRIFFITHS
PHYSICS DEPARTMENT,
UNIVERSITY OF BRITISH COLUMBIA,
VANCOUVER, B.C.

$\Delta M = \pm 3$ Transitions in Dilute Gadolinium Ethyl Sulphate

The seven $\Delta M = \pm 1$ and six $\Delta M = \pm 2$ paramagnetic resonance transitions in dilute gadolinium ethyl sulphate have been studied by Bleaney, Scovil, and Trenam (1954) and Buckmaster (1956) respectively. The sensitivity of the new spectrometer developed by Buckmaster and Scovil (1956) is sufficient to also allow the $\Delta M = \pm 3$ transitions to be observed at 90° K. with signal-to-noise ratios of about 10: 1. Unfortunately, this sensitivity is insufficient to observe these transitions within 25° of the parallel direction. The value of the spectroscopic splitting factor (g) for the perpendicular direction is given in this letter along with a comparison of the calculated and observed positions for the same direction.

The $\Delta M = \pm 2$ and ± 3 transitions both arise from the same admixture of wave functions describing the energy levels due to the largest off-diagonal term $P_2^2(S_x)$ in the spin-Hamiltonian (Elliott and Stevens 1953). It is probable that other off-diagonal terms such as $P_4^2(S_x)$ are also important; however, they do not improve the theoretical agreement with the observed values given below. The transition probabilities for the $\Delta M = \pm 3$ transitions are smaller than those for the $\Delta M = \pm 2$ transitions by the same factor that the $\Delta M = \pm 2$ are smaller than the $\Delta M = \pm 1$. The observed intensities of the $\Delta M = \pm 1$, ± 2, and ± 3 transitions are in the ratio 10^4: 10^2: 1 confirming this. Four of the five $\Delta M = \pm 3$ transitions are shown in Fig. 1.

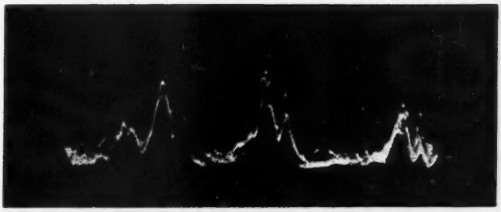

FIG. 1. Four of five $\Delta M = \pm 3$ transitions near crossover point.

The spectroscopic splitting factor for the perpendicular direction is given in Table I.

TABLE I

$\nu = 24.520$ kMc./sec., $T = 90°$ K.

Transition $\Delta M = \pm 3$	Mean field (gauss)	Correction factor (P_2^2)	Corrected field	$g_\perp$
$\pm 7/2 \leftrightarrow \pm 1/2$	2932	+ 4	2936	1.9886
$\pm 5/2 \leftrightarrow \pm 1/2$	2897	+41	2938	1.9875
$+3/2 \leftrightarrow -3/2$	2893	+54	2947	1.9814

Mean value $g_\perp$: uncorrected 2.0085 ± 0.001, corrected 1.9858 ± 0.001
Mean value $g_\perp$: corrected excluding $+3/2 \leftrightarrow -3/2$ transition 1.9881 ± 0.001

The values of $g_\perp$ corrected for ($P_2^2(S_x)$) obtained with the same crystal from the $\Delta M = \pm 1$ and ± 2 transitions (Buckmaster 1956) at 90° K. are

$$\Delta M = \pm 1,\ g_\perp = 1.9901 \pm 0.001;$$
$$\Delta M = \pm 2,\ g_\perp = 1.9901 \pm 0.001.$$

This shows that the effect of other off-diagonal terms such as $P_4^2(S_x)$ is becoming important.

It is not possible to calculate the splitting parameters from the $\Delta M = \pm 3$ transitions. The observed positions for the perpendicular direction are compared in Table II with the positions calculated from the values of the splitting parameters obtained from the $\Delta M = \pm 1$ and ± 2 transitions in this direction (Buckmaster 1956). The agreement is not within the experimental error.

TABLE II

$\nu = 24.520$ kMc./sec., $T = 90°$ K.

Transition $\Delta M = \pm 3$	Observed position (error ± 1 gauss)	Correction factor (P_4^2)	Corrected position	Calculated $\Delta M = \pm 1$ data	Calculated $\Delta M = \pm 2$ data
$+7/2 \leftrightarrow +1/2$	3364	+ 1.7	3366	3374	3369
$+5/2 \leftrightarrow -1/2$	3101	+38.8	3140	3141	3138
$+3/2 \leftrightarrow -3/2$	2893	+53.8	2947	2934	2934
$+1/2 \leftrightarrow -5/2$	2692	+44.2	2736	2727	2731
$-1/2 \leftrightarrow -7/2$	2500	+ 6.8	2507	2494	2500

Recently Cooke (1955) has reported that a resonance from an excited state in dilute dysprosium ethyl sulphate has been observed with $g_{\parallel} = 5.80 \pm 0.02$ and $g_{\perp} = 8.40 \pm 0.2$ which disappeared below 13° K. because of suggested depopulation and above 20° K. because of spin–lattice broadening. A weak resonance ($S/N = 10:1$) has been observed at 4.2° K. with $g_{\parallel} = 5.85 \pm 0.05$ using the high sensitivity spectrometer (Buckmaster and Scovil 1956) in agreement with the above value and confirming the depopulation hypothesis.

BLEANEY, B., SCOVIL, H. E. D., and TRENAM, R. S. 1954. Proc. Roy. Soc. A, **223**: 15.
BUCKMASTER, H. A. and SCOVIL, H. E. D. 1956. To be published.
BUCKMASTER, H. A. 1956. Can. J. Phys. **34**: 150.
COOKE, A. H. 1955. Proceedings of the 9th International Conference of Low Temperature Physics and Chemistry. Paris. In press.
ELLIOTT, R. J. and STEVENS, K. W. H. 1953. Proc. Roy. Soc. A, **219**: 387.

RECEIVED DECEMBER 16, 1955.
PHYSICS DEPARTMENT,
UNIVERSITY OF BRITISH COLUMBIA,
VANCOUVER, B.C.

H. A. BUCKMASTER

THE PHYSICAL SOCIETY

MEMBERSHIP of the Society is open to all who are interested in Physics.

FELLOWS pay an Entrance fee of £1 1*s*. ($3.00) and an Annual Subscription of £2 2*s*. ($6.00).

STUDENTS: A candidate for Studentship must be between the ages of 18 and 26, and pays an Annual Subscription of 5*s*. ($0.75).

MEETINGS: Fellows and Students may attend all Meetings of the Society including the annual Exhibition of Scientific Instruments and Apparatus.

PUBLICATIONS include the *Proceedings of the Physical Society*, published monthly in two sections, and *Reports on Progress in Physics*, published annually. Volume XVIII, 1955, is now available (price 50*s*. ($7.15)). Members are entitled to receive many of the Publications at a reduced rate.

Further information can be obtained from:

THE PHYSICAL SOCIETY

1, LOWTHER GARDENS, PRINCE CONSORT ROAD

LONDON, S.W.7, ENGLAND

CANADIAN JOURNAL OF PHYSICS

Notes to Contributors

Manuscripts

(i) ***General.*** Manuscripts, in English or French, should be typewritten, double spaced, on paper $8\frac{1}{2} \times 11$ in. **The original and one copy are to be submitted.** Tables and captions for the figures should be placed at the end of the manuscript. Every sheet of the manuscript should be numbered.

Style, arrangement, spelling, and abbreviations should conform to the usage of this journal. Names of all simple compounds, rather than their formulas, should be used in the text. Greek letters or unusual signs should be written plainly or explained by marginal notes. Superscripts and subscripts must be legible and carefully placed.

Manuscripts and illustrations should be carefully checked before they are submitted. Authors will be charged for unnecessary deviations from the usual format and for changes made in the proof that are considered excessive or unnecessary.

(ii) ***Abstract.*** An abstract of not more than about 200 words, indicating the scope of the work and the principal findings, is required, except in Notes.

(iii) ***References.*** References should be listed **alphabetically by authors' names,** unnumbered, and typed after the text. The form of the citations should be that used in issues of this journal published in 1956; in references to papers in periodicals, titles should not be given and only initial page numbers are required. The names of periodicals should be abbreviated in the form given in the most recent *List of Periodicals Abstracted by Chemical Abstracts*. All citations should be checked with the original articles and each one referred to in the text by the authors' names and the year.

(iv) ***Tables.*** Tables should be numbered in roman numerals and each table referred to in the text. Titles should always be given but should be brief; column headings should be brief and descriptive matter in the tables confined to a minimum. Vertical rules should be used only when they are essential. Numerous small tables should be avoided.

Illustrations

(i) ***General.*** All figures (including each figure of the plates) should be numbered consecutively from 1 up, in arabic numerals, and each figure referred to in the text. The author's name, title of the paper, and figure number should be written in the lower left corner of the sheets on which the illustrations appear. Captions should not be written on the illustrations (see Manuscripts (i)).

(ii) ***Line Drawings.*** Drawings should be carefully made with India ink on white drawing paper, blue tracing linen, or co-ordinate paper ruled in blue only; any co-ordinate lines that are to appear in the reproduction should be ruled in black ink. Paper ruled in green, yellow, or red should not be used unless it is desired to have all the co-ordinate lines show. All lines should be of sufficient thickness to reproduce well. Decimal points, periods, and stippled dots should be solid black circles large enough to be reduced if necessary. Letters and numerals should be neatly made, preferably with a stencil (**do NOT use typewriting**) and be of such size that the smallest lettering will be not less than 1 mm. high when reproduced in a cut 3 in. wide.

Many drawings are made too large; originals should not be more than 2 or 3 times the size of the desired reproduction. In large drawings or groups of drawings the ratio of height to width should conform to that of a journal page but the height should be adjusted to make allowance for the caption.

The original drawings and one set of clear copies (e.g. small photographs) are to be submitted.

(iii) ***Photographs.*** Prints should be made on glossy paper, with strong contrasts. They should be trimmed so that essential features only are shown and mounted carefully, with rubber cement, on white cardboard with no space or only a **very** small space (less than 1 mm.) between them. In mounting, full use of the space available should be made (to reduce the number of cuts required) and the ratio of height to width should correspond to that of a journal page ($4\frac{3}{4} \times 7\frac{1}{2}$ in.); however, allowance must be made for the captions. Photographs or groups of photographs should not be more than 2 or 3 times the size of the desired reproduction.

Photographs are to be submitted in duplicate; if they are to be reproduced in groups one set should be mounted, the duplicate set unmounted.

Reprints

A total of 50 reprints of each paper, without covers, are supplied free. Additional reprints, with or without covers, may be purchased.

Charges for reprints are based on the number of printed pages, which may be calculated approximately by multiplying by 0.6 the number of manuscript pages (double-spaced typewritten sheets, $8\frac{1}{2} \times 11$ in.) and including the space occupied by illustrations. An additional charge is made for illustrations that appear as coated inserts. The cost per page is given on the reprint requisition which accompanies the galley.

Any reprints required in addition to those requested on the author's reprint requisition form must be ordered officially as soon as the paper has been accepted for publication.

Contents

Page

The Possibility of a Phase Change in Nuclear Matter—*L. E. H. Trainor and W. R. Dixon* - - - - - - - - - - - - - - - - 229

Growth Twins in Germanium—*G. F. Bolling, W. A. Tiller, and J. W. Rutter* - 234

The Photodisintegration of Oxygen Nuclei into Four Alpha-particles—*W. K. Dawson and D. L. Livesey* - - - - - - - - 241

The Far Ultraviolet ($C-X$) Bands of N_2^+—*P. G. Wilkinson* - - - - 250

High-energy Forbidden β-Ray Transitions from Cs^{134} (2.3 yr.), Co^{60} (5.3 yr.), Sc^{46} (84 d.), and Hg^{203} (47.9 d.)—*J. L. Wolfson* - 256

An Examination of Verwey's Model for the Lattice Structure of the Free Surface of Alkali Halide Crystals—*G. C. Benson, H. P. Schreiber, and D. Patterson* - - - - - - - - - - - - - - - 265

The Radiation Force on a Spherical Obstacle in a Cylindrical Sound Field—*T. F. W. Embleton* - - - - - - - - - - - - - - - 276

Evaporation Neutrons from Cosmic Ray Nuclear Interactions in Various Elements—*K. W. Geiger* - - - - - - - - - - - - 288

The Behavior of Ferromagnetics under Strong Compression—*F. D. Stacey* - 304

Selection Rules and Temperature Dependence of the First-order Raman Effect in Crystals—*O. Theimer* - - - - - - - - - 312

Letters to the Editor:

The Resonant Absorption of γ-Rays by N^{14}—*Geo. M. Griffiths* - 339

$\Delta M = \pm 3$ Transitions in Dilute Gadolinium Ethyl Sulphate—*H. A. Buckmaster* - - - - - - - - - - - - - - - - - - - 341

Printed in Canada *by* University of Toronto Press